X-713-69-148
PREPRINT
NASA TM X-63555

PERFORMANCE, SYSTEMS DESIGNS, MODIFICATIONS, RADIOMETRY, OPERATIONAL PROBLEMS, AND CORRECTIVE PROCEDURES ASSOCIATED WITH AN 1.75 METER OFF-AXIS SOLAR SIMULATOR

CHARLES H. DUNCAN

APRIL 1969

GODDARD SPACE FLIGHT CENTER
GREENBELT, MARYLAND

PERFORMANCE, SYSTEMS DESIGNS, MODIFICATIONS, RADIOMETRY, OPERATIONAL PROBLEMS, AND CORRECTIVE PROCEDURES ASSOCIATED WITH AN 1.75 METER OFF-AXIS SOLAR SIMULATOR

Charles H. Duncan

GODDARD SPACE FLIGHT CENTER

Greenbelt, Maryland

PERFORMANCE, SYSTEMS DESIGNS, MODIFICATIONS, RADIOMETRY, OPERATIONAL PROBLEMS, AND CORRECTIVE PROCEDURES ASSOCIATED WITH AN 1.75 METER OFF-AXIS SOLAR SIMULATOR

Charles H. Duncan

ABSTRACT

Solar simulator performance characteristics are defined in terms of system geometry and the definitions of radiant energy. The accuracy, precision, and calibration of the instrumentation utilized for total and spectial irradiance measurements are discussed. The primary standards from which these measurements are derived are identified. The performance, sub-systems designs, modifications, operational problems, and corrective procedures of an 1.25 meter off-axis solar simulator modified to obtain an 1.75 meter test diameter are discussed in detail. The modified simulator is capable of producing an irradiance variable from 164 mw cm^{-2} to 6 mw cm^{-2} over an 1.75 meter diameter test plane with an uniformity of 2% and a stability of 1%. The spectrum correlates with the air mass zero solar spectrum sufficiently for the performance of thermal balance tests, materials degradation tests, and solar energy converter tests. The collimation of the system is 1.5° half-angle. The operational problems discussed are: spectral stability and its effect upon thermal control material absorptance; ozone generation and control; optimization of

spectrum and efficiency of system; degradation of optical and mechanical components resultant from envirroniment; and, electronic and thermal malfunctions. The performance capabilities have been verified by the orbital performance of explorer XXXVIII which received its pre-launch environmental test in this simulator. Explorer XXXVIII is attaining temperatures in orbit within a few degrees of those predicted on the basis of the solar simulation test and has experienced no thermal or power problems during the first eleven months in orbit.

CONTENTS

LIST OF ILLUSTRATIONS

LIST OF TABLES

LIST OF SYMBOLS

A area; aperture, ampere

B point

C centigrade

D diameter

E point

F functional relationship

G gain

H irradiance; principal plane

I current; irradiation

J radiant intensity

K Kelvin

M magnification

N radiance

P power; 1

S plane

T temperature

U radiant energy

V volts; volume

W watt; radiant emittance

a subscript for after modification

b subscript for before modification

c constant

d differential

f focal length

i subscript for image space; summation

j subscript for summation

n index of refraction; number

o subscript for object space

r radius of test volume; coordinate system

s subscript for source

t time

z coordinate system

Γ re-reflected energy

Δ delta

Λ uniformity of irradiance

Υ spectral uniformity

Φ variation between simulator and AMO spectra

X spectral stability

Ψ stability of radint flux

Ω quotient of irradiance in umbra by irradiance in umbra and penumbra

α absorptance; angle

β angle

γ divergence

δ optical path length

ϵ efficiency

ξ conversion efficiency of electrical to radiant power

θ angle in cylindrical coordinates

λ subscript for wavelength

μ transmission of obstructions

π 3.14159

ρ reflectance

τ transmittance

ν capture efficiency

ϕ collimation angle

ψ 1/2 off-axis angle of collimator

ω solid angle

< > average value

′ corresponding point or plane or parameter in image space

o.z. optical axis

|| parallel

$\perp$ perpendicular

0 zero

∞ infinity

° degrees

INDEX HEADINGS

Solar Simulation

Solar Simulators

Off-axis Solar Simulation

Spectral Irradiance

Total Irradiance

Contamination of Optical Surfaces

AMO Solar Irradiance

Optical Design

Testing

Radiometry

Optical Measurements

Detectors

Monochromators

Thermal Control Materials

Spectrum Stability

Compact Arc Lamps

Primary Standards

Large Optics Fabrication

Calibrations

Ozone

Space Environment Simulation

Radiant Energy

Spectral Filters

Uniformity of Irradiance Filters

Explorer XXXVIII

Solar Simulator Systems Design

I. INTRODUCTION

The performance, design characteristics, and operational problems of an off-axis solar simulator, prior and subsequent to a modification which increased the test beam diameter, are the primary subjects of this paper. The optical, radiometric, electronic, thermal, and mechanical design analyses required for the modification are the secondary subjects. The derivation of solar simulator performance and design characteristics from the radiometric definitions of radiant energy[1-4] and simulator geometry is the tertiary subject. The primary emphasis is upon the optical and radiometric aspects of the solar simulation component of a space environment simulator. The components of a space environment simulator which provide pressure and heat sink simulation are not discussed in detail.

The performance and design characteristics of a solar simulator are derived from the definitions of radiant energy[1-4] and system geometry in order to alleviate any confusion which might result from conflicting nomenclatures and symbols currently in use among the various technologies and sciences which involve radiant energy.[5-17] Photometric units and definitions have been avoided because these have no pertinence to either the performance or design of solar simulators.[18-20] The description, calibration, accuracy, and precision of the instrumentation utilized in the measurement of the parameters which characterize solar simulator performance is presented. The primary standard(s) from which the calibration of each instrument is (are) derived is identified. The performance

and design characteristics of the simulator, prior and subsequent to the modification which increased the nominal beam diameter from 1.2 meters to 1.75 meters, are covered in detail. Major problems, which have been experienced, affecting solar simulator performance integrity are identified and discussed in detail. These problems are: 1 - excessive ozone generation by radiant energy sources; 2 - degradation of reflective optics; 3 - degradation of spectrum of simulator; 4 - excessive equilibrium temperatures experienced by components within the system; 5 - electronic malfunctions which compromise the integrity of the performance characteristics of the simulator; 6 - maintenance of irradiance uniformity within test volume; 7 - degradation of efficiency and spectrum of radiant energy source; 8 - thermal control systems malfunctions resulting in destruction of components within system; 9 - source self-destruction; 10 - fluctuations of input voltage to system greater than design tolerances; 11 - pressure fluctuations and contaminants in fluid used for cooling; 12 - corrosion of materials used for various components resulting from environmental conditions; 13 - maintenance of environment around simulator to minimize or eliminate contaminants; 14 - malfunctions introduced by perturbations from data acquisition systems; and, 15 - the acquirement and maintenance of optimum system efficiency. Methods which have been evolved either to eliminate or to minimize each of these problems are given.

The material is presented in the following order: 1 - discussion of the objectives and purposes of solar simulation; 2 - the derivation of solar simulator

performance and design characteristics from considerations of system geometry and definitions of radiant energy; 3 - a description of instrumentation used to measure performance characteristics; 4 - a discussion of the optical design and performance of the system prior to modification; 5 - a description of the constraints, requirements, and objectives imposed upon the modification of the system; 6 - a discussion of the design analyses and final designs involved in the modification; 7 - a description and critique of the performance of the modified simulator; 8 - a discussion of specific operational problems and methods evolved to eliminate or minimize these problems; 9 - a discussion of test experience with Explorer XXXVIII; and 10 - summary.

The experience gained from the operation and performance of the solar simulator described in this paper indicates that adequate characterization of the air mass zero (AMO) solar irradiance[21-31] can be obtained with an off-axis solar simulator utilizing an integrated optical design. This characterization can be obtained with a system which has a large relative aperture, or low f/number. The advantages accruing to a large relative aperture system are: substantial cost reductions over a system utilizing a small relative aperture since total costs of a system are inversely proportional to the relative aperture, and a more compact system with the consequent reduction in space requirements. The disadvantages associated with systems of large relative aperture are: the difficulty of obtaining uniformity of irradiance within the test volume because of imperfections existing in the optical components of the system and the

relatively small distances between points on the effective source of radiant energy and points within the test volume; and, the larger collimator required to obtain irradiance over a specific test area because the projected area of the collimator which provides irradiance within the test volume is an inverse function of the relative aperture of the system. The simulator herein discussed has provided solar simulation for thermal balance tests of spacecraft and spacecraft components which subsequently have performed in space well within design tolerances. It has also provided adequate AMO solar irradiance simulation for thermal control materials degradation tests as well as tests of energy conversion devices.

II. BACKGROUND AND THEORY

A solar simulator is a device used to simulate the AMO solar irradiance. Solar simulators are used for thermal balance tests of spacecraft materials, degradation studies, energy conversion devices calibrations and tests, and calibrations and tests of sensors, experimental packages, and components of spacecraft. In general, the true space environment is not simulated. The true space environment in addition to AMO solar irradiance, consists of energy from the sunlight reflected from the earth, thermal energy from the earth, very low pressures, very low temperatures, low or no magnetic fields, electrons, protons, and other nuclear particles of various energies, cosmic radiation, micrometeoroids, etc. Solar simulators are generally used in conjunction with a

vacuum chamber and thermal shroud which will simulate the space environment sufficiently to allow thermal balance tests to be performed.[32-45] The test and calibration of energy conversion devices, sensors, experimental packages and components of spacecraft are sometimes accomplished using a solar simulator without vacuum or cold shroud. Material degradation studies sometimes employ devices to simulate the charged particle environment (i.e., electrons and protons) in addition to AMO solar irradiance, vacuum, and cold shroud.[46-52] At the present time most medium to large solar simulators (minimum diameter of beam $\geq$ 80 cm) are part of a facility which can maintain pressures $\leq 10^{-6}$ torr and temperatures $\leq 90°K$.[32-45] These types of solar simulators consist of four basic parts: 1 - an enclosure which can maintain a pressure $\leq 10^{-6}$ torr; 2 - a shroud within the enclosure through which fluids, with temperatures $\leq 77°K$, can be circulated; 3 - an optical system to provide radiant energy over a test volume located within the thermal shroud and vacuum enclosure; and, 4 - a source or sources of radiant energy. The optical system design can be either on-axis or off-axis and the sources can be utilized either in a modular or integrated design. Integrated design means more than one source provides radiant energy to any point within the test volume. Solar simulators which characterize AMO solar irradiance most accurately employ off-axis optics and an integrated optical design for the radiant energy sources.[32-45]

The optical design of a solar simulator, in general, consists of four basic elements: 1 - a source mounted inside a collector which images the arc at a

point along the optical axis; 2 - a field lens placed at the position of the arc image; 3 - a projection lens which images the field lens onto the plane of the collimator or some adjacent position; and 4 - a collimator which directs radiant flux into the test volume. Figure 1 represents the geometry of a typical solar simulator system.

The radiometric definitions of radiant energy[1-8] along with the symbols for each definition suggested by references one through four are listed in Table I. The corresponding units, in the cgs system for radiometric quantities, which are used in this paper, are also shown. The column headed "object space" refers to source characterization definitions and the column headed "image space" refers to definitions characterizing radiant energy incident upon a surface from a source of radiant energy.

The characteristic of the source which is most important in solar simulator design is the radiance, symbol N, units of watts cm^{-2} $ster^{-1}$ and the corresponding characteristic within the test volume is the irradiance, symbol H, units of watts cm^{-2}. Radiance always refers to a source of radiant energy and irradiance always refers to radiant energy incident upon a surface from a source of radiant energy.

Other characteristics of the source which are useful in solar simulator optical design are: the radiant intensity, symbol J_0, units of watts $ster^{-1}$; the radiant emittance, symbol W_0, units of watts cm^{-2}; and, the radiant flux, symbol P_0, units of watts.

Other characteristics of the radiant energy within the test volume of a solar simulator which are useful for some applications are: the radiant flux, symbol P_i, units of watts; the irradiation, symbol I_i, units of joules cm^{-2}.

The radiant flux or radiant power (P) is considered as the basic definition in radiometry and is equal to the mean power of the radiant energy averaged over a period much greater than the oscillation period.[8] The relationships among the source characteristics and the radiant power are:

$$U_0 = \int_0^t P_0 \, dt \tag{1}$$

$$J_0 = \frac{\partial P_0}{\partial \omega_0} \tag{2}$$

$$W_0 = \frac{\partial P_0}{\partial A_0 \cos \alpha_0} \tag{3}$$

$$N = \frac{\partial P_0}{\partial \omega_0 \, \partial A_0 \cos \alpha_0} \tag{4}$$

where ω_0 is the unit solid angle, A_0 is the area of the source, and α_0 is the angle formed by a perpendicular to an element of area dA_0 and the direction of emission of the radiant flux. The corresponding relationships among the

characteristics of radiant flux within the test volume of a solar simulator are:

$$U_i = \int_0^t P_i \, dt \tag{5}$$

$$I_i = \frac{\partial U_i}{\partial A_i \cos \alpha_i} \tag{6}$$

$$H = \frac{\partial P_i}{\partial A_i \cos \alpha_i} \tag{7}$$

where α_i is the angle formed by a perpendicular to an element of area dA_i and the direction from which radiant energy is incident upon dA_i. The relationship between radiance and irradiance for any optical system is:

$$H = \frac{\epsilon' N A_0 \cos \alpha_0 \cos \alpha_i}{\delta 2} \tag{8}$$

where ϵ' is the optical efficiency of the optical system, and δ is the optical path length between the source of radiant energy and the surface where H is determined. The relationship between the radiant flux in the test volume of a solar simulator, P_i, and the radiance is obtained by integrating Equation 8 with respect to the area of a plane within the test volume (A_i) and is:

$$P_i = \frac{\epsilon' N A_0 \cos \alpha_0 A_i \cos \alpha_i}{\delta 2} \tag{9}$$

Equation 9 states that the radiant flux incident in the test volume is directly proportional to the optical efficiency of the system, the radiance of the source, the projected area of the source, and the projected area of the collimator; and, inversely proportional to the square of the optical path length between the source and the plane of the test volume where the radiant flux is measured. Figure 1 is an optical representation of a typical solar simulaion system of the type described in this paper.

From an inspection of Figure 1, the following relationships are obtained. The solid angle over which radiant flux is collected from the sources (ω_0) is:

$$\omega_0 = \frac{A_0 \cos \alpha_0}{\delta_0^2} \tag{10}$$

and the solid angle over which radiant flux is incident on the collimator (ω_i) is:

$$\omega_i = \frac{A_i \cos \alpha_i}{\delta_i^2} \tag{11}$$

The relationship between δ_i, δ_0, and δ is:

$$\delta_i + \delta_0 + z_i = \delta \tag{12}$$

where z_i is the optical path length between the collimator and a point in the test volume.

Each of the quantities listed in Table I are also functions of wavelength. The notation used in this paper when spectral properties are discussed will be in accordance with Equation 13:

$$(\text{Symbol})_{\lambda_2-\lambda_1} = \int_{\lambda_1}^{\lambda_2} (\text{Symbol})_{\lambda_i}\, d\lambda \tag{13a}$$

$$\lambda_2 - \lambda_1 = \Delta\lambda \tag{13b}$$

$$\lambda_1 \leq \lambda_i \leq \lambda_2 \tag{13c}$$

where λ_1 is the shortest wavelength for which the quantity is measured, λ_2 is the longest wavelength, and λ_i is the value of the quantity for an infinitesimal bandwidth centered at λ_i.

III. PARAMETERS CHARACTERIZING SOLAR SIMULATOR PERFORMANCE

The parameters which characterize solar simulator performance are listed in Table II together with the symbols, units, and nomenclature for each as used in this paper.

A. Mean Irradiance, Mean Radiant Flux, and Mean Radiant Energy Within Test Volume

The mean or average values of the radiant energy $\langle U_i \rangle_t$, radiant flux, $\langle P_i \rangle_t$, and, irradiance $\langle H \rangle_t$ within the test volume in cylindrical coordinates

at some time t are, from calculus:[53]

$$\langle U_i \rangle_t = \frac{\int_v U_i(r,\theta,z)\, dV}{\int_v dV} \tag{14a}$$

$$\langle P_i \rangle_t = \frac{\int_v P_i(r,\theta,z)\, dV}{\int_v dV} \tag{14b}$$

$$\langle H \rangle_t = \frac{\int_v H(r,\theta,z)\, dV}{\int_v dV} \tag{14c}$$

where $\int_v dV$ is the volume integral of the solar simulator test volume.

The mean values of the radiant energy, radiant flux, and irradiance for a time interval equal to Δt are:

$$\langle U_i \rangle = \langle U_i \rangle_{t_2 - t_1} = \frac{\int_0^t \langle U_i \rangle_t\, dt}{\int_0^t dt} \tag{15a}$$

$$\langle P_i \rangle = \langle P_i \rangle_{t_2 - t_1} = \frac{\int_0^t \langle P_i \rangle_t \, dt}{\int_0^t dt} \qquad (15b)$$

$$\langle H \rangle = \langle H \rangle_{t_2 - t_1} = \frac{\int_0^t \langle H \rangle_t \, dt}{\int_0^t dt} \qquad (15c)$$

The symbol without the subscript, $t_2 - t_1$, will be used throughout this paper to represent the quantities of Equations 15a, b, c when the time interval is one second.

B. Efficiency, Optical, Electrical, and Total

The optical efficiency of a solar simulator, ϵ', is defined as the quotient of the radiant energy incident upon any plane r, θ, at position z within the test volume by the total radiant energy emitted by the sources. The efficiency of the conversion of electrical energy to radiant energy (ϵ'') by the electrical components of the solar simulator is defined as the quotient of the total radiant energy emitted by the sources by the total electrical energy supplied to the sources. The total efficiency of a solar simulator, ϵ, is defined as the product of ϵ' and ϵ''; or $\epsilon = \epsilon' \epsilon''$ and is a function of the transmission, absorption, and reflection characteristics of the optical components of the system, the effective

transmission of apertures and obstructions within the optical system, the efficiency of collection of radiant energy from the sources, the ratio of the useful energy in the test volume to the total energy in the test volume, and the conversion efficiency of electrical to radiant energy for each radiant source. The efficiency of a solar simulator, ϵ, is defined by Equation 16:

$$\epsilon = \epsilon' \epsilon'' = \sum_{i=1}^{n} \xi_i \nu_i \sum_{i=1}^{n'} \tau_i \alpha_i \rho_i \sum_{i=1}^{n''} |\mu_i| \; |\Omega| \qquad (16)$$

where

ξ_i is the conversion efficiency of electrical to radiant energy for each source,

ν_i is the collection efficiency of radiant energy emitted by each source,

τ_i is the radiant transmittance of each optical element in the system,

α_i is the radiant absorptance of each optical element in the system,

ρ_i is the radiant reflectance of each optical element in the system,

μ_i is the effective transmission of each obstruction and aperture in the system,

Ω is the ratio of useful energy in the test volume to the total energy in the test volume.

n is the number of sources used in the simulator,

n′ is the number of optical elements in the optical system of the simulator, and

n″ is the number of apertures and obstructions in the optical system of the simulator.

The total electrical power (P_e) input to the radiant energy sources of a solar simulator is equal to:

$$P_e = \sum_{j=1}^{n} V_j I_j \tag{17}$$

where V is the voltage in volts, I is the current in amperes, and n is the number of radiant energy sources in the system.

Total electrical power input to the system is related to total radiant power output of the sources (P_o) and total radiant power incident in the test volume (P_i) as:

$$P_e = \epsilon'' P_o = \frac{\epsilon}{\epsilon'} P_o \tag{18a}$$

$$P_e = \epsilon P_i = \epsilon' \epsilon'' P_i \tag{18b}$$

From Equations 7, 15b, 15c, 17, and 18b, the following relation between system efficiency, electrical power input, average irradiance and area of a plane in the test volume is obtained:

$$\epsilon = \frac{\left\langle \sum_{j=1}^{n} V_j I_j \right\rangle}{\langle H \rangle A_i \cos \alpha_i} \tag{19}$$

The parameters of Equation 19 are more easily measured than those of Equation 14 and is more useful for determinations of the efficiency of a solar simulator.

C. Uniformity of Irradiance

The uniformity of irradiance within the test volume of a simulator (Λ) is a measure of the deviations of individual irradiances from the mean value of irradiance for all positions within the test volume averaged over a time interval much shorter than any period of system oscillation which would effect the mean irradiance value.

The definiting equation for uniformity of irradiance is:

$$\Lambda = 100 \left(\frac{\Delta H_{(min)} + \Delta H_{(max)}}{2\langle H \rangle} \right) \tag{20}$$

where

$$\Delta H_{(min)} = \langle H \rangle - \left(\frac{\partial P_i}{\partial A_i \cos \alpha_i} \right)_{min} ;$$

and,

$$\Delta H_{(max)} = \left(\frac{\partial P_i}{\partial A_i \cos \alpha_i} \right)_{max} - \langle H \rangle .$$

D. Stability of Radiant Flux

The stability of the mean radiant flux within the test volume of a simulator $(\Psi)_{t_2-t_1}$ is a measure of the variations in radiant flux for the time interval $t_2 - t_1$ from the mean value of the radiant flux averaged over the time interval $t_2 - t_1$.

The defining equation for stability is:

$$\Psi_{t_2-t_1} = 100 \left(\frac{\Delta P_{i(min)} + \Delta P_{i(max)}}{2\langle P_i \rangle_{t_2-t_1}} \right) \tag{21}$$

where

$$\Delta P_{i(min)} = \langle P_i \rangle_{t_2-t_1} - \left(\frac{\partial U_i}{\partial t} \right)_{min} ;$$

and

$$\Delta P_{i(max)} = \left(\frac{\partial U_i}{\partial t} \right)_{max} - \langle P_i \rangle_{t_2-t_1} .$$

E. Mean Spectral Irradiance

The mean spectrum for all positions within the test volume of a solar simulator for some time, Δt, which is much less than any period of system oscillation which effects the spectrum of the simulator is given by a tabulation or graph of H_{λ_i} versus λ_i over all wavelengths of interest. For solar simulators, the variations of H_{λ_i} of the solar simulator as compared to H_{λ_i} of the AMO

solar irradiance are of more interest than the tabulations of H_{λ_i} of the solar simulator. For this reason, the data for the spectrum of a solar simulator are sometimes presented in the form of tabulations or graphs of the percent of the total energy of the simulator per wavelength interval averaged over the measurement interval and the percentage variation from the corresponding AMO solar irradiance averaged over the same wavelength interval. The percentage variation is sometimes represented by the ratio of solar simulator irradiance to the AMO solar irradiance for each bandwidth of interest. The wavelength intervals are generally set equal to 10 nm for wavelengths shorter than 1000 nm and 100 nm for wavelengths greater than 1000 nm when a detailed presentation of the spectrum is desired.

Measurements are usually made from 250 nm to 2500 nm. The equations used to calculate the percent of the total irradiance per bandwidth ΔH_{λ_i} for the solar simulator (S.S.) and the AMO solar irradiance (AMO) for each wavelength interval, $\Delta\lambda$, contained between the shortest wavelength measured, λ_1, and the largest wavelength measured, λ_n; the variation Φ_{λ_i} between the solar simulator and the AMO solar irradiance; and the ratio of solar simulator irradiance to AMO solar irradiance are:

$$\Delta H_{\lambda_i} = 100 \left[\frac{H_{\lambda_i}}{\sum_{i=\lambda_1}^{\lambda_n} H_{\lambda_i}} \right] \tag{22}$$

$$\Phi_{\lambda_i} = 100\left[\left(\frac{\Delta H_{\lambda_{i(S.S.)}}}{\Delta H_{\lambda_{i(AMO)}}}\right) - 1\right] \quad \text{for} \quad \Delta\lambda_{i(S.S.)} \geq \Delta\lambda_{i(AMO)} \tag{23a}$$

$$\Phi_{\lambda_i} = 100\left[\left(\frac{\Delta H_{\lambda_{i(AMO)}}}{\Delta\lambda_{i(S.S)}}\right) - 1\right] \quad \text{for} \quad \Delta\lambda_{i(S.S.)} \leq \Delta\lambda_{i(AMO)} \tag{23b}$$

$$\text{Ratio} = \frac{\Delta H_{\lambda_{i(S.S.)}}}{\Delta H_{\lambda_{i(AMO)}}} . \tag{23c}$$

F. Uniformity of Spectral Irradiance

The uniformity of spectral irradiance within the test volume of a simulator $\left(\Upsilon_{\lambda_i}\right)$ at some wavelength λ_i is a measure of the deviations of individual spectral irradiances from the mean value of the spectral irradiance at wavelength λ_i for all positions within the test volume averaged over a time interval much shorter than any periods of system oscillation which effect the spectral irradiance. The defining equation is:

$$\Upsilon_{\lambda_i} = 100\left(\frac{\Delta H_{\lambda_{i(min)}} + \Delta H_{\lambda_{i(max)}}}{2\langle H_{\lambda_i}\rangle}\right) \tag{24}$$

where

$$\Delta H_{\lambda_{i(min)}} = \langle H_{\lambda_i}\rangle - \left(\frac{\partial P_{i\lambda_i}}{\partial A_i \cos\alpha_i}\right)_{min} ;$$

and

$$\Delta H_{\lambda_{i}(max)} = \left(\frac{\partial P_i X_i}{\partial A_i \cos \alpha_i}\right)_{max} - \left\langle H_{\lambda_i}\right\rangle$$

G. Stability of Spectral Radiant Flux

The stability of the mean spectral radiant flux within the test volume of a simulator $\left(X_{\lambda_i}\right)_{t_2-t_1}$ at some wavelength λ_i is a measure of the variations in the spectral radiant flux for a time interval $t_2 - t_1$ from the mean value of the spectral radiant flux at wavelength λ_i averaged over the time interval $t_2 - t_1$.

The defining equation is:

$$\left(X_{\lambda_i}\right)_{t_2-t_1} = 100\left(\frac{\Delta P_{i\lambda_i(min)} + \Delta P_{i\lambda_i(max)}}{2\left\langle P_{i\lambda_i}\right\rangle_{t_2-t_1}}\right) \qquad (25)$$

where

$$\Delta P_{i\lambda_i(min)} = \left\langle P_{i\lambda_i}\right\rangle_{t_2-t_1} - \left(\frac{\partial U_{i\lambda_i}}{\partial t}\right)_{min};$$

and

$$\Delta P_{i\lambda_i(max)} = \left(\frac{\partial U_{i\lambda_i}}{\partial t}\right)_{max} - \left\langle P_{i\lambda_i}\right\rangle_{t_2-t_1}$$

H. Collimation or Solar Beam Subtense Angle

The collimation of a solar simulator or solar beam subtense angle is defined in the same manner as the solar subtense angle, i.e., the solid angle determined by the quotient of the area of the source array as observed at a point within the test volume by the distance between source and observation point. The apparent area of the source array at any point within the test volume is the product of the magnification of the system (M) and the area of the source array (Ao). When the sources are arranged in a nearly circular array, then the area is proportional to the diameter of the array. The maximum plane angle (ϕ) equivalent of the collimation solid angle (ϕ_{ster}) is generally specified when solar simulators are discussed. The defining equations for the solid and plane collimation angles of a solar simulator are:

$$\phi_{ster} = \frac{M A_0 \cos \alpha_0}{\delta^2} \approx \frac{\pi M (r_0 \cos \alpha_0)^2}{\delta^2} \qquad (26a)$$

$$\phi = 2 \arcsin \frac{M r_0 \cos \alpha_0}{\delta} = 2 \arctan \frac{r_p}{\delta_i} \qquad (26b)$$

where M is the magnification of the optical system at the point of observation in the test volume; A_0 is the area of the source array; α_0 is the angle formed by the plane of the source array and a perpendicular to the optical axis, δ is the optical path length between the source array and the point of observation in the test volume, r_p is the radius of the source array in the principal plane of the

projection lens array, and δ_i is the optical path length along the axis between the principal plane of the projection lens array and the plane containing the surface of the collimator.

I. Divergence or Solar Beam Incident Angle

The divergence or solar beam incident angle (γ_{ster}) of a solar simulator is defined as the solid angle subtended by a plane parallel to the optical axis of the test volume and the radiant energy source array as observed at a point within the test volume. The corresponding plane angle (γ) is defined as twice the angle subtended by a line parallel to the optical axis of the test volume and the point on the source array, as observed in the test volume, which is located most distant from the parallel line to the optical axis. The plane divergence angle (γ) is equal to the sum of the plane collimation angle (ϕ) and the angle formed by the line in the test volume which includes the point of observation and a line parallel to the optical axis of the test volume. This angle is equal to α_i of Equations 6 and 7. The divergence is always equal to or greater than the collimation angle. When the collimation angle bisector is parallel to the optical axis, α_i is equal to zero degrees and the divergence is equal to the collimation. The defining equations for the solid and plane divergence angles of a solar simulator are:

$$\gamma_{ster} = \phi_{ster} + \alpha_{i\ ster} = \frac{MA_0 \cos \alpha_0}{\delta^2} + \frac{\pi \Delta z^2}{4\left(\Delta z^2 + r_i^2\right)} \qquad (27a)$$

$$\gamma = 2 \arctan\left(\frac{r_p}{\delta_i} + \frac{\Delta z}{r}\right) \tag{27b}$$

where Δz is the distance between a perpendicular to the optical axis at radius r equal r_i and a plane perpendicular to the bisector of the collimation angle at r equal $r_i \sec \alpha_i$.

J. Re-reflected Energy

The energy incident within the test volume of a solar simulator which is reflected back into the optical system by a test object and re-reflected back into the test volume is termed re-reflected energy (Γ). The re-reflected energy is determined by the geometry of the simulator optical system, the test object, and the reflectivities of the surfaces of the optical components of the simulator and test object. It is generally expressed as a percent of the mean radiant energy incident within the test volume $\left(\langle U_i \rangle\right)$. The total amount of re-reflected energy within the test volume of an off-axis simulator is small but can be large for an on-axis system. Measurements of the total energy re-reflected into the test volume are difficult since a detector must be used to measure the energy within the test volume and the introduction of the detector into the test volume introduces perturbations which causes uncertainties in the measurements. Γ is defined by Equation 28 where $\langle U_i \rangle$ is the mean value of the energy in the test volume before introduction of the test object and $\langle U_i \rangle'$ is the mean value of the

energy after introduction of the test object.

$$\Gamma = 100 \left[\frac{\langle U_i \rangle' - \langle U_i \rangle}{\langle U_i \rangle} \right] \tag{28}$$

$\langle U_i \rangle'$ is a function of the energy at each point within the test volume U_j and the reflectivity of the test object at that point (ρ_j) as well as the reflectivity of the component of the optical system which causes the re-reflection ρ_k and the transmission of the optical system between the test volume and the optical component which introduces re-reflections (τ_k). $\langle U_i \rangle'$ can be defined by Equation 29:

$$\langle U_i \rangle' = \langle U_i \rangle + \rho_k \tau_k^2 \int_V' U_j \rho_j \, dV \tag{29}$$

where the integration of the volume interval is over all points common to both U_j and ρ_j.

K. Configuration and Dimensions of Test Volume

The configuration of the test volume and the dimensions of the test volume are determined by the optical system of the simulator. The configuration is the surface of revolution which encloses the useful test volume and is generally a quadric surface. A cylindrical coordinate system (r, θ, z) is used to describe the dimensions and configuration in this paper in which z represents the optical axis, $\theta = 0°$ refers to the vertical with respect to the physical dimensions of the enclosure housing the simulator and r is the radius of the test volume.

L. Vacuum

The vacuum obtainable within the enclosure containing the test volume is expressed in units of torr which is equal to 1/760 of a standard atmosphere or 1.33×10^{-2} Newtons cm^{-2}. The vacuum obtainable within the enclosure has no effect upon the optical design or performance characteristics of a solar simulator.

M. Shroud

The shroud inside the enclosure containing the test volume of the solar simulator is maintained at some temperature expressed in degrees Kelvin. The temperature of the shroud has no effect on the optical design but can effect the simulator performance by providing thermal energy into the test volume.

N. Contamination

The molecules inside the simulator enclosure which are detrimental to the reflective and transmissive properties of optical surfaces within the enclosure is called contamination. These molecules come from vacuum pump oil, and other materials which may be located within the enclosure. Contamination manifests itself by a change in the spectral reflectance or transmission characteristics of optical components within the vacuum enclosure and may effect the measurements of spectral irradiance, spectral fidelity, and spectral stability. Contamination can be monitored by placing disks of evaporated aluminum within the enclosure near the optical components and measuring the spectral reflectance at frequent intervals.

A measure of the contamination present can be obtained by the changes in spectral radiant reflectance $\left(\Delta\rho_{\lambda_i}\right)_{t_2 - t_1}$ or spectral radiant transmittance $\left(\Delta\tau_{\lambda_i}\right)_{t_2 - t_1}$ which occur within a wavelength interval $\Delta\lambda$ centered at λ_i within a specific time interval $\left(\Delta t = t_2 - t_1\right)$. The change in reflectance or transmittance for a wavelength interval, $\Delta\lambda = \lambda_2 - \lambda_1$, centered at λ_i is:

$$\Delta\rho_{\lambda_i} = 100 \left[\frac{\left(\rho\lambda_i\right)_{t_1} - \left(\rho\lambda_i\right)_{t_2}}{\left(\rho\lambda_i\right)_{t_1}}\right] \tag{30a}$$

$$\Delta\tau_{\lambda_i} = 100 \left[\frac{\left(\tau\lambda_i\right)_{t_1} - \left(\tau\lambda_i\right)_{t_2}}{\left(\tau\lambda_i\right)_{t_1}}\right] \tag{30b}$$

The change in reflectance $(\Delta\rho)_{t_2 - t_1}$ or transmittance $(\Delta\tau)_{t_2 - t_1}$ of the incident irradiance (H_λ) for all wavelengths included between λ_0 and λ_n is obtained by:

$$(\Delta\rho)_{t_2 - t_1} = \frac{\sum_{i=\lambda_0}^{\lambda_n} \Delta\rho_{\lambda_i} H_{\lambda_i}}{\sum_{i=\lambda_0}^{\lambda_n} H_{\lambda_i}} \tag{31a}$$

$$(\Delta\tau)_{t_2 - t_1} = \frac{\sum_{i=\lambda_0}^{\lambda_n} \Delta\tau_{\lambda_i} H_{\lambda_i}}{\sum_{i=\lambda_0}^{\lambda_n} H_{\lambda_i}} \tag{31b}$$

The contamination of optical components can be expressed by means of Equation 30 when spectrum is a prime performance characteristic of the test and by Equation 31 when total irradiance is the prime performance characteristic of the test

O. Angular Aperture and f/no

The angular aperture on the radiant energy source or object side of a solar simulator (AA_0) is the angle subtended by the source array at the principal plane of the field lens; on the test volume or image side (AA_i), the angular aperture is the angle subtended by the collimator at the principal plane of the projection lens assembly. The f/no on the object side (f/no_0) is the quotient of the focal length of the collector by the diameter of the source array; the f/no on the image side (f/no_i) is the quotient of the focal length of the collimator by the diameter of the collimator upon which radiant flux is incident. The defining equations are:

$$AA_0 = \frac{\pi (D_s)^2}{4 (f_s)^2} \tag{32a}$$

$$AA_i = \frac{\pi D_{coll}^2}{4 f_{coll}^2} \tag{32b}$$

$$f/no_0 = \frac{f_s}{D_s} \tag{32c}$$

$$f/no_i = \frac{f_{coll}}{D_{coll}} \tag{32d}$$

where D_s is the diameter of the source array, f_s is the working focal length of the primary collector, D_{coll} is the diameter of the collimator upon which radiant flux is incident, and f_{coll} is the working focal length of the collimator.

IV. INSTRUMENTATION FOR MEASUREMENT OF SOLAR SIMULATOR PERFORMANCE CHARACTERISTICS

A. Total Radiant Energy Measurement Instrumentation

The characteristic of the total radiant energy which is measured is the irradiance. This is measured with several types of total radiation detectors: 1 - an Eppley normal-incidence pyrheliometer; 2 - an Ångström compensation pyrheliometer; and, 3 - a Hy-Cal pyrheliometer. Uniformity is sometimes measured with a square Heliotek P/N one ohm-cm solar cell of area equal one square centimeter.

The normal-incidence pyrheliometer consists of a fifteen junction bismuth-silver thermopile with a thermistor temperature compensating circuit. It utilizes a circular receiver 5.5 mm is diameter coated with Parson's black lacquer. The thermopile is mounted inside a blackened brass tube with a diaphragm which limits the field of view to an angle of 5°43'30". The tube is filled with dry air at atmospheric pressure during manufacture and is sealed at the viewing end by a removable insert carrying a 1 mm thick quartz crystal window.

The resistance of the pyrheliometer is 510Ω at 25°C. The time constant of the pyrheliometer is approximately twenty seconds and the sensitivity is 1.00 m volt per 2.18×10^{-2} watts cm^{-2}. The pyrheliometer is temperature compensated and the changes in sensitivity which have been observed for the range of temperatures 10°C to 50°C have been less than one quarter of one percent. The pyrheliometer has been in constant use for six years and the observed change in sensitivity has been less than 2% of the initial value.

The Ångström compensation pyrheliometer utilizes two parallel manganin strips which are sprayed with Parson's black optical lacquer on the upper surfaces mounted inside a cyclindrical metal tube diaphragmed so that the rectangular aperature of each strip is 4.2° by 10.6°. The strips are 20.0 mm × 2.0 mm × 0.015 mm in dimensions. A copper-constantan thermocouple is attached to each of the strips so that good thermal contact is provided. The thermocouples are electrically insulated from the strips. One strip is exposed to radiant energy while the other strip receives electrical current. The current from the thermocouples mounted to each strip is then equalized utilizing a galvanometer. The process is repeated with the roles of the strips reversed. Several measurements are averaged to obtain a value for the irradiance. The irradiance is equal to a constant times the square of the current necessary to maintain equal outputs from the thermocouples or:

$$H = cI^2 \tag{33}$$

The value of the constant c is obtained by periodic calibrations and is 86.2 watts cm^{-2} amp^{-2} when H is in watts cm^{-2} and I is in amps. A variation of 3% from

the initial value has been observed in c. This large change was caused by internal damage caused by rough handling when the detector was shipped to Ames Research Center for use aboard the Convair 990 aircraft.

The Hy-Cal pyrheliometer utilizes a proprietary sensor termed an "Asymptotic Hy-Therm" which is a registered trade mark of Hy-Cal Engineering.[54]

This consists of a thin constantan disk over a cavity in a heat sink of copper. The disk is bonded to the heat sink at the periphery of the disk to form the thermocouple junction. A thin copper wire is attached to the center of the disk which forms a differential thermocouple between the center and periphery of the disk which generates a signal directly proportional to the incident radiant flux.[55] The circular sensor is approximately 3 cm in diameter and is coated with colloidal graphite. The sensitivity is approximately one m volt per 2.8×10^{-2} watts cm^{-2} varying about 20% among a group of production pyrheliometers purchased by the author. The sensor is protected with a window fabricated from optical grade quartz and has a response time of approximately 0.25 sec. The pyrheliometer is temperature conpensated for the temperature range 10°C to 50°C.

The Heliotek one cm by one cm P/N solar cell with base resistivity of one ohm centimeter is mounted on a slide within a metal track two meters in length. The slide can be positioned at any point along the track by means of a motor and pulley arrangement. The track is mounted at the geometrical center to a holder placed within the test volume of the simulator. The track can be positioned to any desired angle within ± 1 degree by means of another motor, gear box, and

shaft encoder mechanism. The cell is operated near short circuit current with an electrical load of 0.2 ohms. The cell is used to measure uniformity and stability at atmospheric pressure; no problems are encountered which result from the dependence of near short-circuit current upon the temperature of the cell.[56] The spectral response of the cell covers a bandwidth which is less than the bandwidth of radiant energy incident in the test volume. The cell is sensitive to radiant energy of wavelengths 400 nm to 110 nm. This cell can be used to measure uniformity because the spectral uniformity of the system is equal to zero percent. The spectral response and linearity of cell response with irradiance for this cell is shown in Figures 2 and 3.

The Ångström compensation pyrheliometer is used as the basic standard to calibrate the other detectors. The calibration of the Ångström pyrheliometer is accomplished periodically by comparison with the primary group of pyrheliometers maintained by the Eppley Laboratory at Newport, Rhode Island which are compared frequently with the World Meteorological Organization Standards maintained in Davos, Switzerland.[57-61] The calibrations are based on the International Pyrheliometric Scale 1956 (IPS 1956) which yields an absolute accuracy of ± 1 percent at worst and most probably ± 0.5 percent.[62] The reproducibility or precision of the Eppley group of standards is ± 0.2%[60] based on the Davos standards. The precision of the Ångström compensation pyrheliometer is ± 0.5%. An uncertainty of ± 1.0% is introduced when the other detectors are compared to the Ångström. The precision of both the Eppley normal incidence

pyrheliometer and the Hy-Cal pyrheliometer is about ± 1.0 percent. This yields a root mean square (rms) value of the error in the magnitude of the absolute accuracy of the radiant energy measurement of ± 1.8% when considerable care is taken in the standardization of the secondary pyrheliometers.

The primary standards, upon which the IPS (1965) is based, are:[62] 1 - the absolute calorimeter maintained by the Smithsonian Institution which is used for the calibration of the Abbot silver disk pyrheliometer;[63] and, the absolute ohm and amp which are used for the calibration of the original Ångström compensation pyrheliometer.[64-65] In each case, the calibration is accomplished with the sun as the source of radiant flux. Both calibrations assume no variations occur in the radiant flux from the sun at one astronomical unit (A.U.). The mechanical equivalent of heat (4.186 joules per calorie) is utilized to relate the values obtained from the two types of standards.

B. Spectral Radiant Energy Measurement Instrumentation

The spectral radiant energy measurement instrumentation measures spectral irradiance and utilizes a double monochromator[66] with ultrasil quartz prisms as the dispersive element. An integrating sphere is mounted at the entrance slit of the monochromator. The spectral irradiance transmitted through the exit slit of the monochromator is incident upon one of three detectors which are used to cover the bandwidth of wavelengths. The signals from each of the detectors are amplified by a high gain, high sensitivity synchrous

amplifier[67] and subsequently recorded on either magnetic tape or a strip chart. Calibrations are obtained from a standard of spectral irradiance[68-69] certified by the National Bureau of Standards (NBS).

The monochromator optical design employs reflective optics for all components except the prisms. It is a constant deviation instrument utilizing two ultrasil quartz prisms, each 50 mm in height and 75 mm across the hypotenuse. The refracting angle is 32.5°. The incident radiant flux transverses each prism twice because the rear surface of each is aluminized which results in an effective refracting angle of 65°. The entrance, intermediate, and exit slits are 10 mm in height and are adjustable in width from 0.01 mm to 1.00 mm. The height of the entrance slit can be varied from 10 mm to 1 mm by means of a built-in diaphragm. The ultimate resolution obtainable with the instrument at 500 nm is 1.00 nm which corresponds to a linear dispersion in the exit slit of 5×10^{-2} mm per nm. The stray radiant flux wavelengths, greater or less than 10 nm of the center wavelength which is incident on the exit slit, is less than one part in ten thousand of the incident flux from the center wavelength. The integrating sphere is constructed of two hemispheres each 10 cm in diameter. The entrance aperture is circular and has a diameter of 2.5 cm; the exit aperture is rectangular and is 3 mm wide and 13 mm in height. The exit aperture is mounted coincident with the entrance slit of the monochromator. The apertures are arranged on the surface of the sphere so that all radiant flux incident through the entrance port is reflected a minimum of one time by the wall of the sphere before becoming incident at the

exit port. The sphere wall is coated with five mm of magnesium oxide (MgO) which is obtained by burning magnesium in air. The MgO coating covers approximately 64 percent of the interior sphere walls, with the remainder of the area devoted to entrance and exit ports. The MgO coating is of nearly uniform diffuseness and reflectance. The efficiency of the sphere is approximately five percent.

A multiplier phototube designated 1P-28 with an S-5 response is used to detect signals between 250 nm and 700 nm; a 7102 multiplier phototube with an S-1 response is used between 600 nm and 1000 nm; and, a lead sulfide (PbS) detector is used between 800 nm and 2600 nm. This provides adequate coverage of the spectrum to allow scaling factors to be computed at the overlap regions. The signals from each of these detectors are amplified with a lock-in amplifier which is free of zero-drift and zero-error problems. This amplifier allows the detection of very weak signals superimposed on a high noise background to an accuracy of one percent. The gain stability is 1/4 of one percent. The incident radiant flux is modulated at 11.3 Hz before entering the entrance port of the integrating sphere for one set of instrumentation; and, is modulated at 33 Hz at the position of the intermediate slit for a second set of instrumentation. The strip chart recorder has a gain stability of 1/4 of one percent and a pen error (recording line width) of 1/4 of one percent.

The instrumentation is calibrated with 1000 watt quartz iodine tungsten lamps certified by the NBS. The lamp is calibrated for a current of 8.30 amperes at

approximately 120 volts and 60 Hz. This yields a color temperature of approximately 3100°K. A table of the spectral irradiance of the lamp in units of mw cm^{-2} nm^{-1} per wavelength bandwidth when the detector is 50 cm from the source is supplied with each lamp. The lamp current is maintained within 0.01 amp of the nominal value when the instrumentation is calibrated and is monitored either with a precision ammeter or a digital voltmeter used with a calibrated shunt. The distance between the lamp filament and the entrance aperture of the integrating sphere is measured to an accuracy of one mm when absolute spectral irradiance values are desired. Radiant flux from the standard lamp and the source measured is incident upon the identical portion of the integrating sphere wall for all cases in order to minimize errors which would result from non-uniform diffuseness and reflectance characteristics of the wall material.

The spectral irradiance for the unknown source $H_{\lambda_{i(S.S.)}}$ for each wavelength bandwidth centered at λ_i is calculated from Equation 34:

$$H_{\lambda_{i(S.S.)}} = \left(\frac{G_{(std)}}{G_{(S.S.)}}\right)\left(\frac{V_{(S.S.)}}{V_{(std)}}\right) H_{\lambda_{i(std)}} \qquad (34)$$

where G is the combined gain of the amplifier recorder combination referenced to unit amplification, V is the voltage output from the recorder, S.S. is the solar simulator or unknown source and std is the standard lamp.

The reproducibility of measurements obtained with this instrumentation is ±1 percent when sources of similar spectral irradiance are measured and

±5% when large gains (10^3-10^5) are introduced by the electronics for either the standard or unknown source. The uncertainties inherent in the values of $H_{\lambda_{i(std)}}$ furnished with the standard lamps range from 8% at 250 nm to 3% at 2600 nm.[69-70] This yields a maximum rms value of the error in the values of spectral irradiances of 9.4% at 250 nm and 5.8% at 2600 nm when considerable care is exercised in the performance of the measurement.

The primary standards upon which the spectral irradiance is based are two blackbodies maintained by the NBS; one operated at 1400°K and the other at 2400°K. The temperatures were obtained by the use of platinum vs. platinum 10 percent rhodium thermocouples for the 1400°K blackbody and an optical pyrometer for the 2400°K blackbody. The thermocouple and pyrometer were calibrated by the Heat Division of NBS. The values of the spectral irradiances of the blackbodies were obtained from Planck's radiation law using a value of 1.19088×10^{-12} watt cm^2 and 1.4380 cm°K for the first and second radiation constants respectively. The scale used to determine temperature is the International Practical Temperature Scale (IPTS) which is based on six fixed points from the boiling point of oxygen to the freezing point of gold.[71-73]

C. Goniometric Measurement Instrumentation

Goniometric measurements are obtained with either a pinhole camera or theodolite. The pinhole camera used consists of a cyclindrical tube 36 cm in length and 5 cm in diameter. A circular aperature, 1.0 mm in diameter is placed

at the geometrical center of the tube at one end and a ground glass screen is placed at the opposite end. Circles are inscribed on the screen corresponding to planar angles, in respect to the geometrical axis of the cylinder, of 1/2°, 1°, 1-1/2°, 2°, and 2-1/2°. For very accurate measurements of collimation and divergence a theodolite positioned on the optical axis of the solar simulator or a line parallel to the optical axis is utilized. The accuracy of the pinhole camera is ten minutes of arc; and, the accuracy of the theodolite is one second of arc.

V. OPTICAL DESIGN AND PERFORMANCE CHARACTERISTICS OF SIMULATOR BEFORE MODIFICATION

A brief description of the optical design of the simulator before modification is given below. More detailed descriptions exist in the literature.[73-78]

The sources for the simulator are mounted to the top of a vertical cyclindrical tank which is located adjacent to the horizontal vacuum enclosure. Power supplies and electronics for each source are mounted in a rack located beyond the entrance aperture to the vacuum enclosure, a control console to operate and monitor the simulator is located nearby. The housing for the optical system connects the source array with the vacuum enclosure by means of a transition tube which utilizes an optical element to accomplish the vacuum seal. The cyclinder housing the source array and the transition tube are equipped with liquid and gas cooling systems to remove thermal energy from the enclosures

which could damage either the sources or the optical, electronic, and mechanical components of the subsystems.

An optical schematic of the system before modification is shown in Figure 4. Nineteen 2500 watt high pressure xenon compact arc lamps were used as the source of radiant energy. Each xenon arc was provided with a power supply, starter, cables, and electronic control system so that independent operation of each source could be accomplished. Each source was mounted to the top of the source tank within an aconic collector and was provided with mechanical adjustment capabilities in three dimensions to enable precise positioning of the arc plasma with respect to the aconic surface of the collector. The aconic collector is a three zone ellipse with a nominal focal length of 385 cm. The clear aperture of the collector is 25.4 cm in diameter. Radiant flux from the xenon arc is collected over a solid angle which includes most of the flux emitted by the xenon plasma. The xenon plasma is reimaged at the position of the field lens. The "zoned" ellipse provides a smear focus of the arc plasma at this position. The uniformity of irradiance in the plane of the field lens is directly proportional to the uniformity which can be obtained in the test volume. The xenon plasma is smear focused to eliminate the large variations in the radiance of the source which is characteristic of high-pressure arc lamps. A more uniform irradiance over the plane of the field lens can be obtained by placing properly designed uniformity filters at this position in the optical system. The field lens becomes the source for the projection lens assembly and is

located in respect to the principal planes of the projection lens assembly such that the image of the field lens is coincident with the plane containing the surface of the collimating element. Filters which modify the spectral irradiance of the image existing in the plane of the field lens are generally placed at a position near the front projection lens element. The collimating element, which was an off-axis parabola, reflects the irradiance incident upon the front reflecting surface into the test volume of the vacuum enclosure. The field lens and first component of the projection lens assembly consisted of seven optical elements each. Each of the seven elements of the field lens was magnified to the dimensions of the collimator by the projection lens assembly. This allowed seven additional integrations of the radiant flux from the sources to be accomplished before the flux was incident within the test volume. The more integrations of the radiant flux from the sources, the more uniform the irradiance within the test volume. The total number of integrations of the radiant flux is equal to the product of the number of radiant sources and the number of elements in the field and projection lens assemblies or $n_T = n_s\, n_{opt}$, where n_T is the total number of integrations of the radiant flux, n_s is the number of sources used, and n_{opt} is the number of elements in the field lens.

The performance characteristics of the simulator before modification are shown in Table III.

The area of the plane located at the center of the test volume and perpendicular to the optical axis was 1.24×10^4 cm^2, the radiant flux incident on this plane was

variable from 3×10^3 watts to 1.6×10^2 watts with no spectral filters in the system and from 1.8×10^3 watts to 97 watts with seven spectral filters in the system. The mean irradiance obtainable within the test volume was variable from 8 mw cm^{-2} to 242 mn cm^{-2} by the use of one to nineteen sources and the adjustment of the power input to the sources. The maximum irradiance when seven spectral filters were inserted into the optical system was 148 mw cm^{-2}. The uniformity of irradiance within the test volume was five percent. Figure 5 represents the uniformity of irradiance over a typical plane in the test volume. The solar cell described above was used to obtain the data. The diameter of the plane was scanned for 22°30' increments of θ starting with $\theta = 0°$. The stability of irradiance was one percent for intervals of t greater than 1 second and less than 10^5 seconds. The maximum plane angle collimation was 4° total or, as more generally stated, 2° half angle. The dimensions of the test volume, which was a section of an ellipsoid, were: minor axis diameter equal 120 cm; major axis diameter equal 132 cm; and, depth equal 244 cm. The test volume was located concentric to the center of the vacuum enclosure and cold shroud which provided a cyclindrical volume within the enclosure with a diameter of 280 cm and a depth of 460 cm for location of fixtures, collimator, and test objects. The ultimate vacuum obtainable within the chamber is 10^{-9} torr and the shroud can be maintained at any temperature between 77°K and 525°K. The f/no of the collimator, which was a 43°10' off-axis section of a parabola was f/2 and the f/no on the object side was f/2.8.

The contamination within the vacuum chamber varies with the test objects placed within the chamber; the contamination in the chamber as determined by a change in the spectral reflectance of aluminum ($\Delta\rho$) for the system without test objects was: $\Delta\rho \leq 2\%$ for each 10 nm spectral bandwidth in the interval from 250 nm to 2500 nm.

The spectrum of the simulator was: either xenon modified by the optics of the simulator; or, xenon modified by spectral filters as shown in Figure 6. The spectrum was invariant with position within the test volume so that the spectral uniformity was zero percent. Spectral stability was $\leq 5\%$ for tests of 2×10^5 sec or less but became quite large (40-60%) for some wavelength bandwidths for tests conducted over a period of several months. This is discussed in detail below under Simulator Operational Problems.

VI. OBJECTIVES, REQUIREMENTS, AND CONSTRAINTS FOR MODIFICATION OF SYSTEM

The objectives to be obtained through modification and redesign of the optical system of the solar simulator were:

1 - Increase minor axis diameter of test volume to 180 cm;

2 - Irradiance within test volume to equal 168 mw cm^{-2} with seven spectral filters in optical system;

3 - Uniformity of irradiance within test volume to equal 5%;

4 - Collimation angle to be $<40°$;

5 - Stability of irradiance to be $\leq 1\%$ for periods of one second to 10^5 seconds;

6 - Spectrum of simulator to correspond to spectrum of AMO solar irradiance for spectral intervals of 10 nm to 1000 nm and intervals of 100 nm from 1000 nm to 2600 nm as shown in Equation 35:

$$1.40 \geq \frac{\langle H \rangle (400\ \text{nm} - 250\ \text{nm})_{\text{S.S.}}}{\langle H \rangle (400\ \text{nm} - 250\ \text{nm})_{\text{AMO}}} \geq 0.60 \ ; \qquad (35a)$$

$$1.10 \geq \frac{\langle H \rangle (700\ \text{nm} - 400\ \text{nm})_{\text{S.S.}}}{\langle H \rangle (700\ \text{nm} - 400\ \text{nm})_{\text{AMO}}} \geq 0.90 \ ; \qquad (35b)$$

$$1.20 \geq \frac{\langle H \rangle (1000\ \text{nm} - 700\ \text{nm})_{\text{S.S.}}}{\langle H \rangle (1000\ \text{nm} - 700\ \text{nm})_{\text{AMO}}} \geq 0.80 \ ; \qquad (35c)$$

$$1.30 \geq \frac{\langle H \rangle (2500\ \text{nm} - 1000\ \text{nm})_{\text{S.S.}}}{\langle H \rangle (2500\ \text{nm} - 1000\ \text{nm})_{\text{AMO}}} \geq 0.70 \ . \qquad (35d)$$

7 - Spectral uniformity to equal zero percent;

8 - Spectral stability to be $\leq 5\%$ for periods of one second to 10^6 seconds;

9 - Re-reflected energy to be $\leq 2\%$.

The requirements imposed upon the optical redesign were:

1 - Increase minor axis diameter of test volume to 162 cm;

2 - Irradiance within test volume to be $\geq 1.40 \times 10^{-1}$ w cm^{-2} with no spectral filters in the optical system;

3 - Spectrum to be spectrum of xenon modified by optical system;

4 - Uniformity of irradiance to be 10% for test volume 162 cm in diameter and 80 cm in depth;

5 - Stability of irradiance to be $\leq$1% for periods of 60 seconds to 10^5 seconds;

6 - Collimation angle to be $\leq 6°$;

7 - Spectral uniformity to be $\leq$10%;

8 - Spectral stability to be $\leq$10% for periods of 60 seconds to 2×10^5 sec.

The constraints imposed upon the modification of the system were:

1 - Vacuum enclosure not to be enlarged;

2 - Source housing not to be enlarged or repositioned with respect to vacuum enclosure;

3 - No modifications to be made to vacuum enclosure or thermal shroud;

4 - Test volume to remain concentric with axis of vacuum enclosure within fifteen cm;

5 - All components of existing system to be utilized insofar as possible except for new collimator and new sources of radiant energy;

6 - Solar simulator to remain operational throughout modification except for period of 21 days when new collimator would be installed;

7 - Modification to be completed within 120 days;

8 - Modification to be accomplished with no increase in man power and limited increase in budget;

9 - Whether modification was successful or not, a solar simulation test had to provided for spacecraft Radio Astronomy Explorer-A (RAE-A) before

scheduled launch date which was 150 days from the start of the modification. Test to be performed with existing solar simulator system if the requirements of the modification were not accomplished in time for the RAE-A test.

VII. MODIFICATION DESIGN ANALYSES, SPECIFICATIONS, AND FINAL DESIGNS

A. General

The performance specifications which were required of the modified system dictated the procurement of a new collimator and new source of radiant energy. The new source of radiant energy required modification of the power supply, starter, cables, and electronics control system associated with each source. The new source introduced additional radiant energy onto components of the system which required modifications to the liquid and gas cooling systems. The new optical design required mechanical modifications to the transition tube between the source housing and the vacuum chamber. The specification and procurement of a new collimator were identified as the most critical items in the modification. Qualification of a new source of radiant energy and the specification of the optical design to be used in the modified system were identified as the next most critical items. The modifications to the electronic, thermal, and mechanical sub-systems and components could not be specified until the new source was qualified; and, the optical design was established within reasonable limits.

B. Collimator

The schedule for completion of the modification negated the procurement of an off-axis parabola for the collimating element. The surface of the collimator which could be manufactured within the schedule had to be spherical. The dimensions of the collimator were established by the geometry of the existing enclosures of the solar simulator system, the mechanical stability of the material of the collimator, and the design requirement for the minimum diameter of the test volume. The material from which the collimator was to be formed was to be government furnished equipment (GFE) to the vendor who contracted to manufacture the collimator. A disk of radius r and thickness z would be GFE to the vendor. The radius of the disk was determined from Equation 36:

$$r_{vac} \geq r_0 \geq r_{coll} \geq \frac{r_{i(min)}}{\cos \psi} \tag{36}$$

where r_{vac} is the radius inside the shroud of the vacuum chamber, r_0 is the radius of the useful portion of r_{vac}, r_{coll} is the radius of the collimator, r_i is the minimum radius required in the modified simulator and ψ is the angle a normal to the center of the collimator forms with the optical axis of the solar simulator test volume. Values for r_{vac}, r_0, and r_i were 145 cm, 120 cm, and 81 cm respectively. ψ was limited to $21° \pm 1°$ by the mechanical restraints of the modification, i.e., no modifications to be made to vacuum enclosure and position of source housing with respect to vacuum chamber to be invariant.

These values were substituted in Equation 32 for the worst case condition of ψ which was 22° as:

$$145 \text{ cm} \geq 120 \text{ cm} \geq r_{coll} \geq \frac{83.5}{.92718} = 87.4 \text{ cm} .$$

The radius of the collimator which was procured was 116 cm. The thickness of the disk was determined by the material of the collimator blank and the diameter of the blank. Past experience with the existing collimator, which was constructed of 6061 aluminum, indicated that aluminum should be used for the new collimator. The collimator would be attached to a mounting frame inside the vacuum chamber at three points. The approximation was made that the center of mass of the disk before forming would equal the center of mass after forming. The displacement of any point on the surface of the collimator from the equilibrium position could not exceed one minute of arc or 2.88×10^{-4} radians. The ratio of stress to strain was calculated for elements of the surface which were maxima and compared to the values of elastic moduli for 6061 aluminum. The calculations indicated that ten cm of 6061 aluminum would be sufficient so that the displacement of any point of the surface would be $\leq 2.88 \times 10^{-4}$ cm per cm.

The thickness of the blank which would yield a collimator with ten cm thickness at the center would depend upon the method of fabrication. Three methods were possible, machine to proper contour, form proper contour by bumping technique, or form by explosive technique. The first method would require a

blank of thickness >> 10 cm and would increase weight by an undesirable amount. The latter two techniques had not been used in fabrication of components as large as 232 cm in diameter but had been used for much smaller components. Either of these latter techniques would remove a minimum of material so that a 10 cm thick blank could be used. The bumping technique involved pounding the surface into the proper shape and the explosive technique involved igniting a charge of high explosive at the proper distance from the blank inside a suitable enclosure. Each of these techniques involved the risk of blank destruction but each had the advantage of minimizing weight, cost, and fabrication time. The blank procured was 234 cm in diameter, 10.2 cm thick and weighted 1180 kilograms. The material was 6061 aluminum. The initial forming was accomplished by use of the explosive technique which yielded the required radius of curvature without additional machining. The surface of the blank was Kanigen plated after forming to a thickness of 0.155 ± 0.025 mm in order to obtain a more suitable surface for optical polishing.[1] The collimator was coated with evaporated aluminum after it was placed within the vacuum chamber of the simulator. No protective overcoat was applied because the collimator can be realuminized whenever the reflectance drops below an acceptable level more economically than it could be cleaned if the surface were protected by an overcoat. Not using an overcoat offers the additional advantage of increased reflectance at all wavelengths with a consequent increase in efficiency of the system. The spectral radiant reflectance of the surface, of the mirror is about 2% less than that obtained

[1]Collimator was fabricated by Tinsley Laboratories, Inc., Berkeley, California on Contract NAS-5-14337

for aluminum deposited upon glass or quartz which would be equivalent to an integrated absorptance of about 10%. Figure 7 is a photograph of the collimator mounted inside the vacuum enclosure.

C. Optical System

Solar simulator optical design differs from most other design of optical instruments in that a faithful representation of the source in the image plane is not desired but rather a transformation of the source into an image of uniform irradiance is desired. Solar simulator design is similar to searchlight design in this respect.[79-83] Uniform irradiance within the test volume is obtained by reimaging the source within the optical system in such a manner that an area of uniform irradiance is obtained. This image then becomes the object for the projection lens assembly which is located in respect to the collimator so that uniform irradiance is obtained in the test volume. Irradiance which is invariant with position along the z axis can be obtained only when the secondary source is imaged at infinity by the collimator projection lens combination and the variation of z is less than or equal to a functional relationship of the radius of the collimator, the angle a normal to the collimator forms with the optical axis of the test volume and the collimation angle of the simulator or, to a first approximation, $z_{i(uniform)}$ is:

$$z_{i(uniform)} \leq r_{(coll)} \cos \psi \operatorname{ctn} \frac{\omega_i}{2} \tag{37}$$

where $z_{i(uniform)}$ is the range of z over which irradiance is uniform with the origin of z at the collimator, ψ is the angle formed by a tangent to the surface of the collimator and a perpendicular to the optical axis of the test volume and is equal to one half of the off-axis angle at which the collimator is placed. Substituting the values of $r_{coll} = 81$ cm, $\cos \psi = 22°$, $\operatorname{ctn} \omega_i/2 = 3°$; Z_i (uniform) (minimum) is:

$$Z_{i(uniform)_{min.}} = (81 \text{ cm})(.927)(19.1) = 1432 \text{ cm} .$$

The radius of the test volume with uniformity = 0% at any point z_i will be:

$$r_{T.V.} = r_{coll.} \cos \psi - z_i \tan \frac{\omega_i}{2} \tag{38}$$

The geometrical requirements for the modification were:

$$r_{T.V.} \geq 81 \text{ cm for } z_i \text{ between 157 cm and 237 cm} \tag{39a}$$

$$\omega_i \leq 6° \tag{39b}$$

$$r_{T.V.} \cong r_{f\ell_j} M' \tag{39c}$$

$$20° \leq \psi \leq 22° \tag{39d}$$

where $r_{f\ell_j}$ is the radius of each element of the field lens and M' is the magnification of the system between the field lens and the test volume.

The geometrical constraints on the modification were:

$$\Delta z \leq 304 \text{ cm (distance from collimator to field lens)} \tag{40a}$$

$r_{f\ell} \geq 20$ cm fixed by collector design (40b)

$(\Delta r(oz) \leq 15$ cm) (40c)

$\delta_i + \delta_0 \cong \delta_i + \delta_0$ (before modification) ≤ 1094 cm (40d)

field lens to be aperture stop of system (40e)

collimator to be field stop of system (40f)

Equations 33-36 were the basis for the optical redesign of the system. Substitution of the requirements of Equation 35 into Equation 34 showed that the desired radius of the test volume could be achieved by imaging the field lens on the collimator. However, a ray trace of the system indicated that the shroud inside the vacuum chamber would become the field stop for the system unless the position of the field projection lens array was changed. The field and projection lens assembly had to be repositioned 60 cm toward the collimator in order for the shroud not to become the field stop of the system which was within the constraint imposed by 36a.

The relocation of the field-projection lens array allowed the calculation of the focal lengths and apertures of the field projection lens array to be accomplished by use of Equations 41:

$$M_{ang} = \frac{\tan \omega_i}{\tan \omega_0} \tag{41a}$$

$$M = -\frac{\delta_i'}{\delta_0'} \tag{41b}$$

where ω_i and ω_0 are the plane angles corresponding to Equations 10 and 11 and δ_0'' and δ_i' are the object and image distances of each optical component of the system. The requirement of uniformity $\leq 10\%$ for a test volume of radius 81 cm

and depth 80 cm imposed upon the modification also had to be considered in the calculation of the optical characteristics of the field, projection, and collimator elements. This was equivalent to a ±10% variation in angular magnification $(\Delta M)_{ang}$ for all points within the total volume or:

$$\frac{\tan \omega_i}{M_{ang} - \Delta M_{ang}} \leq \tan \omega_0' \leq \frac{\tan \omega_i}{M_{ang} + \Delta M_{ang}} \qquad (42)$$

Calculations of the uniformity obtainable with various optical configurations were performed by computer using Gaussian optics.* The field lens which was the secondary source for the system was assumed to radiate as a series of point sources onto equal areas of the collimator. Each of these areas of the collimator was traced into the test volume. A comparison of the ratios of the areas in the various planes of the test volume indicated the uniformity which would be obtained with the optical parameters introduced into the calculations. Similar traces of the skew rays were also made. The field-projection lens array which resulted from these calculations is shown in Figure 8. The optimum optical design which resulted from these calculations is shown in Figure 9. The field lens array is imaged at the plane BE which is determined by the intersection of the marginal rays from the outer elements of the projection lens assembly. This results in irradiance on plane BE which is conjugate to the irradiance on each element of the field lens. The uniformity of irradiance on this plane approaches zero and is limited by imperfections in the optical system and the

*Performed by Spectrolab, Division of Textron, Inc., Sylmar, California on contract NAS-5-9244.

uniformity of irradiance obtainable on each field lens element. The nominal beam diameter is defined by the marginal rays emanating from the central element of the field lens. Uniformity along the z axis is a strong function of position as can be seen from the figure since the marginal rays from the outer elements of the field lens diverge rapidly beyond plane BE with a consequent reduction in the diameter of the usable test volume. Each element of the field lens provides irradiance over a cone angle equal to the off-axis angle of the collimator, consequently each element of the field lens irradiates a portion of the collimator with only the central cone angle, equal to the off-axis angle, being irradiated by all of the elements. The optical path lengths for radiant energy emanating from each of the field lens elements to any plane perpendicular to the optical axis of the test volume vary by approximately 8% which increases the value of the uniformity of irradiance.

D. Radiant Energy Source

A xenon compact arc high pressure lamp rated at 2500 watts was used in the simulator prior to the modification. A xenon arc was selected because of the spectral radiance and operational characteristics of the lamp. These sources have been reported in the literature.[84-92]

The radius of the minor axis of the test volume was required to be increased to 81 cm from a previous value of 60 cm. The assumption was made that the efficiency of the system after modification (ϵ_a) would be related to the efficiency

of the system before modification ϵ_b within the limits shown in Equation 43:

$$\epsilon_b \geq \epsilon_a \geq \epsilon_b \ (0.70) \tag{43}$$

A mean irradiance of .140 w cm^{-2} was desired in the test volume with a maximum of seventeen lamps providing radiant energy. Two lamps were to be available in case of a malfunction during a thermal balance test. Equation 17 shows the relationship between electrical power input to the system as a function of the efficiency of the system, mean irradiance and area of the test volume. The increase in area (ΔA) of the test volume was obtained from Equation 44:

$$\Delta A = \left(\frac{r_a^2 - r_a^2}{r_b^2} \right) A_b \tag{44}$$

Substituting the minimum value for efficiency shown in Equation 43 along with the increase in area of the test volume determined by Equation 44 and the requirements listed above into Equation 19 yields:

$$\sum_{i=1}^{17} V_i \ I_i = \frac{140 \text{ mw cm}^{-2} \ (A_b + \Delta A) \cos \alpha_i}{0.70 \ \epsilon_b} = \frac{(.140 \text{ mw cm}^{-2})(1.82 \ A_b) \cos \alpha_i}{0.70 \ \epsilon_b}$$

$$= \frac{.364 \ A_b \cos \alpha_i}{\epsilon_b} \tag{45}$$

The values for A_b and ϵ_b were 1.24×10^4 cm^2 and 6.5×10^{-2} respectively. Setting $\cos \alpha_i = 1$ we obtain:

$$\sum_{i=1}^{17} V_i I_i = \frac{(.364)(1.24 \times 10^4)}{6.5 \times 10^{-2}} = 6.94 \times 10^4 \text{ watts} \quad (46)$$

The wattage (W) required of each lamp is then this value divided by seventeen or:

$$W = \frac{6.94 \times 10^4 \text{ watts}}{17} = 4082 \text{ watts} \quad (47)$$

The worst case condition would require a source rated at 4082 watts to obtain 1.40×10^{-1} watts cm^{-2} within the test volume with no spectral filters in the system. The comparable value for the lamp with seven spectral filters in the system is 6632 watts.

The only xenon compact arc which was available commerically which could be used without extensive modifications to the lamp cage and collector was rated at 4200 watts, since this lamp would provide sufficient radiant energy to meet the requirements of the modification, it was selected for use in the modified system. The lamp is 41 cm in length with a bulb diameter equal 61 cm, operates at 30 volts and 140 amperes at rated wattage, requires 50 K volts ignition voltage, and will withstand 200°C temperature on the quartz to metal seals at the electrodes. The effective area of the arc is an ellipsoid with

major and minor diameters of 6.0 mm and 1.5 mm. The lamp can be operated from 1800 watts to 4600 watts and has a rated life of 1000 hours.

The spectral irradiance of one of these lamps was obtained at the following intervals: 0, 24, 48, 136, 216, 428, 520, and 652 hours total elapsed operation time. The lamp was operated at a constant power of 3660 watts with the current maintained at 133 ± 2 amperes. The radiant energy from the lamp was collected over a solid angle of $5.41 \times 10^{-5}\,\pi$ ster and compared to a standard of spectral irradiance obtained from the National Bureau of Standards. The Leiss instrumentation described previously was used to obtain the data. Figure 10 shows the spectral irradiance of the lamp at $t \leq 4 \times 10^3$ sec; $t \leq 10^5$ sec; $t \leq 10^6$ sec; and $t \leq 2 \times 10^6$ sec. The lamp exhibits a rapid spectral diminution for wavelengths ≤600 nm during the first 24 hours, or 4×10^3 sec, maintains a nearly constant spectrum for the next 100 hours, ($t \leq 10^6$ sec) decreasing to the spectrum shown for 312 hours ($t \leq 10^6$ sec) which remains constant to 520 hours, ($t \leq 2 \times 10^6$ sec) then another rapid diminution of the spectrum begins. This study indicated that the useful life of the lamp is about 500 hours and that the lamp should be operated for 24 hours before spectral measurements of the irradiance in the test volume of the simulator are obtained to allow for the initial diminution of the spectrum below 600 nm.

The geometry of the lamp, viz., the limitations imposed by the anode and cathode, is such that radiant energy is radiated into a solid angle of approximately $2.7\,\pi$ steradians. The surface area of the arc which provides this radiant

energy is approximately 2.83×10^{-1} cm^2. The radiant flux from the lamp averages 1890 watts, the radiant intensity averages 23 watts $ster^{-1}$ and the radiance averages 788 watts cm^{-2} $ster^{-1}$. The conversion efficiency of electrical energy to radiant energy for the lamp is the quotient of the radiant flux by the electrical power or approximately 0.45.

E. Electronic

The source of radiant energy to be used with the modified system required a current input to the source and operating voltage for the source to be within the limits of Equation 48:

$$28 \text{ volts} \leq V_i \leq 32 \text{ volts} \tag{48a}$$

$$60 \text{ amps} \leq I_i \leq 160 \text{ amps} \tag{48b}$$

The power supplies, starters, and cables before modification, were limited to a maximum current of 110 amperes and provided voltages in excess of those specified by equation 48a. The power supplies were mounted in a rack located near the source housing with individual shelves provided for each supply. The starters were located on the top of the source housing and were connected to the power supplies with a cable approximately 6 meters in length. The modification to the power supplies was accomplished by the installation of new power transformers, filter chokes, silicon controlled rectifiers, and rectifier diodes. The only complication in the modification was the requirement to package the new components into the same space occupied by the old

components. The complication was thermal, not electrical in that the new components generated more thermal energy which had to be dissipated. Two small fans were installed to furnish air to the heat sink of each supply and performed adequately. New cables with a current capacity of 160 amperes were installed in the system. The same starter was used for the lamps as previously with a parallel circuit consisting of a shorting bar and solenoid installed which provides a conduction path for more than 80% of the current to the lamp after lamp ignition is accomplished. The ignition of the lamp activates the solenoid which completes the parallel circuit by pulling the shorting bar into position. The electronic control system consists of an error amplifier, radiant flux sensor and control circuitry to control the current output either as a function of some predetermined current or as a function of some predetermined radiant flux incident upon the sensor. These two modes of operation are referred to as current mode and light mode respectively. In the current mode of operation, lamp current is maintained at a predetermined level by a frequent comparison of the potential difference across a shunt internal to the power supply and a stable reference potential difference. Constant current is maintained by the control circuitry which varies the firing angles of three silicon control rectifiers in a three phase bridge network. In the light mode, the irradiance incident upon the sensor generates a voltage which is compared to the reference voltage by means of a feed back loop with the error amplifier and the current is adjusted by the control circuitry as before to maintain a constant voltage output from the sensor. The sensor is

provided with circuitry so that the position of the sensor in respect to the source of radiant energy is not critical and the voltage generated by the sensor can be adjusted to any value which is convenient for comparison to the reference voltage.

F. Thermal

The source housing and transition tube is cooled by a recirculating gas system and a heat exchanger. Figure 11 is a photograph of the source housing and Figure 12 is a photograph of the transition tube with cover installed. The heat exchanger coils, the holder for the field lenses, and the turning flat inside the source housing are provided with a liquid recirculating cooling system connected to a cooling tower located outside the building. The tower operated near rated capacity before modification of the system when the outside air temperature exceeded 30°C. It was immediately obvious that the thermal capacity of the cooling system would have to be increased. The additional thermal energy which had to be dissipated was approximately that given by Equation 49

$$\Delta U_{Thermal} \cong U_{Thermal(b)} \left(\frac{W_a}{W_b} - 1 \right) \cong 0.68\ U_{Thermal(b)} \qquad (49)$$

where W_b and W_a is the power input to the sources before and after modification. The components of the system dependent upon the cooling tower liquid to maintain operational temperatures at less than the maximum permissible temperatures were: field lens assembly, seal lens flange, source holder, blower

motors, turning flat, and heat exchange coils. The flow rate of gas through the source housing could not be increased without major modification to the source housing, heat exchanger, and connecting ducts. The components of the system dependent upon the recirculating gas system were: 1 - source of radiant energy; 2 - aconic collectors; 3 - light sensor in control circuit of power supply; 4 - transfer optics assembly; and 5 - transition tube connecting the source housing to the vacuum chamber. The transfer optics and transition tube obtained additional cooling above that provided by the gas recirculating system flow by means of two blowers which directed gas within the source housing onto the components.

The flow rate obtainable with the gas recirculating system was not sufficient to provide adequate cooling of the aconic collectors with a 4200 watt source. Additional cooling was provided to each collector by bonding 6.4 mm diameter copper coils to the rear surface of the collector. Bonding was accomplished with a high temperature epoxy cement. A solenoid value was placed in series with each inlet supply line to the collectors to control the flow of coolant.

The heat exchanger was provided with additional coils which doubled the effective area for thermal energy transfer to the coolant.

The materials of the liquid coolant system were fabricated of materials which were compatible with water, ethylene gylcol, or liquid nitrogen.

The liquid circulating subsystems are connected in parallel with coolant either from the cooling tower or water lines in the building so that the capacity of the cooling tower is not exceeded. Coolant is supplied to the subsystems at

pressures in excess of 5×10^3 gm cm^{-2} through the use of pumps installed in the supply lines.

The transfer of thermal energy from the electrodes of the radiant source to the gas recirculating through the housing is a function of the electrode surface area and velocity of gas flow. The velocity of the gas provided by the blower of the heat exchanger was too low to provide sufficient thermal energy transfer between the electrodes and the gas to maintain the temperature of the electrode $\leq 200°C$. Additional surface area was provided for the cathode of each source instead of increased velocity of air flow. A small fan located near the cathode would be required to provide the additional gas velocity required. This would introduce an additional obstruction into the system which would decrease efficiency and engender additional thermal problems. The additional surface area was obtained by mounting ten brass fins, each 6 cm wide by 8 cm long by 0.25 mm thick, in good thermal contact with the cathode of the lamp. Each fin is mounted perpendicular to the direction of emission of radiant energy from the collectors. The obstruction factor for the fins of each lamp is less than 5×10^{-3}. The addition of the fins to each lamp resulted in a reduction of 50°C or more in the equilibrium temperature obtained by the cathode of the lamp. Figure 13 is a photograph of a lamp assembly with the cooling fins installed. Figure 14 is a photograph of the source array showing the water cooling coils added to the collector, source base plate, lamp cage, starter posts, and adjustment controls.

The transfer of thermal energy from the turning flat to the coolant is accomplished by circulating the coolant through copper coils attached to the rear of the mirror. The mirror is constructed of aluminum which is nickel plated by the Kanigen process to a thickness of $1.55 \pm 0.25 \times 10^{-1}$ mm. The reflective surface is evaporated aluminum of thickness equal 70 nm with a protective overcoat of SiO_x of thickness equal to one half wave at 560 nm. The coating of the mirror reflects on the average about 85% of the incident energy and absorbs 15%. The equilibrium temperature obtained by this mirror before modification was $20° \pm 3°C$. The equation of heat flow for thermal equilibrium conditions[93-94] indicated that the change in temperature between the front face of the turning flat and the coolant was directly proportional to the energy per unit time incident upon the surface of the mirror and inversely proportional to the constants of the material. Therefore, it was assumed that empirical data could be used to predict the equilibrium temperatures which would be attained by the components after the modification since the only change would be an increase in the thermal energy incident per unit time upon the component.

Empirical data which had been obtained for several values of electrical power input indicated that the maximum temperature rise of the mirror would not exceed 5°C with the projected 68% percent increase in electrical power input. Similar data for the field lens array and vacuum seal flange indicated no modification to the thermal control systems for these components was necessary.

The temperatures achieved by these components after the modification verified the previous empirical data as no deviations greater than ±2°C from those predicted were obtained. Temperature vs electrical power to the system for each of these components plus a typical collector are shown in Table IV. An inspection of this table indicates that all of the components are attaining equilibrium temperatures which are less than the established minimum allowable temperatures. The temperature attained by the atmosphere of the source housing can be further reduced by the circulation of liquid nitrogen through heat exchanger coils of the source housing thermal control system. This has not been done to date because the cooling fins installed on the negative seals of the radiant energy sources have maintained the seal temperatures at an acceptable level. The temperature of the projection lens array could be reduced by the addition of water cooling coils to the lens holder. No problems have resulted from the temperatures attained by the projection lens to date. The thermal systems provide adequate capacity to dissipate the thermal energy which would result if the sources were operated at 5000 watts.

G. Mechanical

A new transition tube was necessary because of the revised optical design which resulted in a movement of the field and projection lens assembly 60 cm along the optical axis toward the collimator. The rear element of the projection lens was the vacuum seal element of the system before modification and was placed at the position of the penetration into the vacuum chamber. Figure 15 is a photograph of this tube installed in the system as seen from the test volume. The images of the source array in each of the projection lens elements can be seen in this view. The optical redesign required two vacuum seals to be accomplished with the disadvantage that the field and projection lens assemblies would not be accessible for adjustment without the aid of some mechanical linkage mechanism. The mechanism was designed into the system which allowed accurate positioning of each of the elements of the array. The transition tube was constructed of 9.35 mm thick stainless steel which was rolled into a cyclinder 60 cm in length and 42.5 cm in diameter. Flanges were installed at either end of the cyclinder to accomplish the vacuum seals. An indium seal was used at the position of penetration into the vacuum system and the quartz lens with a silastic gasket* was installed on the other end. The temperature limits for the indium and silastic seals are 156°C and 200°C respectively.

*Gasket molded from 916 silastic manufactured by Dow Corning

VIII. PERFORMANCE CHARACTERISTICS OF MODIFIED SIMULATOR

The performance characteristics of the modified simulator are listed in Table V. The area of the plane located at the center of the test volume and perpendicular to the optical axis is 2.42×10^4 cm^2, the radiant flux incident on this plane is variable from 4×10^3 watts to 2×10^2 watts with no spectral filters in the system and from 2.7×10^3 watts to 1.4×10^2 watts with seven spectral filters in the system. The mean irradiance within the test volume with no spectral filters is variable from 8.6 mw cm^{-2} to 164 mw cm^{-2}. This variation is obtained by the use of one to nineteen of the sources and the adjustment of the current input to each of the sources. The mean irradiance with seven spectral filters in the optical system is variable from 5.9 mw cm^{-2} to 113 mw cm^{-2}.

The uniformity of irradiance within the test volume is 10%. The uniformity of irradiance for the plane perpendicular to the optical axis located at z = 250 cm is 1.9% and is shown in Figure 16. The view is from the rear of the test volume looking toward the collimator, the minor axis of the test volume is the plane defined by θ = 48°38' and 228°38', the major axis is the plane defined by θ = 138°38' and 318°38'. The off-axis angle of the collimator is indicated by ψ in the figure and is equal to the angle formed by the vertical with respect to the vacuum enclosure and the major axis of the test volume. Contours are shown for areas in wich the variation of ΔH from $\langle H \rangle$ is 10^{-3} watts cm^{-2}. The stability is 1% for periods of one second to 24 hours. The collimation is 3° for any point within the test volume; the divergence is $\leq 5°$. The test volume is a

section of an elliptic paraboloid with minor axis 86.5 cm, major axis 89 cm and depth 244 cm. The optical axis of the test volume is parallel to the geometric axis of the vacuum chamber and is the line defined by r = 1.8 cm, θ = 270° when r = 0 is the geometrical axis of the vacuum chamber and θ = 0° as shown in Figure 7. The ultimate vacuum obtainable in the chamber remained constant at 10^{-9} torr. The temperature range of the shroud also remained constant, 77°K to 523°K. The modifications performed had no effect on the contamination present in the system which remained constant, i.e., no changes in spectral reflectance $\geq$0.02 for 10 nm bandwidths to 1000 nm and 100 nm bandwidths to 2500 nm of an aluminum sample located within the vacuum enclosure.

The spectra of the simulator with no spectral filters and with seven spectral filters in the optical system are shown in Figure 17 along with the AMO solar irradiance. The correlation of H_λ (s.s.) to H_λ (AMO) is much better than that obtained with the unmodified simulator for both spectra. The spectral uniformity (T) of the simulator is 0%; the spectral stability (X) is less than 5% for periods less than 2×10^5 sec. Spectral stability is an extremely critical parameter for most solar simulation tests and is discussed in detail below under Operational Problems.

The re-reflected energy is less than or equal to 2% over 75% the test volume. The portion of the test volume included within the planes defined by the re-reflection line of Figure 5 and the test volume diameter at θ = 90° can introduce re-reflections from this portion of the test volume to the collimator and back

into this portion of the test volume. The maximum energy that can be re-reflected within this portion of the test volume is determined by the geometry and spectral reflectance of the test object. The general formula for the computation of this energy has been given as Equation 29. The maximum value of the reflected energy observed to date with a test object located within the portion of the test volume which can introduce re-reflections from the collimator is 3%.

IX. CRITIQUE OF PERFORMANCE CHARACTERISTICS OF MODIFIED SIMULATOR

The performance characteristics of the modified simulator equal or exceed the requirements imposed upon the modification. However, the constraints imposed upon the modification compromised the performance characteristics which are possible to achieve with this type of simulator. In particular, performance was compromised by these constraints:

1. Vacuum enclosure not to be enlarged;
2. Source housing not to be repositioned with respect to vacuum enclosure;
3. No modifications to vacuum enclosure or thermal shroud;
4. Same aconic collectors to be used; and,
5. Modification to be completed within 120 days.

The constraints imposed by one through four of the above determined the geometry of the system. Item 4 was not compatible with items 1 to 3 with the result being a loss in efficiency of the system. The efficiency of the system was

reduced approximately 25% (from .065 to .048) by these constraints in that the collectors were used to form an image of each radiant energy source at a distance greater than the initial position of the image by 60 cm. The collector design gives maximum efficiency of radiant flux transfer from object to test volume at the original position which corresponded to an optical pathlength of 385 cm from arc plasma to field lens. The collectors could have been used to form an image at this optimum position if modifications to the thermal shroud and vacuum enclosure could have been accomplished.

An additional serious effect of this refocusing of the image of the arc by the collector was the non-uniformity of irradiance over the field lens elements obtained at this new position. A uniformity filter had to be placed in the optical system in order to meet the performance requirements of the modification. Uniformity of 6% was obtained in one plane and of 15% in the required test volume before the filter was installed. One filter is used at the position of the center element in the field lens array. The effective system transmission of this filter is 0.92 which also reduces the efficiency of the system. The filter is a series of concentric circles with density increasing toward the center. The filter is formed from vapor deposited platinum with a protective coating of one half wave of SiO_x at 560 nm. The substrate is ultra-violet grade quartz. The spectral transmission of a filter of this type with $\tau = 0.69$ at 560 mm for 0, 24, 1000 hours is shown in Figure 18. The shape of the spectral transmission curve is invariant for the range $.05 \leq \tau \leq .90$. The filter is shown in Figure 19

and consists of 9 zones with the outer zone having no material deposited upon the quartz. The transmission at 560 nm of each zone progressing toward the center is: .92, .84, .75, .66, .58, .50, .42, .27, and .17. The collimator f/no is 1.4 compared to f/2 previously which accentuates the effects of optical component imperfections upon uniformity, both spectral and total. However, the quality of the optical components in the modified system is such that minimum deterioration of performance has resulted from this low f/no. The exceptional quality of the collimator surface is the prime factor contributing to the uniformity, both spectral and total, obtainable with the modified system.

Uniformity in depth can be achieved with a high f/no system utilizing a spherical collimator or with a parabola in a low f/no system. Constraint no. five negated the procurement of a parabola which resulted in the rapid change of irradiance with position along the optical axis of the test volume. The cost of the total simulator system is a function of the f/no of the system. The higher the f/no. the larger the vacuum enclosure becomes and the greater the distance between source and test volume. This results in additional expenses for building and chamber modifications as well as the utilization of additional laboratory space for the housing of the simulator. Uniformity in depth comparable to the planar uniformity obtainable with the modified simulator utilizing the present spherical collimator would involve expenses equal to the cost of the system before modification.

However the present spherical collimator could be refigured into a parabola at a fraction of the above costs. Based on past experience, uniformity throughout the test volume would be 2% or less if a parabola of excellent optical quality were substituted for the spherical collimator.

Item one of the constraints resulted in a compromise in the re-reflected energy characteristic of the simulator. The test volume should be located beyond the plane of the re-reflection line shown in Figure 9. This plane intersects the nominal beam diameter at: $\theta = 90°$, z = 355 cm, which is 45 cm from the rear door of the vacuum chamber. A minimum addition of 200 cm of vacuum enclosure is essential to obtain a test volume 244 cm in depth. Several thermal vacuum tests have been conducted in the modified system with the test objects partially situated inside the plane of no re-reflection from the collimator. The maximum value of Γ which has been observed is 3%. All of the surfaces tested to date have had surface reflectances of less than 0.30 for more than 90% of the area of the test object.

The average irradiance within the test volume could be increased either by providing more radiant energy input to the optical system or by increasing the efficiency of the system. Sources of increased radiant energy could be used to replace one or all of the present sources. An arc research program presently in progress at GSFC indicates that a modified vortex stabilized radiation source of 20 kw utilizing a mixture of eight parts neon to one part of xenon would increase the average irradiance in the test volume by providing

increased radiant energy and improving efficiency through the elimination of the use of seven spectral filters. The replacement of the present radiant energy sources in the center and first ring of the source array with 20 kw sources would provide an additional power input of 60.2 kw. Assuming the efficiency of the system which would provide adequate spectral correlation with AMO solar irradiance remained at 0.048, the irradiance possible in the test volume with eight sources would be:

$$H = \frac{\epsilon W}{A_i} = \frac{(4.8 \times 10^{-2})(1.4 \times 10^{5} \text{ watts})}{(2.42 \times 10^{4} \text{ cm})} = 0.278 \text{ watts cm}^{-2} \qquad (50)$$

or approximately two solar constants. The collimation angle could also be reduced with some optical redesign if a lower efficiency for the system would be acceptable.

X. SIMULATOR OPERATIONAL PROBLEMS AND CORRECTIVE PROCEDURES

A. Spectral Stability, Spectral Uniformity and Material Absorptance

Spectral stability and uniformity which approach zero are critical requirements for thermal balance tests of materials with reflectance characteristics which are strong functions of wavelength;[95] for thermal control materials degradation tests; and for tests of energy conversion devices.

The total energy absorbed by each material is a function of the absorption characteristic of the material and the spectral energy incident upon the material.

The equilibrium temperatures of test items which are neither gray nor black in thermal balance tests have no meaning unless the spectral energy incident upon the material is known. The spectral energy in each bandwidth of interest has to be known to apply the results of materials degradation tests and energy conversion tests.

The integrated spectral absorptance (α_x) of each material as a function of the spectral energy incident in the test volume of the simulator is obtained for all materials used in each of the above tests. The absorptance of each material is calculated from Equation 51:

$$\alpha_x = \frac{\sum_{i=1}^{n} \alpha(\lambda)_i \; H(\lambda)_i}{\sum_{i=1}^{n} H(\lambda)_i} = \frac{\int_0^{\infty} \alpha(\lambda)\, H(\lambda)\, d\lambda}{\int_0^{\infty} H(\lambda) d\lambda} \qquad (51)$$

where $\alpha(\lambda)_i$ is the mean absorptance of the material for wavelength interval $\Delta\lambda$ centered at λ_i and $H(\lambda)_i$ is the corresponding irradiance. The summation is taken over one percent of total radiant energy bandwidths. The total radiant energy absorbed (U_x) by the material during the test is the product of the total incident radiant energy (U_T) and the absorptance of the material integrated over time and wavelength or:

$$U_{(x)} = \int_{\lambda_0}^{\lambda_f} \int_0^t U_{(T)}\, \alpha_x \, dt \, d\lambda \qquad (52)$$

where $U_{(T)}$ and α_x are in general functions of time and wavelength. The spectral energy absorbed for each wavelength bandwidth of interest for the period of the test is obtained from periodic measurements of the spectral irradiance and the assumption that the spectral energy U_{λ_i} varies linearly between measurements to a first approximation. This assumption is based upon extensive spectral measurements of several solar simulation systems which indicate that the spectral energy characteristics of any system can be reproduced for any time $t \leq 4 \times 10^6$ sec. Some of the data upon which this assumption is based are shown in Figure 20 which represents the spectral irradiance of a solar simulator system at $t \leq 4 \times 10^3$ seconds and $t \leq 10^6$ seconds for two series of measurements on the same system when the above procedures were followed. The spectral degradation of the unmodified solar simulator discussed in this paper is shown in Figure 21, curve A was obtained at $t = \leq 4 \times 10^3$ sec, curve B was obtained at $t \leq 1.3 \times 10^6$ sec. The total elapsed time between curves A and B was 60 days. Curve C was obtained 180 days after curve A when all the reflective optics were realuminized and all the radiant energy sources with operational times in excess of 2×10^5 sec were replaced.

A smaller simulator* which utilized identical components as the unmodified simulator with the difference in optical design which effects spectral stability being the addition of two reflective flats in the optical system has been studied extensively. An optical schematic of this system is shown in Figure 22. The change in spectrum with time is shown in Figure 23 which represents the

*X-25 solar simulator manufactured by Spectrolab Division of Textron Inc., Sylmar, Calif.

spectrum at $t \leq 4 \times 10^3$ sec, $t \leq 1.6 \times 10^5$ sec, $t \leq 1.1 \times 10^6$ sec and $t \leq 1.2 \times 10^6$ sec with the simulator in continuous use for the period of the measurements.

Curve D corresponding to $t \leq 1.2 \times 10^6$ sec was obtained when the simulator was extinguished so that the transmission optics could be cleaned and the reflective optics realuminized. The same source was utilized for curve D as for curves A-C.

It is apparent from the above figures that the spectral energy obtained from a simulator is a function of the interval between periods of use as well as the total operation time. This may not be true in all laboratories, especially those which maintain extremely clean environments. Serious errors in test data may result if the assumption is made that the spectrum of a system is invariant with time even if the simulator has not been in use. This is shown in Table VI which is a tabulation of several materials relevant to spacecraft thermal design with the absorptance of each material shown for various spectra.

The column headed α_s contains the integrated absorptance values for the material of the corresponding row calculated for all wavelengths between 0 and ∞ according to values of AMO solar irradiance given by Reference 22. The column headed α_x contains the integrated absorptance value of the material of the corresponding row for the wavelength bandwidth as shown in column 5 and the source indicated at the head of each set of columns. Values of the integrated solar al orptance for this same wavelength bandwidth are shown in the column various spectra.

headed $\alpha(\lambda)$s. The values of $\alpha(\lambda)$ utilized in the calculations were obtained from measurements of the subject materials which were made for various spacecraft except for gold, silver, and aluminum which were obtained from published data.[96]

B. Spectral Filters

The spectral filters which are used to obtain irradiance similar to AMO solar irradiance have been in use for several years. The spectral transmission of a typical filter at t = 0 sec and t = 4×10^6 sec operation time is shown in Figure 24. No serious degradation of reflectance characteristics have been observed in any of the filters used in a simulation system. One filter was exposed to a thermal environment of 540°C and one was exposed to 2 watts cm^{-2} total irradiance and 4×10^{-1} watts cm^{-2} in the bandwidth 200 nm to 400 nm to ascertain the stability of the filter as a function of temperature and ultra-violet irradiance. Measurements of the spectral transmission of the filter were obtained at periodic intervals viz., time t = 0, 8.6×10^4 sec, and 2.6×10^5 sec. The results for the filter exposed to 540°C are shown in Figure 25 for times equal to 0 sec, 8.6×10^4 sec, and 2.6×10^5 sec. The transmission properties of the filter changed by a large amount. Physically, the filter appeared to have a thin coating of powder on the surface after an exposure of 10^3 sec which was not disturbed for the duration of the test. At the conclusion of the test, the filter was washed with distilled water which removed the powder. The spectral transmission was again measured with the results shown in curve D. The spectral transmission characteristic of the filter had completely changed.

The results for the filter exposed to 4×10^{-1} watts cm^{-2} in the wavelength interval 200 nm to 400 nm are shown in Figure 26 for times equal 0 sec, 8.6×10^4 sec, 2.6×10^5 sec, and 8.6×10^5 sec. The spectral transmission of the filter is invariant with time. The total energy between 200 nm and 400 nm incident upon unit area of the filter during the test was equal to approximately 3.4×10^5 joules. The radiant flux was approximately 250 times the AMO solar irradiance in this wavelength interval.

The conclusion obtained from these two tests is obvious. The spectral filters are very stable in the presence of high ultra-violet radiant fluxes but are easily destroyed by high temperatures. The physical appearance of the filter is a good indication of filter fidelity in that the filter appears to have a layer of powder upon the surface when the transmission characteristics of the filter have changed.

C. Uniformity Filters

The uniformity filters which were supplied with the simulator did not maintain the initial transmission as a function of position on the filter surface when exposed to the severe environment existing at the field lens of the simulator with a resulting compromise in uniformity of irradiance. A test program was initiated to identify a coating which would be compatible with the environment existent at the position of the field lens. Platinum (Pt) with a protective overcoat of one half wave of silicon monoxide-oxide (SiOx) at 560 nm deposited

on ultra-violet grade quartz proved resistant to the extant environment at the field lens. Filters of this type can be produced with any transmission pattern and effective transmission desired. This is accomplished by multiple depositions of the platinum with an appropriate mask inserted between the platinum and the quartz substrate of the filter. These filters have maintained the initial spectral transmission characteristic for periods up to four years. Typical spectral transmission characteristics of these filters are shown in Figure 15. Since these filters have been in use, no degradation of uniformity has been experienced with the system. The transmission characteristics which are desired for the filter can be obtained from irradiance measurements over a plane within the test volume because each point on the test plane is conjugate to a point on one of the field lens elements.

D. Degradation of Components Resultant From Environment

The environment of a solar simulator should be as free of air borne particles, water vapor, dust, and dirt as possible. The reflective optics of the system are especially susceptible to degradation resulting from foreign matter deposited upon the surfaces. The combination of high temperatures, ultraviolet radiant flux, ozone, and large thermal gradients which are attained when a solar simulator is used also result in degradation of electronic, mechanical, optical and thermal components and subsystems. Most of the degradation which effects the mechanical, electronic, optical, and thermal

components can be avoided by the selection of materials resistant to the corrosive environment, viz, gold plated components, stainless steel components, use of pure water or non-corrosive coolant in the liquid cooling systems, proper cooling of components, maintenance of minimum thermal gradients in components and subsystems, good mechanical contact between igniter and lamp, cables capable of conducting the maximum current with minimal losses and use of paints on subsystems which are ultra-violet and temperature stable.

The most serious of these problems has been the degradation of reflective surfaces which results in spectrum degradation and loss of system efficiency. An enclosure has been built around the optical system of the simulator which is supplied with filtered air. This has reduced the degradation somewhat. Humidity control is not practical although most desirable because of the nature of the building in which the simulator is housed and the physical location of the simulator adjacent to an outside entrance to the building which cannot be blocked.

Some of the methods employed to reduce the degradation of the reflective optics are: application of SiOx overcoat to aluminum surfaces, control of temperature of surfaces within a small temperature interval, deposition of a barrier layer of SiOx between the nickel substrate and the evaporated aluminum, use of pure, dry nitrogen to purge the lamp housing and installation of an electronic air filter to condition the atmosphere of the simulator room. None of these methods have eliminated the problem. The deposition of a barrier

layer of SiOx between the nickel substrate and the evaporated aluminum had no effect on the degradation but presented a relatively major problem when the components had to be realuminized. The process of stripping the old aluminum from the component in preparation for realuminizing also stripped parts of the SiOx layer but not all of it. The remainder of the layer had to be removed by optical polishing which was expensive and time-consuming. The major advantage to the protective overcoat of SiOx on the aluminum surfaces is: cleaning of the surfaces can be accomplished without destroying the aluminum surface.

The reflective optics of the simulator discussed in this paper are: the nineteen aconic collectors; the turning flat; and, the collimator. The solution to this problem which is used is to realuminize all components before a major test or whenever spectrum is a major requirement of the test. All of the components can be realuminized within a 48 hour period if necessary and can be accomplished as a matter of routine within ten days. The collectors and turning flat are removed from the optical system when realuminized but the collimator can be realuminized in the vacuum enclosure of the solar simulator. This is a decided advantage because the size and mass of the collimator make it difficult to handle.

The reflective surfaces should not be operated at too low or too high a temperature. The optimum temperature for minimum degradation has not been established to date. The temperature of the collimator should never be less than the shroud temperature while the chamber is evacuated. When the

simulator was first installed, the collimator was allowed to attain its equilibrium temperature during a solar simulation test. No temperature sensors were mounted on the collimator at the time so the temperature could not be monitored. When the shroud temperature was raised to 20°C and the vacuum chamber was opened, the surface of the collimator was immediately covered with a thick deposit of frost and other contaminants. The temperature of the collimator was approximately -50°C and had trapped most of the particles which were trapped on the cold shroud before the shroud temperature was increased prior to opening the chamber. This deposit was very difficult to remove and could not be completely removed by cleaning. Subsequently, heaters and thermal sensors were installed to the rear of the collimator to prevent a reoccurrence of such depositions. The collimator is always maintained at least 10°C above the shroud temperature and no further problems have developed. The collectors and turning flat are always maintained at a temperature at least 5°C above the dew point to prevent condensation upon the surfaces. Condensation always leaves a deposit upon the surfaces which cannot be completely removed by cleaning. These components are presently operated between 25°C and 80°C in order to obtain data to establish an optimum operational temperature.

E. Optimization of Spectrum and Efficiency of System

The requirement of close correlation of the solar simulator spectrum to the AMO solar spectrum results in a loss in efficiency of the system which can

be as large as fifty percent. The basic problem results from the spectrum of the source which for compact arc xenon lamps deviates grossly from the AMO solar spectrum between 800 nm and 1000 nm. To attain a close spectrum correlation to AMO solar irradiance with xenon lamps requires the selective filtration of the radiant flux between 800 nm and 1000 nm. The spectral filters used to accomplish this filtration also filter the radiant flux between 400 nm and 500 nm which results in a deficiency of radiant flux in this wavelength interval. In addition, after transmission through the optical system of the simulator, xenon deficient in radiant flux below 350 nm as compared to AMO solar irradiance.

Results from a program of spectral dependence as a function of gas, impurities, pressure, and current indicated that compact arc lamps filled with krypton, argon, or 10% hydrogen -90% xenon would provide additional radiant flux below 350 nm. Several prototype lamps were obtained with each of these gases, each with a nominal power rating of 2500 watts. Spectra of argon, hydrogen-xenon, xenon and mercury-xenon arc lamps are shown in Figure 27. Each lamp was operated at 2500 watts when the measurement was obtained. The hydrogen xenon lamp was not suitable for use in a solar simulation system because the quartz envelope of the lamp was transparent to the hydrogen when the lamp was operated. The argon lamps all failed violently before 25 hours of operation could be obtained. The krypton lamps exhibited acceptable lifetimes i.e., 500 hours, but degraded rapidly in the emission of radiant flux

below 400 nm in the first 100 hours of lamp operation as shown in Figure 28. Five of the krypton lamps were placed into the optical system of the solar simulator. The spectrum of the simulator was obtained with various combinations of krypton and xenon lamps with and without spectral filters. The spectra of the simulator with: five krypton and five xenon; five krypton and ten xenon with no spectral filters are shown in Figure 29. Corresponding spectra of the simulator with seven spectral filters in the optical system are shown in Figure 30. An examination of these two figures indicates that a combination of krypton and xenon lamps is superior to xenon alone and should be considered for some types of solar simulation tests. However, the krypton lamps were 30% less efficient in the conversion of electrical power to radiant power which negated the use of these lamps to improve the efficiency of the system. The major advantage accruing to the use of krypton lamps is the increased amount of radiant flux below 400 nm which is incident in the test volume. However, with the advent of higher powered xenon arc lamps which exhibit enhanced radiant flux below 400 nm, the advantages offered by krypton lamps are largely negated except for specialized tests requiring a substantial excess of radiant flux below 400 nm as compared to the AMO solar irradiance. An added advantage of the higher powered xenon lamps is the increased conversion efficiency of electrical to radiant power, ranging from 40% for a 2.5×10^3 watt lamp to 65% for a 2×10^4 watt lamp.

Desirable spectral characteristics have also been obtained in a vortex stabilized arc source using a mixture of 8 parts neon to one part of xenon. A typical spectrum of this mixture is shown in Figure 31. However the conversion efficiency of the vortex stabilized arc between 5×10^3 watt and 2×10^4 watt electrical input is approximately 30% to 40% which again negates its use except for specialized tests. However, if the conversion efficiency of the arc can be increased to efficiencies attained at comparable wattages with xenon arcs, a definite improvement in the optimization of spectrum and efficiency of a solar simulator can be attained.

F. Ozone

The ozone generated by solar simulators sometimes approaches concentrations which are hazardous to the health of personnel. In addition to the health hazard, ozone absorbs radiant energy at many wavelengths throughout the spectrum. Ozone absorption between 220 nn and 300 nm (Hartley band) is especially detrimental when a close correlation of the spectrum of the simulator to the AMO solar spectrum is required.

The American Council of Governmental and Industrial Hygienists[97] have established the maximum acceptable concentrations (MAC) of ozone in which personnel may work at one part per ten million in air or, a concentration of 10^{-7} by volume. This is equal to 2×10^{-7} grams per liter of air or a concentration of 1.6×10^{-7} by weight. Concentrations of 1.5×10^{-8} by volume produce

the characteristic odor of ozone which is detectable by the olfactories of personnel.

Ozone is produced when oxygen is exposed to radiant energy of wavelength shorter than 210 nm.[98] Since the quantum yield in this wavelength interval is approximately two, small quantities of radiant energy in this interval can easily produce ozone concentrations detrimental to the health of personnel. The photochemical production of ozone by the radiant energy sources of a solar simulator can be reduced either by removing all oxygen from contact with the radiant energy or by enclosing the radiant energy source with a quartz envelope containing trace of aluminum, titanium, or iron which will not transmit radiant energy below 210 nm.[99] The most practical of these methods in the past was to remove the oxygen from the housing which contains the radiant energy sources by use of a closed loop oxygen free gas cooling system. The system used on the simulator described herein utilizes nitrogen to replace the air in the source housing. The source housing is maintained at a slight positive pressure in respect to the atmosphere to inhibit oxygen migration into the source housing. No problems have resulted with this arrangement when the simulator is operated. However, when the requirement exists to operate the simulator sources with components of the source housing removed, the nitrogen system is no longer effective and concentrations of ozone greater than 10^{-7} by volume are common, especially when the relative humidity is low.

Ozone production is inversely proportional to the relative humidity; is enhanced when nitrogen is present with oxygen; and is directly proportional to the temperature and velocity of air movement around the source of radiant energy. The rate of decomposition of ozone is proportional to the relative humidity, and temperature.[100-101] Personnel are issued respirators to wear on these occasions. Concentrations of ozone as high as 10^{-6} by volume have been observed inside the source housing on these occasions. The operation of a solar simulator poses a definite hazard to the health of personnel if proper precautions are not taken to control the production of ozone. Ozone concentrations in the areas where personnel are present should always be monitored whenever a solar simulator is operated.

G. Electronic Malfunctions

Electronic malfunctions have occurred as a result of faulty components, overheating of components, spurious signal inputs to the control circuits by data acquisition systems, mechanical failures, and voltage fluctuations of the input power to the system. One of the more serious malfunctions was caused when the input power to the system exceeded the design specification by 1 to 10 volts. The power supplies were designed for input power of 460 v ± 20 v. Tantalum capacitors located in the power supply which was used to supply the reference voltage to each of the lamp power supplies failed regularly when the voltage exceeded the design specifications until replaced by capacitors with higher ratings.

The failure of these capacitors introduced instabilities in the irradiance in the test volume and eventually caused the power supply to short out and extinguish the lamp.

Each power supply-lamp circuit has several thermal switches which open when the temperature of the component exceeds a predetermined value. These switches are located at the base of the igniter, the casting to which the source cage is attached, the heat sink in the power supply to which the silicon controlled rectifiers are attached, and the input terminals to the power supply. A considerable number of power outages have occurred due to power contact between the igniter posts and the lamp terminals. In each instance, sufficient heat was produced to cause the thermal switch to open. Some problems have also been encountered which resulted from defective thermal switches. Some switches designed to open at 100°C have actually opened when the temperature exceeded 46°C.

A malfunction of the system also occurred when a new data acquisition system was installed. The ground potential of the data acquisition system was several volts different from the ungrounded neutral of the control circuit of the power supplies which resulted in power supply outage. This malfunction was corrected by the proper interfacing of the ground and neutral potentials between the two subsystems.

One mechanical failure has occurred which caused extensive damage to the components of one power supply when a partial short developed in the

insulating material on one of the lamp cages which separated the cathode and anode voltages. The lamp continued to draw excessive current for a short time before the circuit breaker was activated and the molten metal of the lamp cage fell onto the turning flat in the source housing which caused the formation of several lacunae on the surface of the mirror. The surface had to be remachined and optically polished before it could be reused. This failure also resulted in the violent failure of the radiant energy source which completely destroyed the collector but did minimal damage to other components in the system. The excessive damage caused by this malfunction could have been prevented if the main line circuit breaker had controlled only one power supply. Each power input line circuit breaker supplies current to a group of four power supplies. The total current through the breaker did not exceed the breaker rating, because of the nature of the short circuit, quickly enough to prevent damage to components of the system. A circuit breaker was subsequently installed for each power supply to prevent excessive damage from future malfunctions of this type.

H. Thermal Malfunctions

No thermal malfunctions have occurred which resulted in substantial damage to any components of the system. The most serious malfunction occurred in the course of a thermal balance test of a satellite when the liquid cooling lines to the field lens and seal lens became partially blocked by debris in the

cooling fluid. This resulted in equilibrium temperatures of these components which were near the maximums permissible and the test could only be continued to completion by the introduction of additional cooling air upon the components. The cover of the transition tube which connects the source housing and the vacuum enclosure was removed and two large fans were directed onto the components. The debris in the cooling fluid was subsequently removed by the installation of several filters into the main fluid supply and no further problems have developed.

XI. PRE-FLIGHT QUALIFICATION TEST AND ORBITAL PERFORMANCE OF EXPLORER XXXVIII

The modification described above was performed in order to provide a pre-flight qualification test for the Radio Astronomy Explorer-A (RAE-A) Satellite which was designated Explorer XXXVIII after successful insertion into an earth orbit. The spacecraft was launched on 4 July 1968 from the Western Test Range at Lompoc, California. The apogee and perigee of the orbit are 5858 km and 5850 km, respectively. The orbit inclination is 120.8° from the equator, the period is 224 minutes and the weight of the spacecraft is 190.5 kg. The primary purpose of the experimental instruments aboard the spacecraft is to obtain data of electromagnetic radiations within the radio frequency spectrum ($1\ m \geq \lambda \geq 10^4\ m$) originating from cosmic, solar, and earth sources.

Figure 32 is a photograph of the spacecraft taken prior to the solar simulation test. The view is toward the rear of the vacuum enclosure in the direction of radiant flux incidence from the collimator. The rear door of the vacuum enclosure is mounted on a track which extends 5 meters beyond the rear of the vacuum enclosure. This provides sufficient space to attach the test objects to the three support rails which are welded to the rear door of the chamber. When the test object is attached to the support rails and all sensors have been attached, the rear door is motor driven to the rear of the chamber. This places the test object within the test volume of the simulator and accomplishes the chamber vacuum seal. Sensors which are used to measure the temperatures of various components of the spacecraft are connected to a data acquisition system located nearby. Signals from other sensors which are an integral part of the spacecraft are transmitted directly to the GSFC mission control center. All power for the spacecraft subsystems was provided by the power system of the spacecraft, which for Explorer XXXVIII was an array of four solar panels with solar cells attached to both front and rear sides.

The spacecraft was tested for two positions, one as shown in Figure 32 and one with a 180° rotation of the spacecraft about the vertical axis. The satellite required 18 hours to attain the initial temperature equilibrium at which time it was remotely rotated 180° and required an additional 11 hours to attain the second temperature equilibrium. The test was started at 1700 on 10 May 1968 and completed near midnight on 11 May 1968.

The spacecraft including the solar paddles was approximately a square 150 cm on a side. The maximum diameter of the spacecraft was approximately 190 cm. Since the maximum diameter of a plane in the solar simulator test volume was 178 cm, the ends of the solar paddles did not receive any radiant flux during the test. Approximately one half of the spacecraft was located within the portion of the simulator test volume which could introduce re-reflections from the collimator. The forward edge of the spacecraft was located 200 cm from the center of the collimator. The rear edge of the satellite was approximately 45 cm from the LN_2 shroud of the rear door. The geometrical center of the spacecraft was located at the geometrical center of the vacuum enclosure and not coincident with the optical axis of the solar simulator. Figure 33 is a side view of the spacecraft in the test volume.

The surface of the spacecraft was covered with black paint, white paint, sandblasted aluminum and solar cells. The absorptance of each of these materials for the spectrum of the simulator and AMO solar irradiance are shown in Table 7. The mean irradiance within the test volume before the spacecraft was introduced was 135 mw cm^{-2} measured with the normal-incidence pyrheliometer described above. The uniformity was 2.5 percent and was measured with the solar cell scanner described above. When the spacecraft was placed within the test volume, the mean irradiance increased to 137 mw cm^{-2} and the uniformity decreased to 5%. The irradiance at various positions on the spacecraft surface which were designated by the thermal design engineer were measured with the

Hy-Cal pyrheliometer after the spacecraft was placed into a position within 25 cm of the test position. This corresponded to the distance between the rear door and the end of the vacuum enclosure. The door was not completely closed because no facilities were available to supply oxygen into the test volume to the personnel performing the measurements.

The irradiance during the test was monitored by a black groved plate detector supplied by the thermal design engineer which was placed at a position in the test volume corresponding to: $\theta = 0°$, r = 85 cm, z = 250 cm.

The temperatures which had been predicted by the thermal analytical model developed for the spacecraft corresponded within a few degrees centigrade to those obtained during the simulation test. The solar paddles supplied sufficient power to all systems of the spacecraft even though two of the paddles were partially shaded in each orientation. All of the spacecraft subsystems functioned without mishap for the duration of the test.

The temperatures attained by the spacecraft in orbit corresponded to those predicted by the thermal analytical model within a few degrees centigrade. The power generated by the solar paddles in space also correlates well with the values obtained in the simulation test.

The spacecraft will not orient itself in respect to the sun for either of the aspects tested until it has been in orbit approximately one year. This variation between solar simulation test aspect and orbital aspect resulted from limitations

imposed upon orientations of the spacecraft in the test volume of the simulator by the mechanical positioner which held the spacecraft during the test.

The spacecraft has been declared a success by NASA Headquarters and no problems have developed with either the thermal or power systems during the first nine months in orbit.

XII. SUMMARY AND CONCLUSIONS

The solar simulator has been modified to obtain a nominal 1.75 meter test diameter with a mean irradiance greater than one solar constant. Uniformity of 2% has been obtained over this test diameter and uniformity of 10% has been obtained over a test volume of 244 cm in depth. Uniformity in depth was compromised from that previously obtained by the constraints imposed upon the modification. The spectrum of the simulator can be altered by the use of filters to obtain an adequate correlation with the AMO solar spectrum for thermal balance tests, energy conversion device tests, and materials degradation tests. The system has an overall efficiency ranging from 4.8% with no spectral filters to 3.3% with seven spectral filters. The efficiency of the system decreased approximately 25% as a result of the constraints imposed upon the modification. The performance characteristics are equal or superior to all other solar simulation systems which have been reported in the literature to date.[32-45,102] The solar simulator also has the potential to provide one solar constant irradiance over a nominal two meter diameter.

The performance of this system prior and subsequent to the modification described in this paper establishes the feasibility, at the current state of the art, of obtaining 2% uniformity over a test volume $\geq$2 meters in diameter and $\geq$8 meters in depth with a mean irradiance of one earth solar constant. The stability and spectrum of the irradiance within the test volume is of adequate quality to provide solar simulation tests for all types of space hardware now existent. All of the operational problems which have developed in the operation of the system have either been resolved completely or adequately controlled by the establishment and use of definitive maintenance procedures. The solar simulation fidelity of the simulator has been established by the orbital performance of Explorer XXXVIII which received the final pre-launch simulation test in this system. Explorer XXXVIII performance in orbit is duplicating the performance exhibited during the solar simulation test within the experimental errors associated with the data acquisition and telemetry systems of the spacecraft and ground stations.

REFERENCES

1. J. Opt. Soc. Am., 34, 183, 246 (1944).

2. Ibid., 52, 490, 954 (1962).

3. Ibid., 57, 854 (1967).

4. Optical Society of America, Committee on Colorimetry, The Science of Color (Thomas Y. Crowell Company, New York, 1953).

5. G. A. W. Rutgers, S. Flügge, ed., Handbuch Der Physik. (Springer-Verlag Berlin, 1958) Vol. XXVI, p. 131.

6. Max Born, E. Wolf, Principles of Optics (Pergamon Press, London, 1959) Chap. IV, Sect. 4.8, p. 180.

7. Phys. Today, 15(6), 20 (June 1962).

8. Mikael' A. Bramson, Infrared Radiation (Plenum Press, New York, 1968) Chap. I, Sect. 2, p. 12.

9. William E. Forsythe, Ed., Measurement of Radiant Energy (McGraw-Hill Book Company, Inc., New York, 1937) Chap. 1, p. 3.

10. Earle B. Brown, Modern Optics (Reinhold Publishing Corporation, New York, 1965) Chap. 5, p. 219.

11. Darii Y. Svet, Thermal Radiation (Consultants Bureau, New York, 1965) Chap. I, p. 3.

12. Norman H. Nachtrieb, Principles and Practices of Spectrochemical Analysis (McGraw-Hill Book Company, Inc., New York, 1950) Chap. 6, p. 125.

13. Thomas R. Harrison, Radiation Pyrometry and its Underlying Principles of Radiant Heat Transfer (John Wiley and Sons, Inc., New York, 1960) Chap. 2, p. 9.

14. Tom J. Love, Radiative Heat Transfer (Charles E. Merrill Publishing Company, Columbus, Ohio, 1968) Chap. 1, p. 2.

15. Georg Bauer, Measurement of Optical Radiations (The Focal Press, London, 1965) Chap. II, p. 18.

16. Max Garbuny, Optical Physics (Academic Press, New York, 1965) Chap. 2, p. 28.

17. Robert A. Smith, F. E. Jones, R. P. Chasmar, The Detection and Measurement of Infra-red Radiation (Oxford University Press, London, 1960) 3rd ed., Chap. II, p. 21.

18. John W. T. Walsh, Photometry (Constable and Company, Ltd., London, 1958) 3rd ed., Chap. V, p. 120.

19. Howard H. Seliger, W. D. McElroy, Light: Physical and Biological Action (Academic Press, New York, 1965) Chap. 1, p. 8.

20. Ray P. Teele; R. Kingslake, ed., Applied Optics and Optical Engineering (Academic Press, New York, 1965) Vol. I, Chap, 1, p. 1.

21. M. Nicolet, Ann. Astrophys. 14, 249 (1951).

22. P. R. Gast, Handbook of Geophysics and Space Environments (McGraw-Hill Book Company, Inc., New York, 1967) Chap. 16, p. 16-1.

23. Francis S. Johnson, Satellite Environment Handbook (Stanford University Press, Stanford, Calif., 1961) Chap. 4, p. 78.

24. F. S. Johnson, J. Meteorol. 11, 431 (1954).

25. M. P. Thekaekara, R. Kruger, C. H. Duncan, Appl. Opt. 8, (1969).

26. Dietrich Labs, H. Neckel, Z. Astrophys. 69, 1 (1968).

27. E. A. Makaroua, A. V. Kharitonov, Astronomicheskii Zhur. 45, 752 (1968).

28. J. C. Arvesen, R. N. Griffin, Jr., B. D. Pearson, Jr., Appl. Optics 8, (1969).

29. M. P. Thekaekara, Solar Energy 9, 7 (1965).

30. D. Labs, H. Neckel, Z. Astrophys. 55, 269 (1962).

31. R. Stair, H. T. Ellis, J. Appl. Meteorol. 7, 635 (1968).

32. L. Schneider, D. Wenzel, Technische Mitteilungen AEG-Telefunken, 58, 74 (1968).

33. H. D. Strong, Jr., Proc. of I. A. S. (Los Angeles, Calif. June 1962)

34. R. G. T. Munday, Raumfahrtforschung 2, 68 (1964).

35. M. W. Mitchell, Proc. of AIAA Space Simultation Testing Conference (Pasadena, Calif. Nov. 1964) p. 135.

36. Op. cit., R. A. Griest, J., p. 162.

37. Op. cit., H. K. Strass, D. L. Hannaford, p. 251.

38. D. Q. Durant, T. H. Allen, E. S. J. Wang, Proc. of AIAA/IES/ASTM 1st Space Simulation Conference (Houston, Texas Sept. 1966) p. 17.

39. Op. cit., K. Oshima, F. Tamaki, C. Hayashi, I. Umezu, p. 138.

40. A. D. LeVantine, G. A. Harter, J. E. Norris, Proc. of AIAA/IES/ASTM 2nd Space Simulation Conference (Philadelphia, Penn. Sept. 1967) p. 132.

41. Op. cit., A. R. Lunde, J. W. Yerkes, R. L. Haslund, p. 162.

42. Op. cit., R. E. Rolling, J. P. Kirkpatrick, K. N. Marshall, p. 141.

43. R. Eddy, Proc. of AIAA/IES/ASTM 3rd Space Simulation Conference (Seattle, Wash. Sept. 1968) p. 22.

44. Op. cit., A. D. LeVantine, p. 58.

45. Op. cit., A. R. Lunde, p. 67.

46. Op. cit., S. J. Babjak, J. F. Scannapieco, A. M. Goldis, p. 105.

47. Op. cit., L. B. Fogdall, S. S. Cannaday, R. R. Brown, p. 110.

48. Op. cit., D. W. Clifford, R. J. Schmitt, p. 157.

49. Op. cit., B. E. Cunningham, R. E. Eddy, J. Spacecraft and Rockets, 4, 280 (1967).

50. L. A. McKellan, J. V. Steward, R. L. Olson, J. Env. Sciences, 8, 22 (1965).

51. R. E. Gannon, R. J. Hill, T. S. Laszlo, Proceedings of IES Annual Meeting (1966) p. 463.

52. W. J. Courtney, . E. Gilligan, ibid., p. 21.

53. H. B. Phillips, Analytic Geometry and Calculus (John Wiley and Sons, Inc. New York, 1946) 2nd ed., Chap. XVII, p. 455.

54. D. R. Hornbaker, D. L. Rall, Proc. of IES annual meeting (San Diego, Calif., April 1966) p. 639.

55. J. W. Baughn, J. E. Arnold, Proc. of Instrument Society of America annual conference (Los Angeles, Calif., Oct. 1965) p. TR-196.

56. J. D. Sandstrom, Proc. of Intersociety Energy Conversion Engr. Conf. (Boulder, Colo. Aug. 1968) p. 138.

57. A. J. Drummond, Solar Energy V, 19 (1961).

58. A. J. Drummond, ISA Transactions 7, 194 (1968).

59. A. J. Drummond, J. R. Hickey, Solar Energy 12, 217 (1968).

60. A. J. Drummond, J. R. Hickey, W. J. Scholes, E. G. Laue, Nature 218, 259 (1968).

61. Annals of the International Geophysical Year (Pergamon Press, London, 1958) Vol. V, Part VI, p. 396.

62. Op. cit., p. 378.

63. C. G. Abbot, Ann. Astrophys. Obs. Smithson. Instn. 3, 47 (1913).

64. K. Ångström, Annalen der Physik and Chemie 67, 633 (1899)

65. K. Ångström, Astrophys. J. 9, 334 (1899).

66. K. Leiss, Z. Physik 69, 680 (1931).

67. R. Brower, Electronics, 41(14), 80 (1968).

68. R. Stair, W. E. Schneider, J. K. Jackson, Appl. Opt. 2, 1151 (1963).

69. F. J. Studer, R. F. Van Beers, J. Opt. Soc. Am. 54, 945 (1964).

70. R. Stair, R. G. Johnston, E. W. Halback, J. Res. Nat. Bur. Stds. 64A, 291 (1960).

71. G. A. Hornheck, Appl. Opts. 5, 179 (1966).

72. H. J. Kostkowski, R. D. Lee, Temperature, Its Measurement and Control in Science and Industry (Reinhold Publishing Corporation, New York, 1962) Vol. 3, Part 1, pg. 449.

73. A. E. Mann, F. N. Benning, Proc. of AIAA Space Simulation Testing Conference (Pasadena, Calif. Nov. 1964) p. 123.

74. A. E. Mann, F. N. Benning, Environmental Quarterly June 1964.

75. Ibid., Sept. 1964.

76. M. A. Lillywhite, R. McIntosh, D. L. Lester, Proc. of AIAA/IES/ASTM Space Simulation Conference (Houston, Texas Sept. 1966) p. 23.

77. F. N. Benning, Tutorial Lecture Series of Institute of Environmental Sciences (St. Louis, Missouri April 1968) Section 5.

78. J. A. Castle, ibid., section 8.

79. L. C. Martin, Technical Optics (Sir Isaac Pitman & Sons, Ltd., London, 1961), 2nd ed., Vol. II, Chap. VI, p. 272.

80. John W. T. Walsh, Photometry (Constable and Company, Ltd., London, 1958) 3rd ed., Chap. XIV, p. 458.

81. R. J. Bracey, The Technique of Optical Instrument Design (The English Universities Press, Ltd., London, 1960) Chap. 10, p. 302.

82. Arthur C. Hardy, F. H. Perrin, The Principles of Optics (McGraw-Hill Book Company, Inc., New York, 1932) Chap. XIX, p. 412; Chap. XXVI, p. 534.

83. Francis A. Jenkins, H. E. White, Fundamentals of Optics (McGraw-Hill Book Company, Inc., New York, 1957) 3rd ed., Chap. 7, p. 114.

84. E. A. Boettner, L. J. Miedler, J. Appl. Opts. 2, 105 (1963).

85. W. O. Hamlin, Instruments and Control Systems, 39, 91 (1966).

86. W. B. Reese, J. Soc. Motion Picture Television Engrs., 67, 392 (1958).

87. Kurt Larché, Z. Physik, 136, 74 (1953).

88. H. Schirmer, ibid., p. 87.

89. W. Budde, J. Opt. Soc. Am., 52, 343 (1962).

90. W. E. Thouret, H. S. Strauss, Illuminating Engr., LVII, 150 (1962).

91. O. E. Lienhard, J. A. McInally, ibid., p. 173.

92. W. E. Thouret, ibid., LV, 295 (1960).

93. J. C. Slater, N. H. Frank, Introduction to Theoretical Physics (McGraw-Hill Book Company, Inc., New York, 1933) Chap. XVIII, p. 198.

94. John Strong, Procedures in Experimental Physics (Prentice-Hall, Inc., New York, 1938) Chap. XII, p. 493.

95. M. A. Lillywhite, R. McIntosh, C. H. Duncan, J. A. Colony, J. Env. Sciences, 11(2), 9 (1968).

96. Dwight E. Gray, ed., American Institute of Physics Handbook (McGraw-Hill Book Company, Inc., New York, 1957) Sect. 6, p. 6-108.

97. N. I. Sax, Dangerous Properties of Industrial Materials (Reinhold Publishing Corp., New York, 1957), p. 977.

98. Michael Ardon, Oxygen (Elementary Forms) (W. A. Benjamin, New York, 1965) Sect. 3, p. 51.

99. H. Mohn, Glastechn. Ber. 29, 483 (1956).

100. A. W. Ewell, J. Appl. Phys. 13, 759 (1942).

101. L. R. Koller, J. Appl. Phys. 16, 816 (1945).

102. R. Liebmann, Appl. Opt., 7, 315 (1968).

Table I

Radiant Energy Definitions, Terminology, Symbols, and Units

	Object Space		Image Space		
Terminology	Symbol	Units	Symbol	Units	Definitions
Radiant Energy	U_0	joules	U_i	joules	Energy transported by electromagnetic radiation, equal to product of radiant flux and duration of radiation
Radiant Power or Flux	P_0	watts	P_i	watts	Power of electromagnetic radiation averaged over a time much greater than the oscillation period
Radiant Intensity	J_0	watts $ster^{-1}$	-	-	Spatial density of radiant power of emitted electromagnetic radiation
Radiance	N	watts $ster^{-1}$ cm^{-1}	-	-	Surface density of radiant intensity in a given direction
Radiant Emittance	W	watts cm^{-2}	-	-	Surface density of radiant power emitted by a surface
Irradiance	-	-	H	watts cm^{-2}	Surface density of radiant power incident on a surface
Irradiation	-	-	I*	joules cm^{-2}	Surface density of radiant energy incident on a surface

*The symbol I for irradiation is used in this paper as no symbol has been recommended by references one to four.

Table II

Solar Simulator Performance and Design Characteristics

Parameter	Symbol	Units
Mean irradiance	$\langle H \rangle$	watts cm^{-2}
Mean flux	$\langle P_i \rangle_{t_2-t_1}$	watts
Area of plane in test volume	A_i	cm^{-2}
Efficiency	ϵ	%
Uniformity	Λ	%
Stability	$\Psi_{t_2-t_1}$	%
Mean spectral irradiance	ΔH_{λ_i}	watts cm^{-2} nm^{-1}
Spectral uniformity	Υ_{λ_i}	%
Spectral Stability	$\left(X_{\lambda_1}\right)_{t_2-t_1}$	%
Collimation	ϕ	degrees or radians
Divergence	γ	degrees or radians
Re-reflected energy	Γ	%
Test volume dimensions	r, θ, z	cm, degrees, cm
Test volume configuration	-	-
Vacuum	P_V	Newtons cm^{-2} or torr
Shroud temperature	T_s	°K
Contamination	$\Delta\rho_{\lambda_i}$; $\Delta\tau_{\lambda_i}$	%
Angular Aperature	AA_0; AA_i	ster
Relative aperature or f/no	$f/_0$; f/i	
System off-axis angle	2ψ	degrees
Diameter of collimator	D_{coll}	cm
Optical surface of collimator	-	-
Type of radiant energy source	-	-
Number of radiant energy sources	n	
Interior dimensions of vacuum enclosure	D, z	
Diameter of source array	D_s	
Axial optical path length from H_s to H_f	δ_0	
Axial optical path length from H_p to H_c	δ_i	
Type, number, and capacity of vacuum pumps		

Table III

Performance and Design Characteristics of Simulator Before Modification

Parameter	Symbol	Performance
Mean Irradiance	$\langle H \rangle$	Variable from 242 mw cm^{-2} to 12.7 mw cm^{-2} (no filters) Variable from 148 mw cm^{-2} to 7.8 mw cm^{-2} (7 spectral filters)
Mean Flux	$\langle P_i \rangle_{t_2-t_1}$	Variable from 3×10^3 watts to 1.57×10^2 watts (no filters) Variable from 1.83×10^3 watts to 96.7 watts (7 spectral filters)
Area of plane in test volume	A_i	1.24×10^4 cm^2
Efficiency	ϵ	6.5% with no spectral filters, 4.0% with 7 spectral filters
Uniformity	Λ	5% (1 cm × 1 cm detector)
Stability	$\Psi_{t_2-t_1}$	1% 1 sec to 10^5 sec
Spectral uniformity	Υ_{λ_i}	0%
Spectral stability	$\left(X_{\lambda_i}\right)_{t_2-t_1}$	$\leq$2% 1 sec to 10^5 sec for all λ_i
Collimation	ϕ	4°
Divergence	γ	$\leq 6°$
Re-reflected Energy	Γ	$\leq$2%
Test volume dimensions	D_{max}, D_{min}, z	132 cm × 120 cm × 244 cm
Test volume configuration	-	Section of ellipsoid
Vacuum, ultimate	P_V	10^{-9} torr
Shroud temperature	T_s	523°K $\geq T_s \geq$ 77°K
Contamination	$\Delta\rho_{\lambda_i}, \Delta\tau_{\lambda_i}$	$\Delta\rho_{\lambda_i} = \Delta\tau_{\lambda_i} \leq$ 2% for all λ_i
Angular aperature on object side	AA_0	20°20'
Angular aperature on image side	AA_i	28°26'
f/no on object side	f/o	f/2.8
f/no on image side	f/i	f/2.0
Systems off-axis angle	2ψ	43°10'

Table III (Continued)

Parameter	Symbol	Performance
Diameter of collimator	D_{coll}	152 cm
Optical surface of collimator		Parabola
Type of radiant energy source		2500 watt xenon compact arc
Number of radiant energy sources	n	nineteen
Interior dimensions of vacuum enclosure	D, z	290 cm × 460 cm
Diameter of source array	D_s	138 cm
Axial optical path length from H_s to H_f	δ_0	385 cm
Axial optical path length from H_p to H_c	δ_i	299 cm
Type, number, and capacity of vacuum pumps		Three 50,000 liter sec^{-1} diffusion pumps

Table IV

Thermal Data of Modified Solar Simulator

Component	Equilibrium Temperature for Electrical Power Input Of: 20 kw	40 kw	80 kw	Maximum Allowable Temperature
Optical Turning Flat	22°C	26°C	36°C	150°C
Field Lenses	39	60	102	300
Projection Lenses	46	88	166	300
Vacuum Seal Lens	36	54	92	150
Aconic Collector (Typical)	42	58	89	150
Negative Seal of Radiant Energy Source (Typical)	100	110	130	200
Solar Cell Sensor of Power Supply Control Circuit (Typical)	39	53	76	150
Atmosphere of Source Housing	34	45	63	100

Table V

Performance and Design Characteristics of Simulator After Modification

Parameter	Symbol	Performance
Mean irradiance	$\langle H \rangle$	Variable from 164 mw cm^{-2} to 8.6 mw cm^{-2} (no spectral filters) Variable from 113 mw cm^{-2} to 5.9 mw cm^{-2} (7 spectral filters)
Mean flux	$\langle P_i \rangle_{t_2-t_1}$	Variable from 3969 watts to 208 watts (no spectral filters) Variable from 2734 watts to 143 watts (7 spectral filters)
Area of plane in test volume	A_i	2.42×10^4 cm^2
Efficiency	ϵ	4.8% with no spectral filters; 3.3% with 7 spectral filters
Uniformity	Λ	2% for plane; 10% for volume (1 cm × 1 cm detector)
Stability	$\Psi_{t_2-t_1}$	1% for 1 sec $\leq$ t $\leq 10^5$ sec
Spectral uniformity	Υ_{λ_i}	0%
Spectral stability	$\left(X_{\lambda_i}\right)_{t_2-t_1}$	$\leq$2% for 1 sec $\leq$ t $\leq 10^5$ sec
Collimation	ϕ	3°
Divergence	γ	$\leq$5°
Re-reflected energy	Γ	$\leq$3%
Test volume dimensions	D_{max}, D_{min}, z	178 cm × 173 cm × 244 cm
Test volume configuration		Section of elliptic paraboloid
Vacuum, ultimate	P_V	10^{-9} torr
Shroud temperature	T_S	523°K $\geq$ T_S $\geq$ 77°K
Contamination	$\Delta\rho_{\lambda_i}$, $\Delta\tau_{\lambda_i}$	$\Delta\rho_{\lambda_i} = \Delta\tau_{\lambda_i} \leq$ 2% for all λ_i
Angular aperature on object side	AA_0	17°37'
Angular aperature on image side	AA_i	26°54'
f/no on object side	f/o	f/3.2
f/no on image side	f/i	f/1.2
System off-axis angle	2ψ	41°22'

Table V (Continued)

Parameter	Symbol	Performance
Diameter of collimator	D_{coll}	232 cm of which 200 cm is utilized
Optical surface of collimator		Spherical
Type of radiant energy source		4200 watt xenon compact arc
Number of radiant energy sources	n	Nineteen
Interior dimensions of vacuum enclosure	D, z	290 cm × 460 cm
Diameter of source array	D_s	138 cm
Axial optical path length from H_s to H_f	δ_0	445 cm
Axial optical path length from H_p to H_c	δ_i	239 cm
Type, number, and capacity of vacuum pumps		Three 50,000 liters sec^{-1} diffusion pumps

Table VI

Absorptances of Spacecraft Materials As a Function of Various Spectra

Material	Air Mass Zero Solar Irradiance	Off-Axis Solar Simulator							Krypton	Argon	Hydrogen-Xenon	Mercury-Xenon	Xenon	X-25L
		No Filters	6 Spectral Filters	7 Spectral Filters	No Filters 5 Xenon 5 Krypton	7 Filters 5 Xenon 5 Krypton	No Filters 10 Xenon 5 Krypton	7 Filters 10 Xenon 5 Krypton						
Evaporated Aluminum	7.64%	8.0%	7.5%	7.4%	7.8%	7.1%	7.7%	7.2%	7.3%	5.5%	7.2%	6.5%	7.1%	7.3%
Evaporated Gold	19.8	14.5	17.3	18.5	14.4	17.4	14.6	18.3	12.8	7.1	14.0	23.5	12.6	13.5
Evaporated Silver	4.96	4.1	3.6	3.2	3.8	3.3	4.3	3.3	6.0	3.2	5.2	13.4	4.9	2.6
K_2SiO_3-TiO_2	19.7	15.6	18.2	17.5	17.6	19.1	18.2	18.8	23.4	26.9	22.6	35.8	22.5	16.9
TiO_2-rutile in methyl silicone	18.9	17.4	17.7	17.1	18.1	18.0	18.6	17.9	22.3	22.1	21.0	32.7	21.0	16.6
K_2SiO_3-ZnO	23.5	20.3	22.4	21.3	22.6	23.5	23.1	22.9	29.4	34.8	28.2	40.5	28.4	21.9
ZnO-SP500 from New Jersey Zinc in methyl silicone	21.2	19.7	20.1	19.5	20.4	20.3	20.8	20.3	24.4	23.7	23.1	35.3	23.0	18.7
TiO_2 in Epoxy	17.6	14.8	16.4	15.5	16.4	16.9	17.0	16.7	21.9	24.6	20.8	32.7	20.9	15.7
Leafing Aluminum (Al in Phenylated silicone)	28.2	28.2	28.1	28.1	28.2	27.9	28.0	28.0	28.0	26.6	27.7	27.5	27.6	27.9
MMM Velvet Black (Carbon black and spherical glass beads in a non-linear polyester)	97.2	97.2	97.2	97.2	97.2	97.2	97.2	97.2	97.3	97.3	97.2	97.2	97.2	97.2
Cat-a-Lac Black (Carbon black in epoxy)	94.7	94.9	94.8	94.8	94.8	94.8	94.8	94.8	94.7	94.7	94.8	94.5	94.8	94.8

Table VII

Absorptance of Explorer XXXVIII Materials as a Function of AMO Solar and Simulator Spectra

Material	α_{SS}'	α_{AMO}
Sandblasted Aluminum	.68	.67
[1] Black Paint (Carbon black in epoxy)	.95	.93
[2] White Paint (TiO_2-rutile in methyl silicone)	.17	.18
Solar Cell (Typical)	.80	.80

[1]Cat-a-Lac black manufactured by Finch Paint and Chemical Company.
[2]Q-92-007 manufactured by Dow Corning over a primer coat of Cat-a-Lac white manufactured by Finch Paint and Chemical Company.

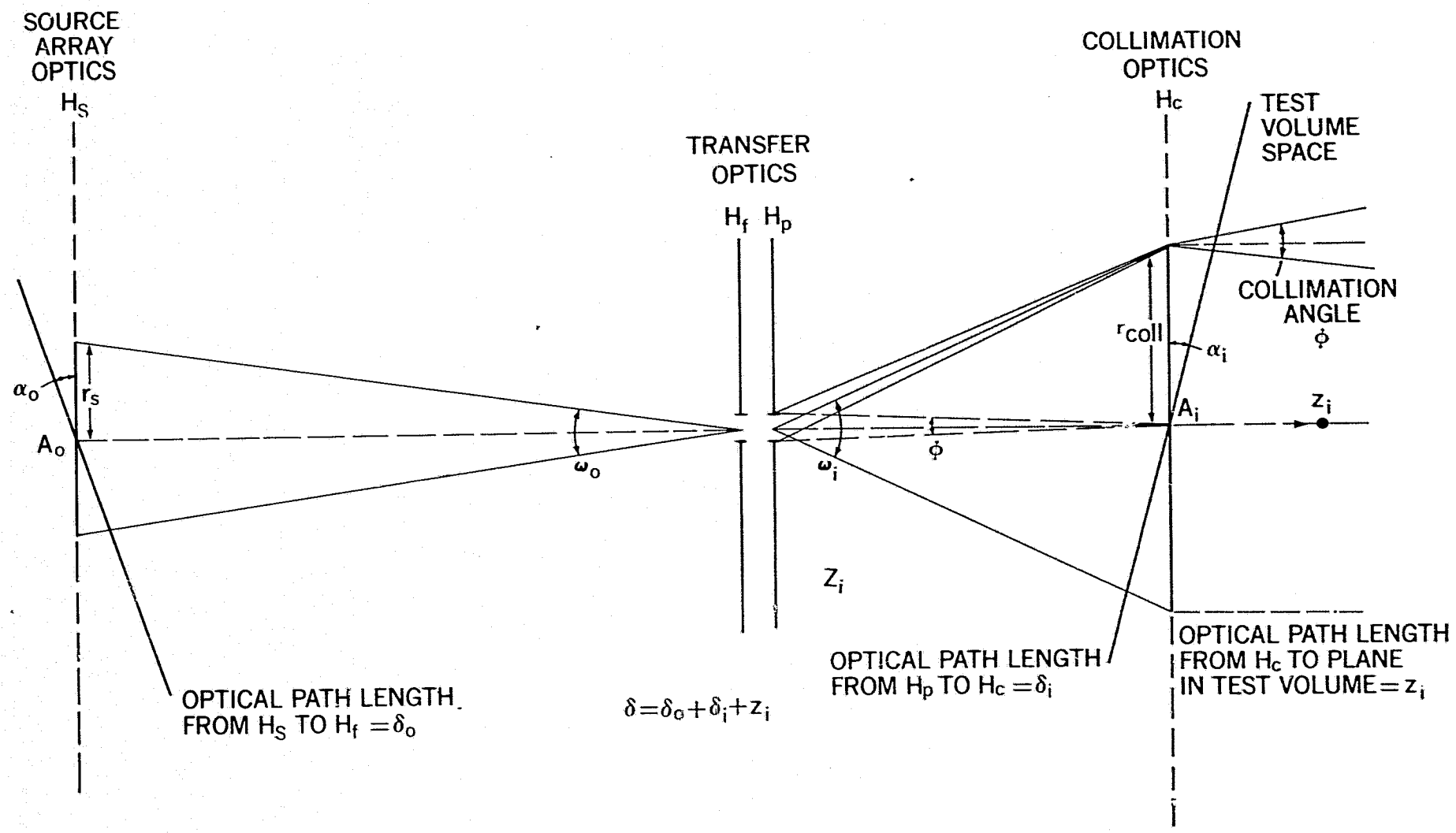

Figure 1. Geometry of a Typical Solar Simulator System

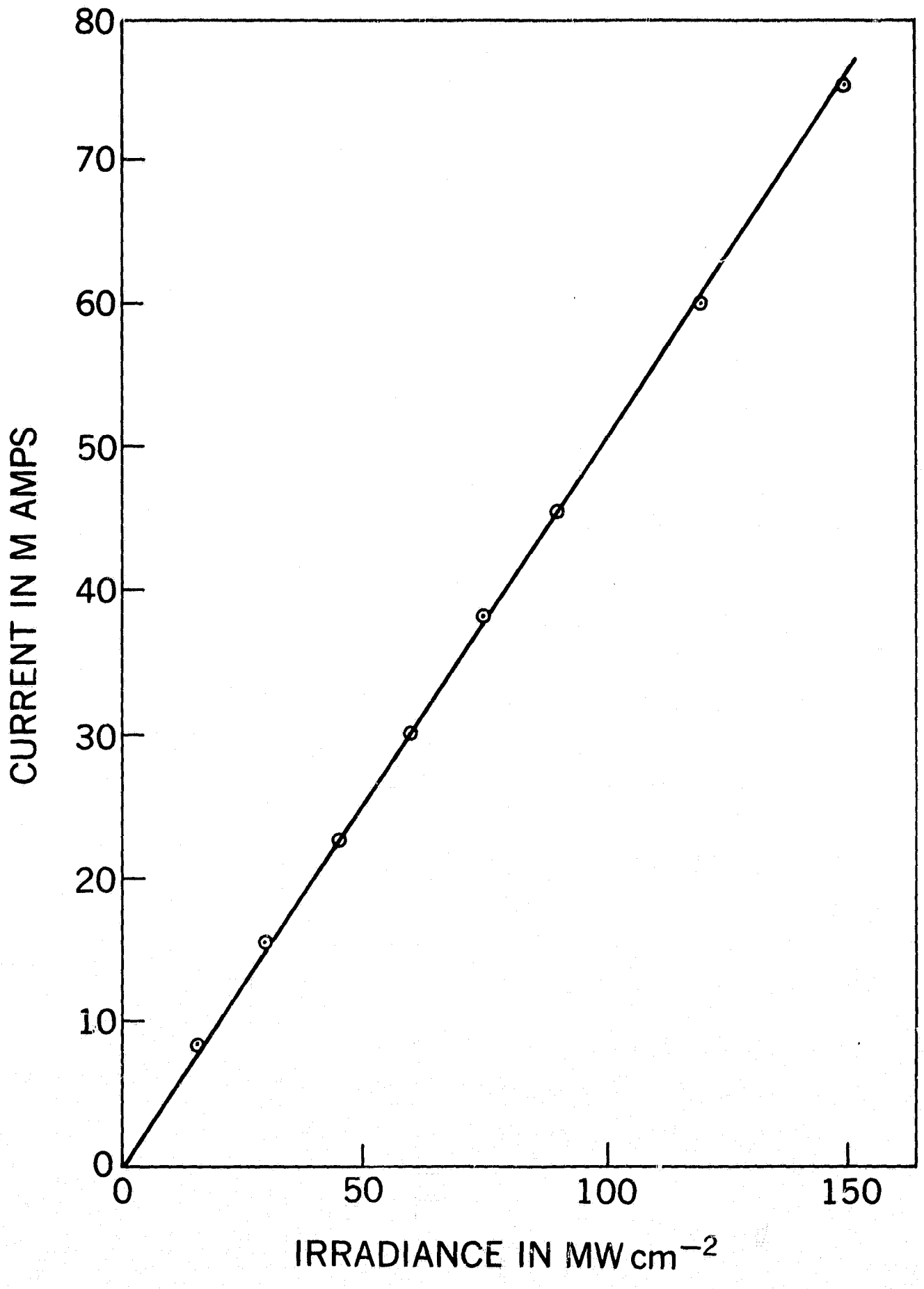

Figure 2. Irradiance - Short Circuit Current Characteristic of Solar Cell at 23°C

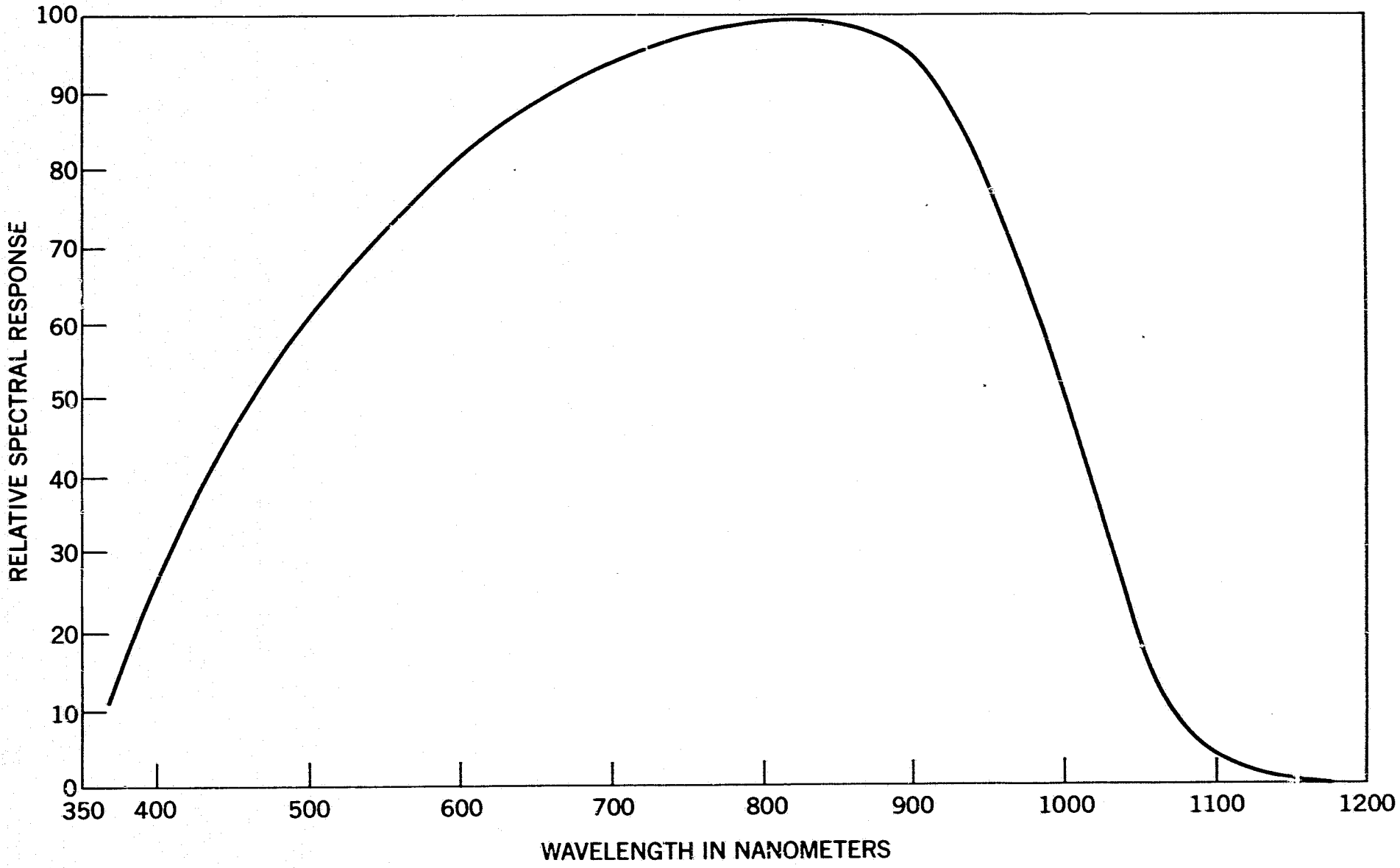

Figure 3. Relative Spectral Response of Solar Cell

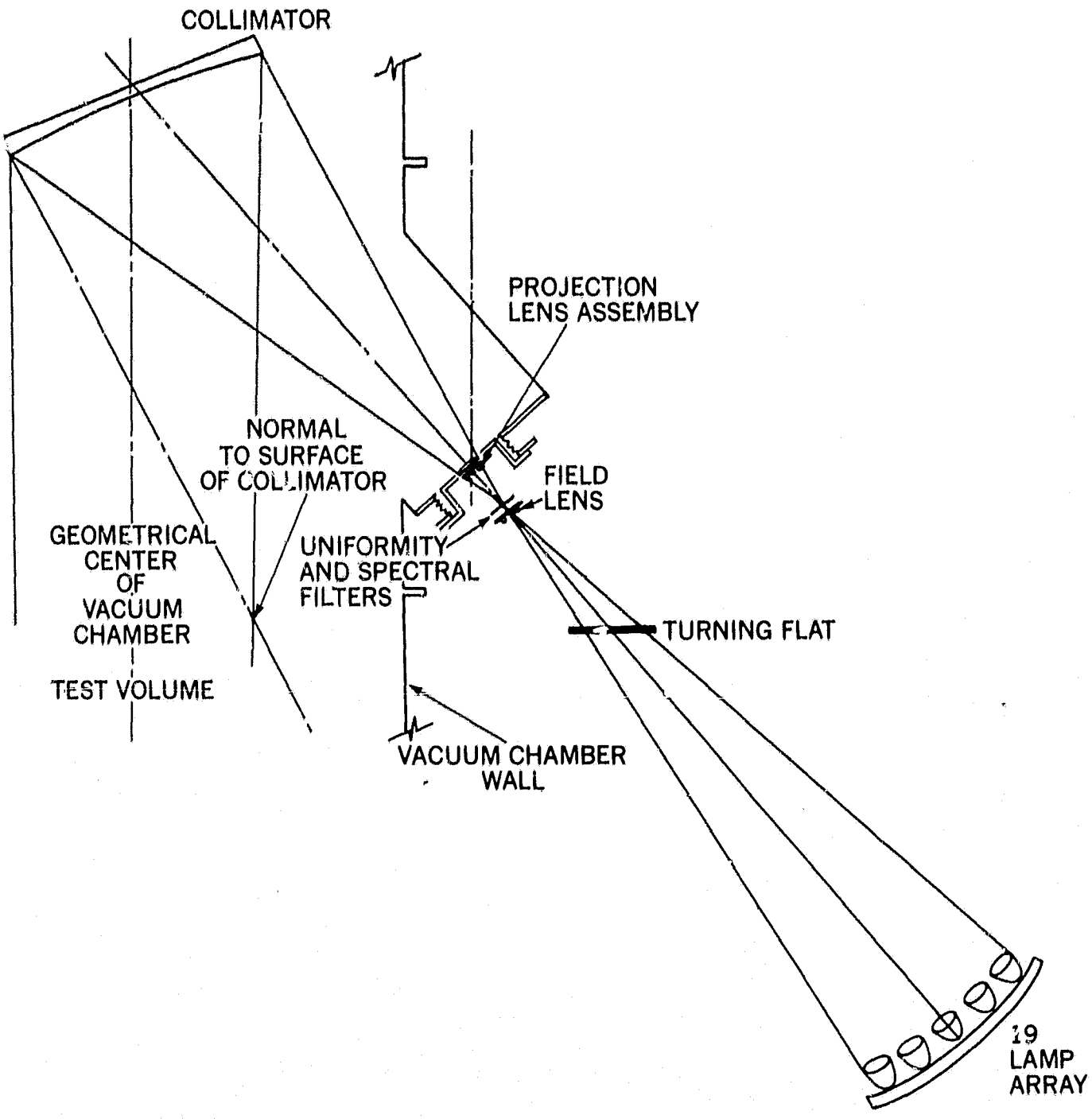

Figure 4. Optical Schematic of Solar Simulator Before Modification

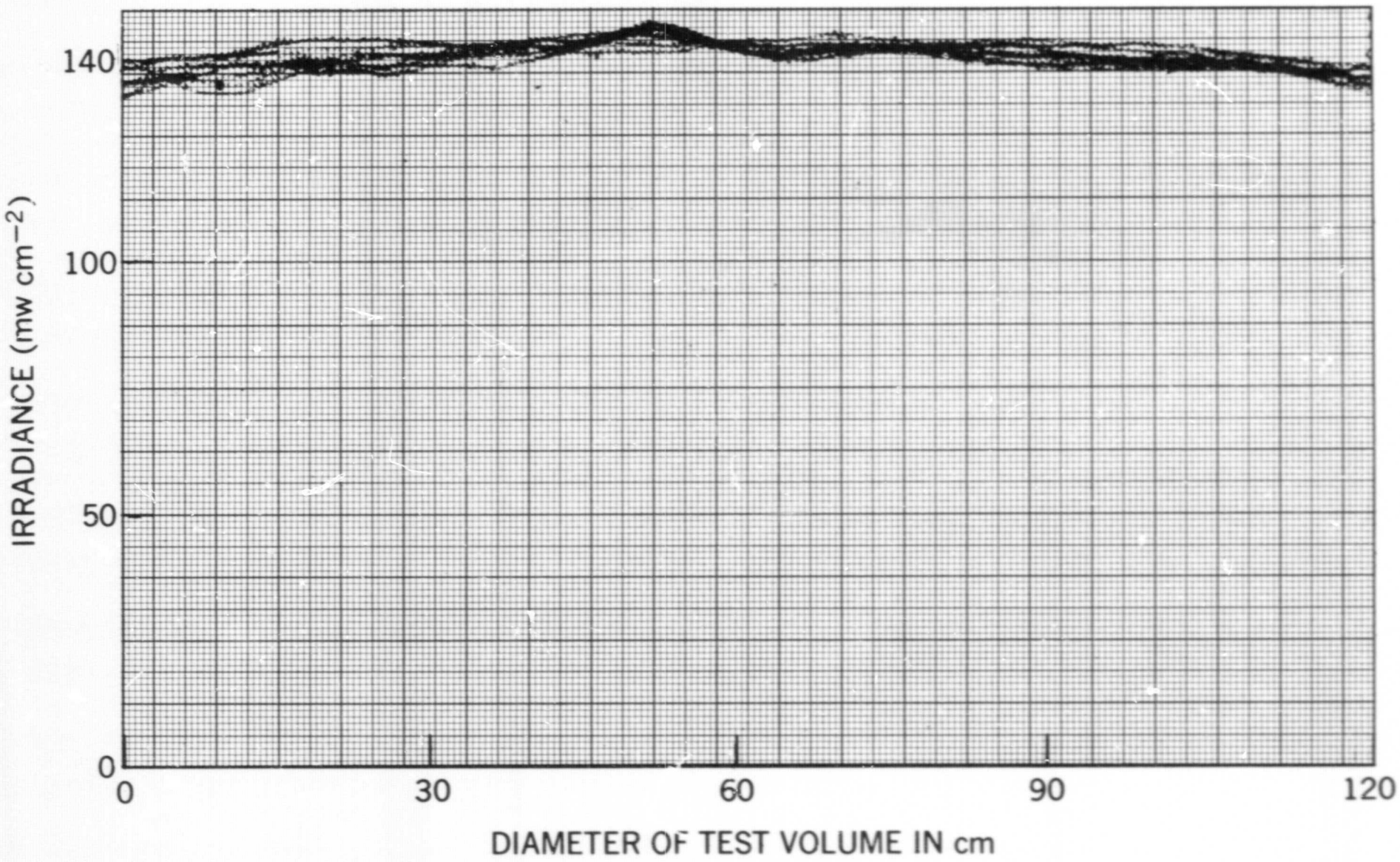

Figure 5. Uniformity of Irradiance Within Test Volume of Solar Simulator Before Modification

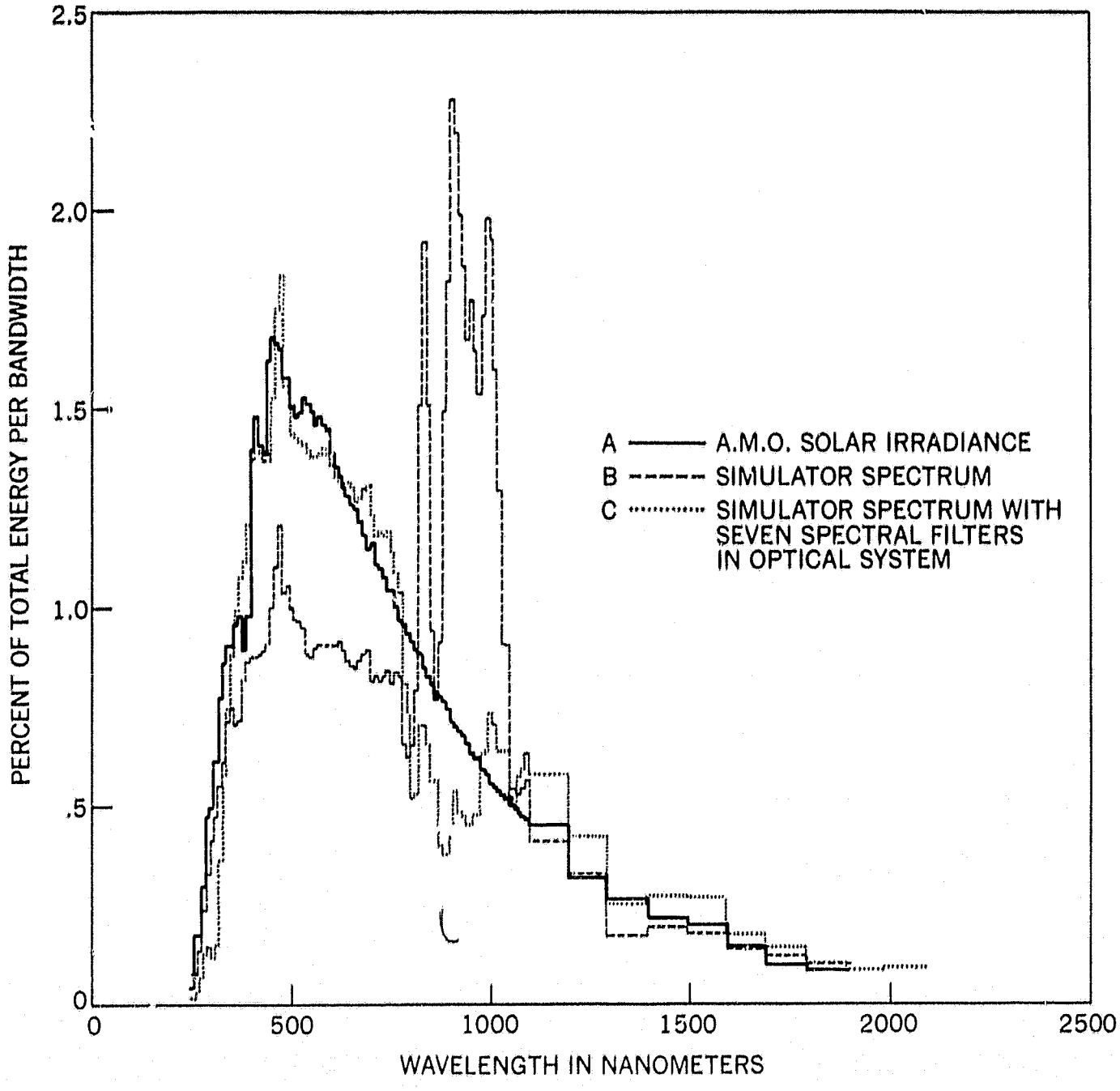

Figure 6. Spectra of Simulator Before Modification

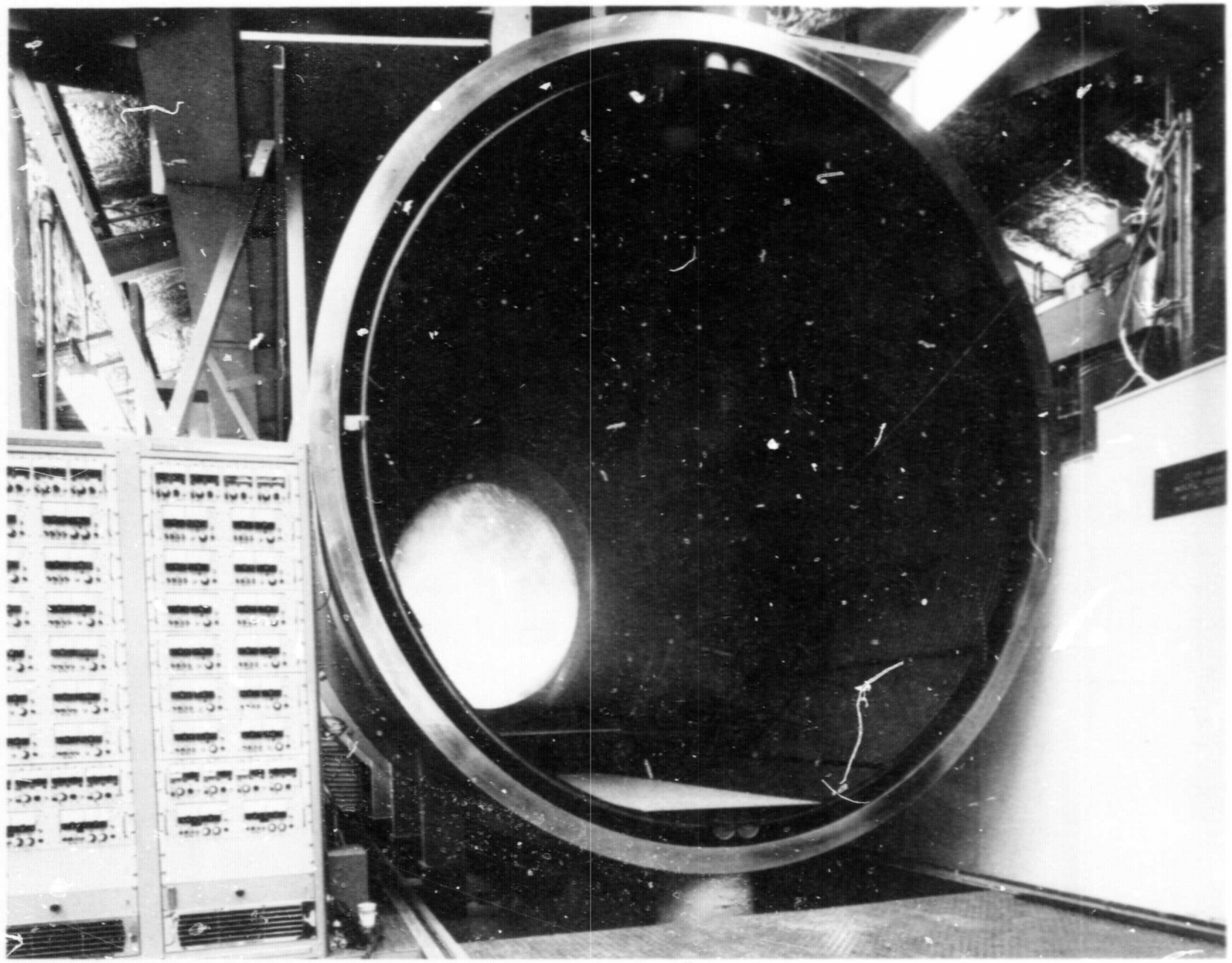

Figure 7. Collimator of Solar Simulator

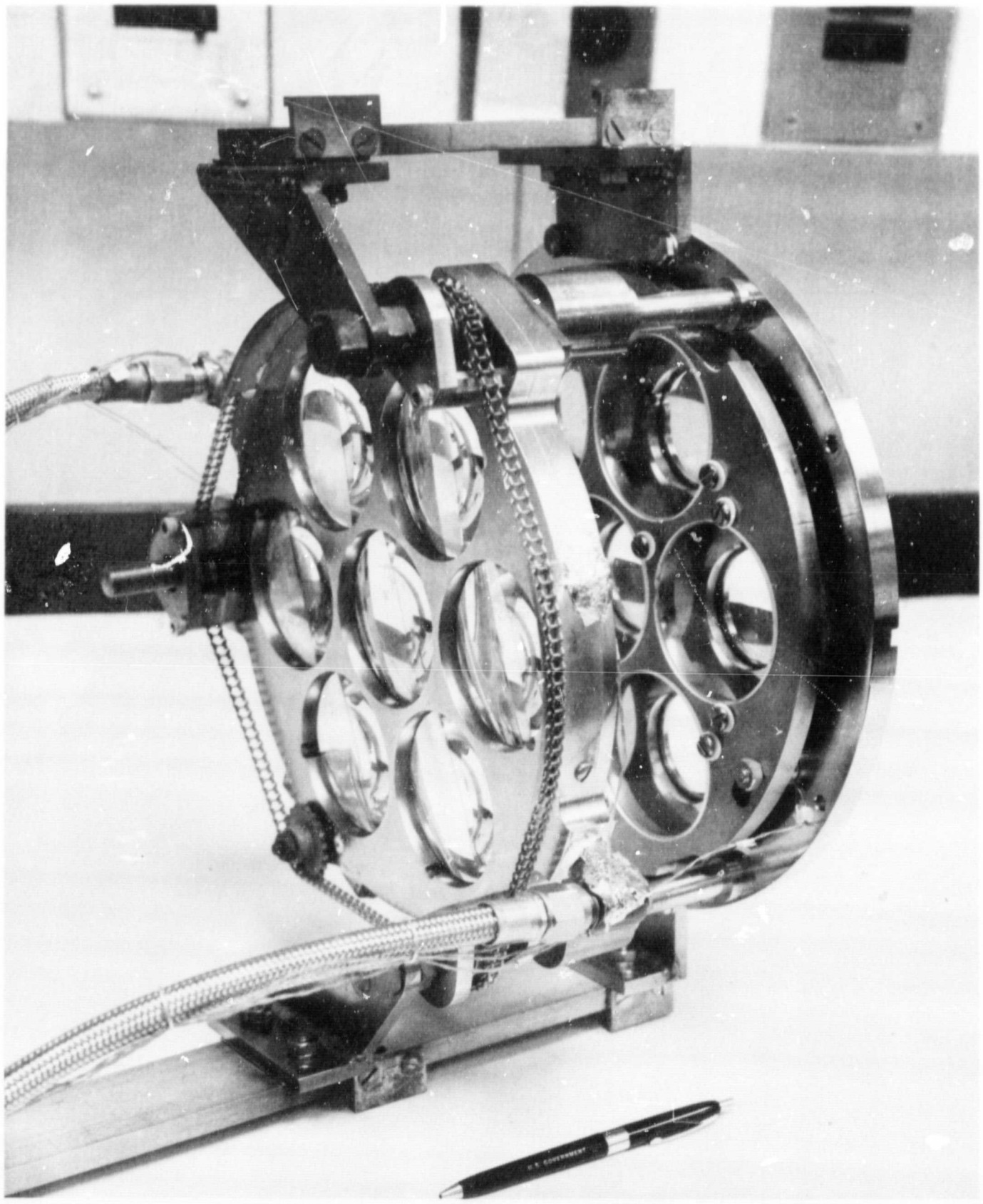

Figure 8. Field-Projection Lens Array for Modified System

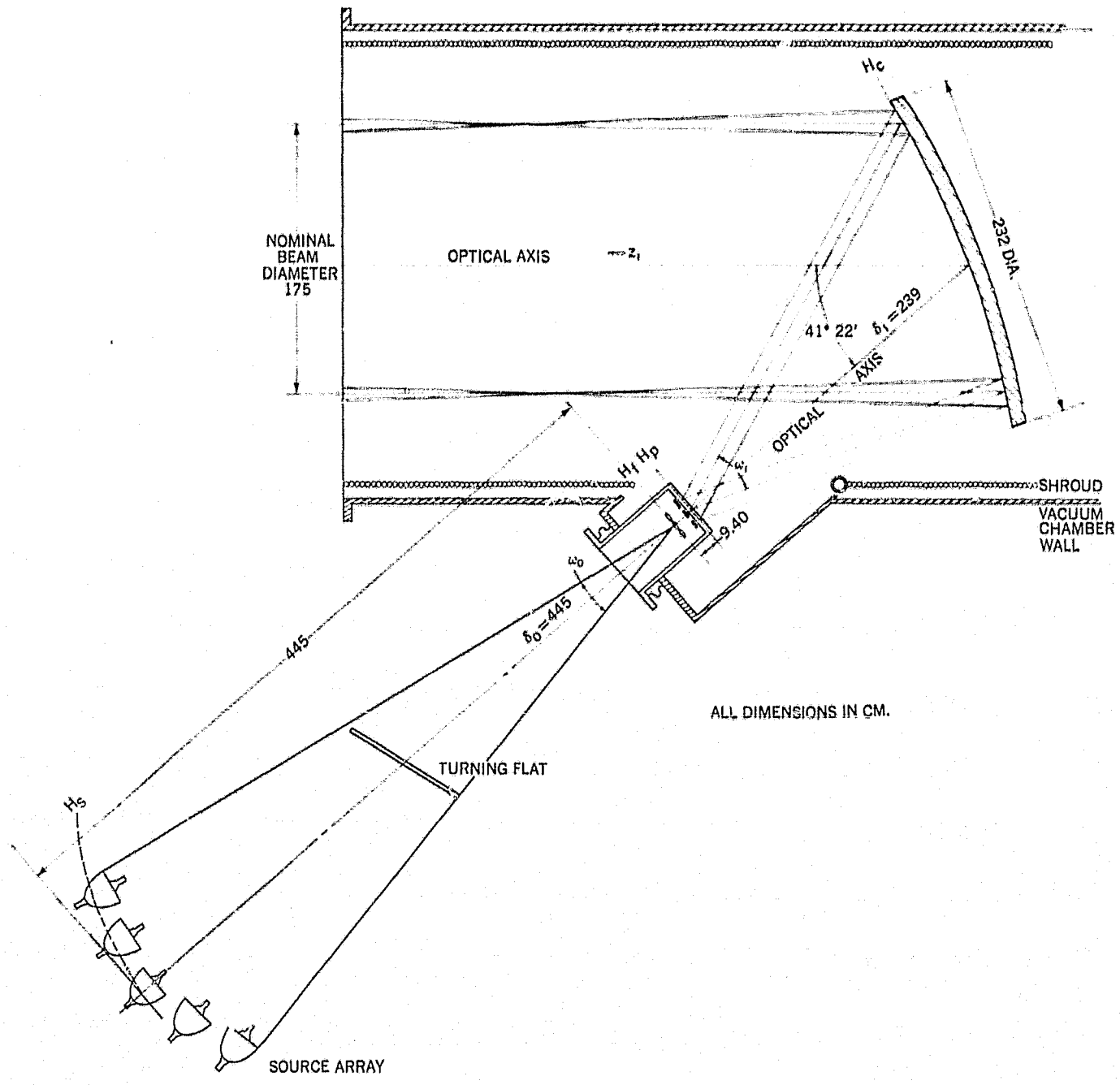

Figure 9. Optical Schematic of Solar Simulator After Modification

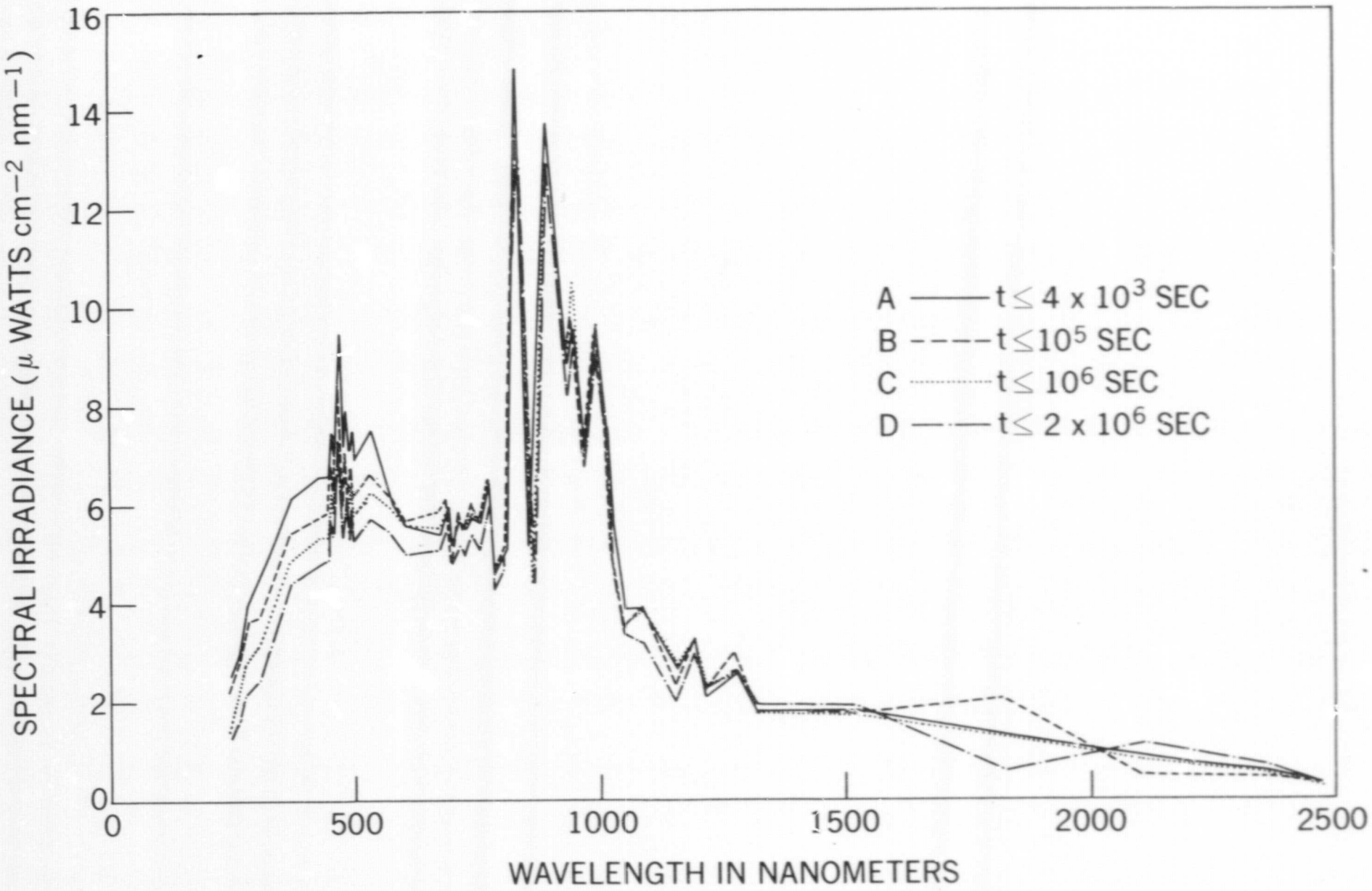

Figure 10, Spectra of 4.2 kw Xenon Arc Source as a Function of Operation Time

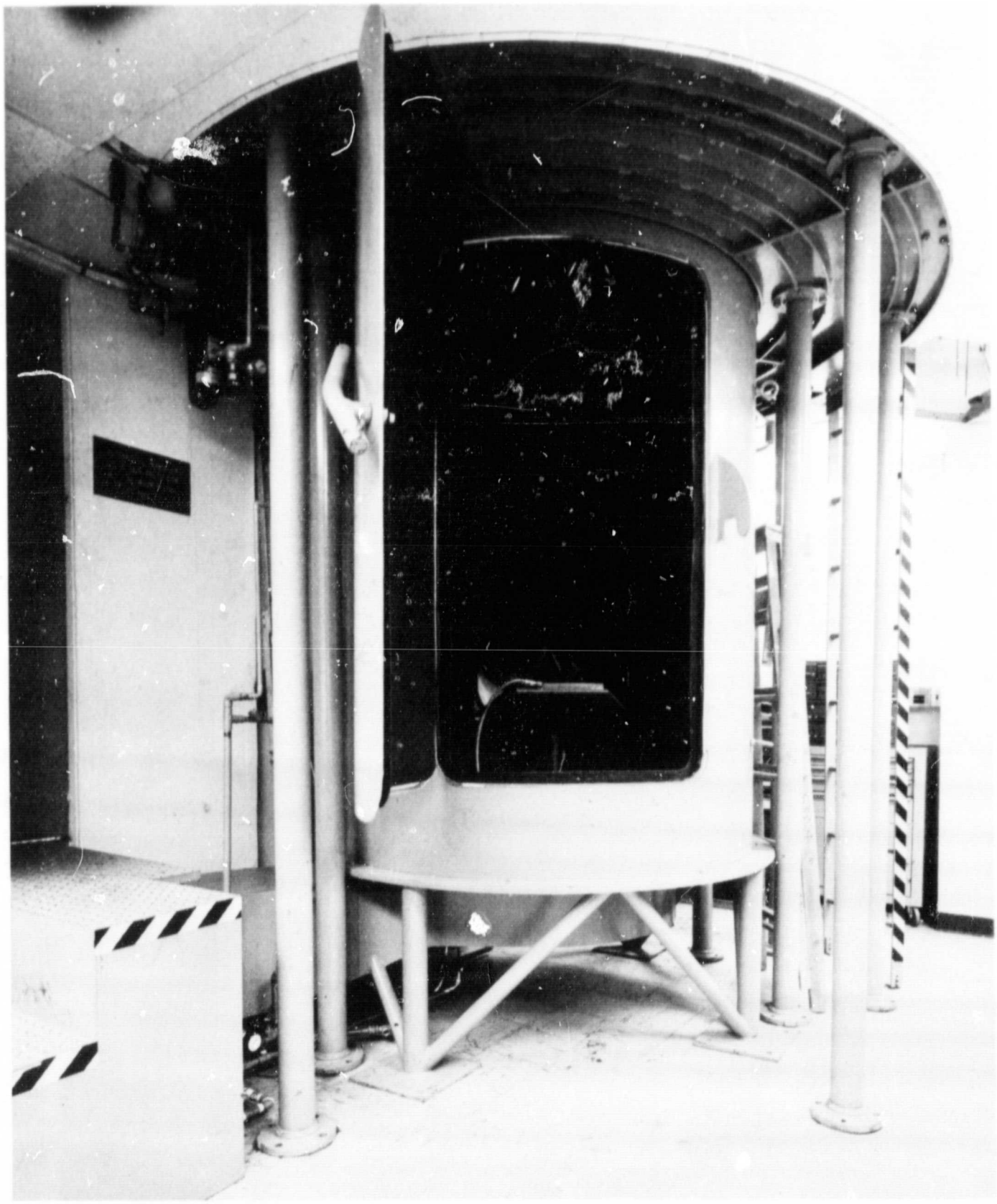

Figure 11. Simulator Source Enclosure

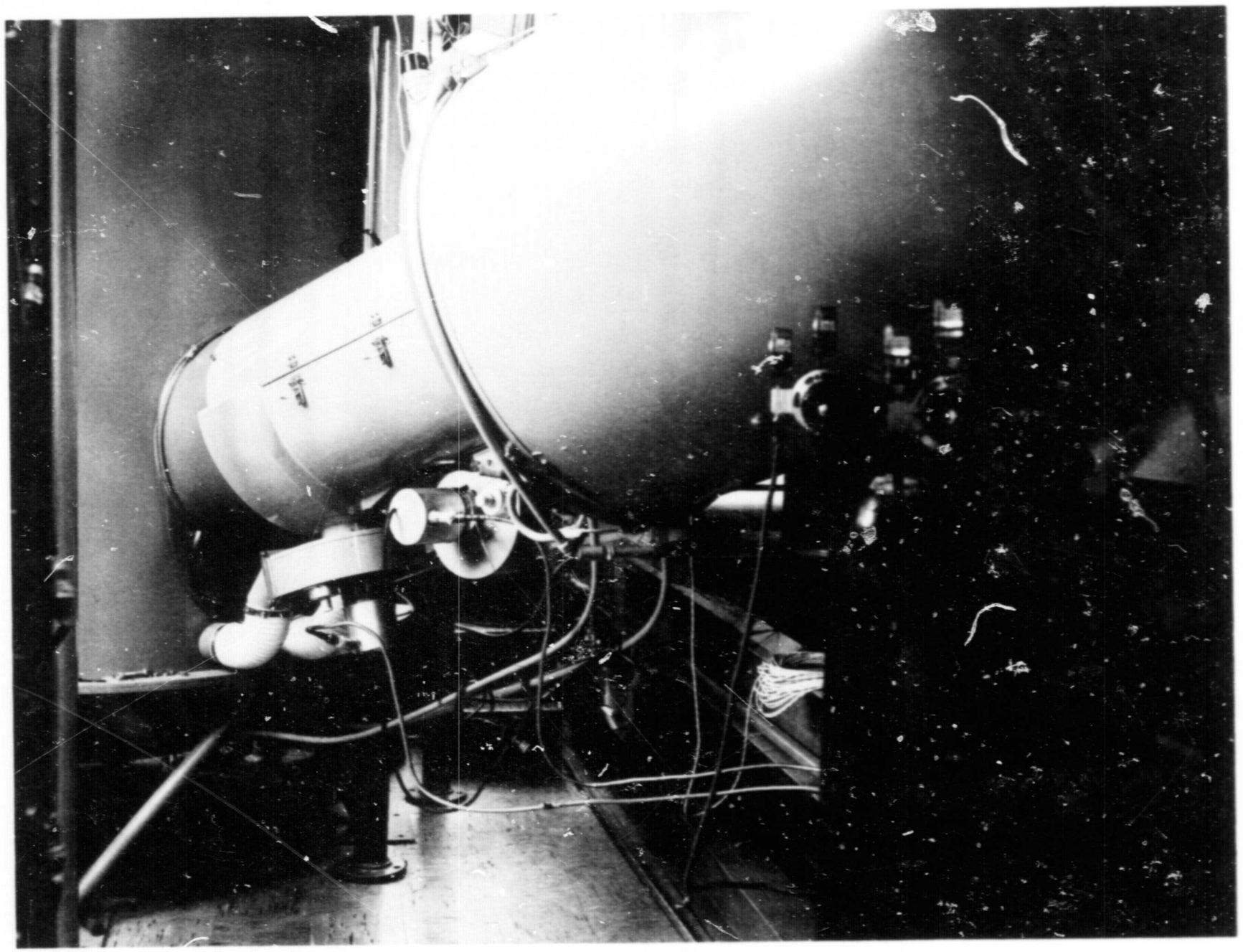

Figure 12. Transition Tube With Cover Installed

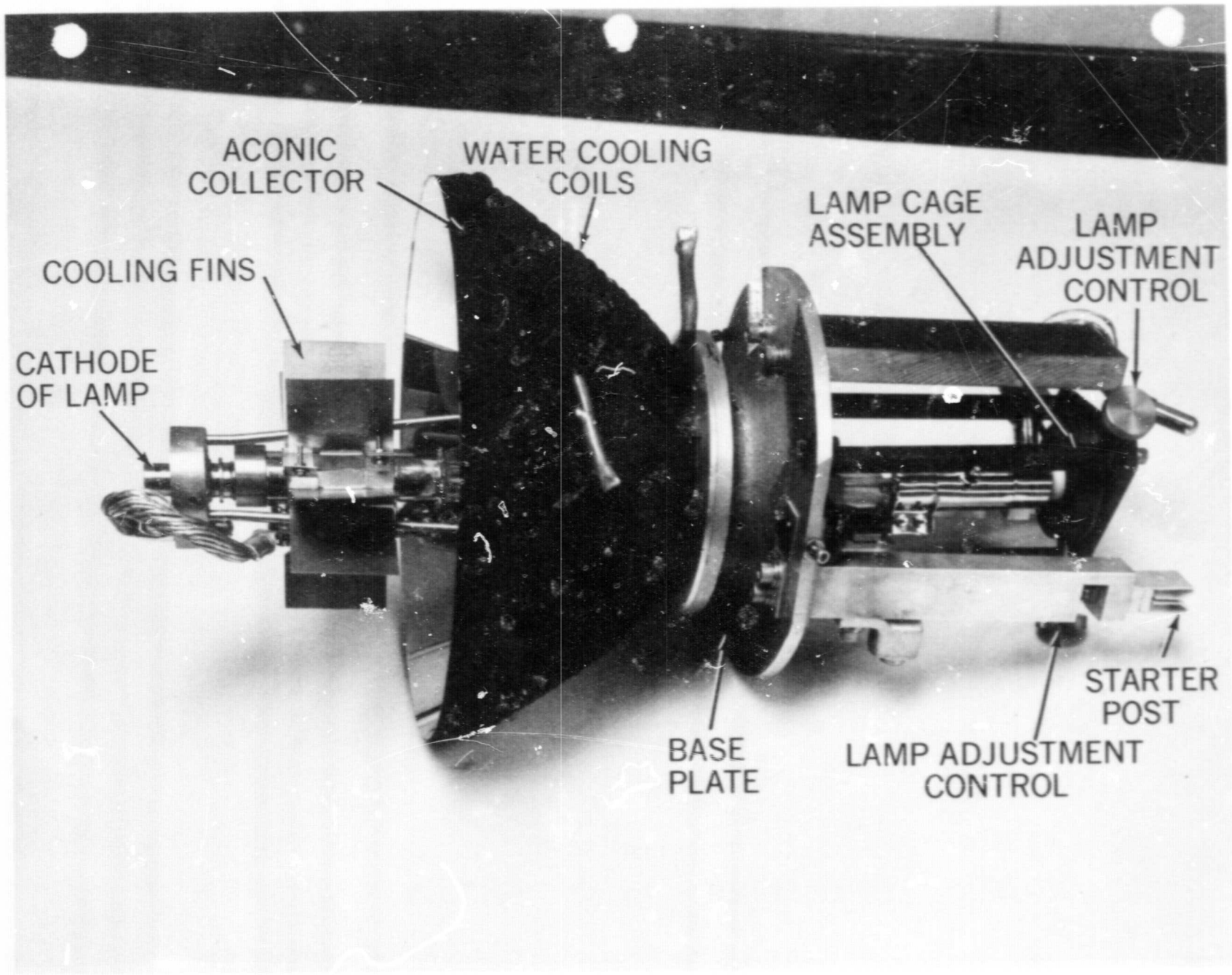

Figure 13. Radiant Energy Source Assembly Module

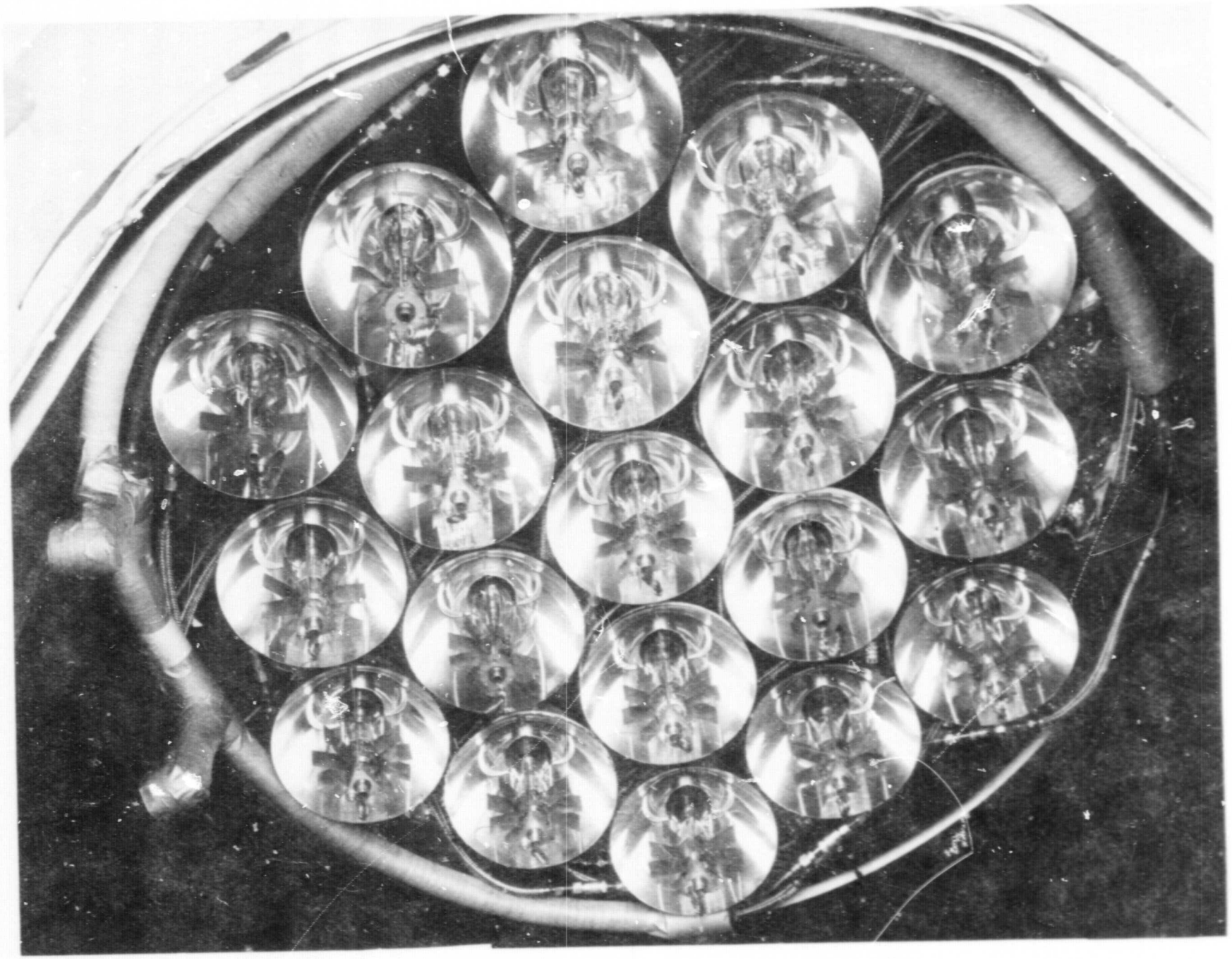

Figure 14. Radiant Energy Soruce Array Installed in Optical System

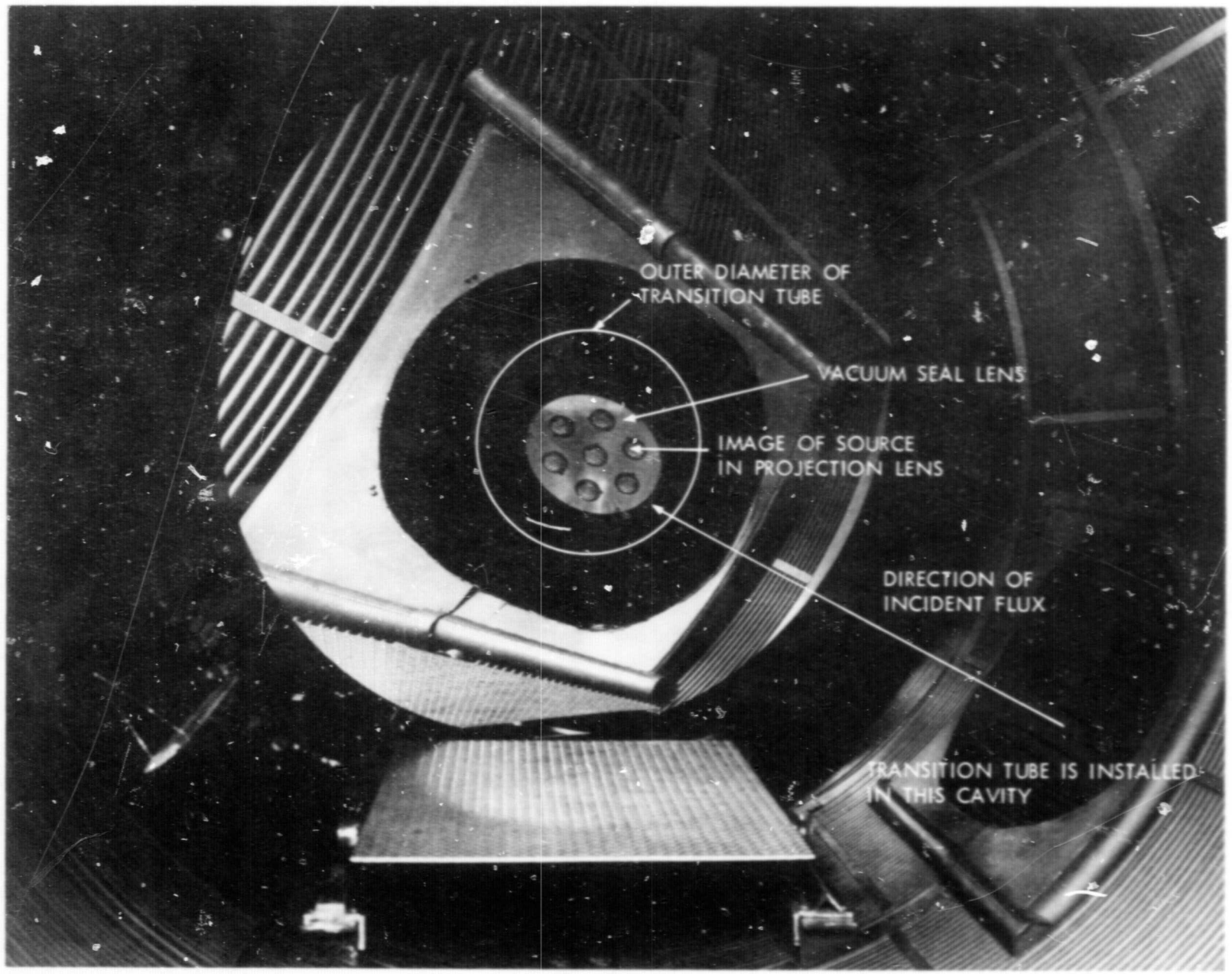

Figure 15. Vacuum-Atmosphere Transition Tube Installed in System

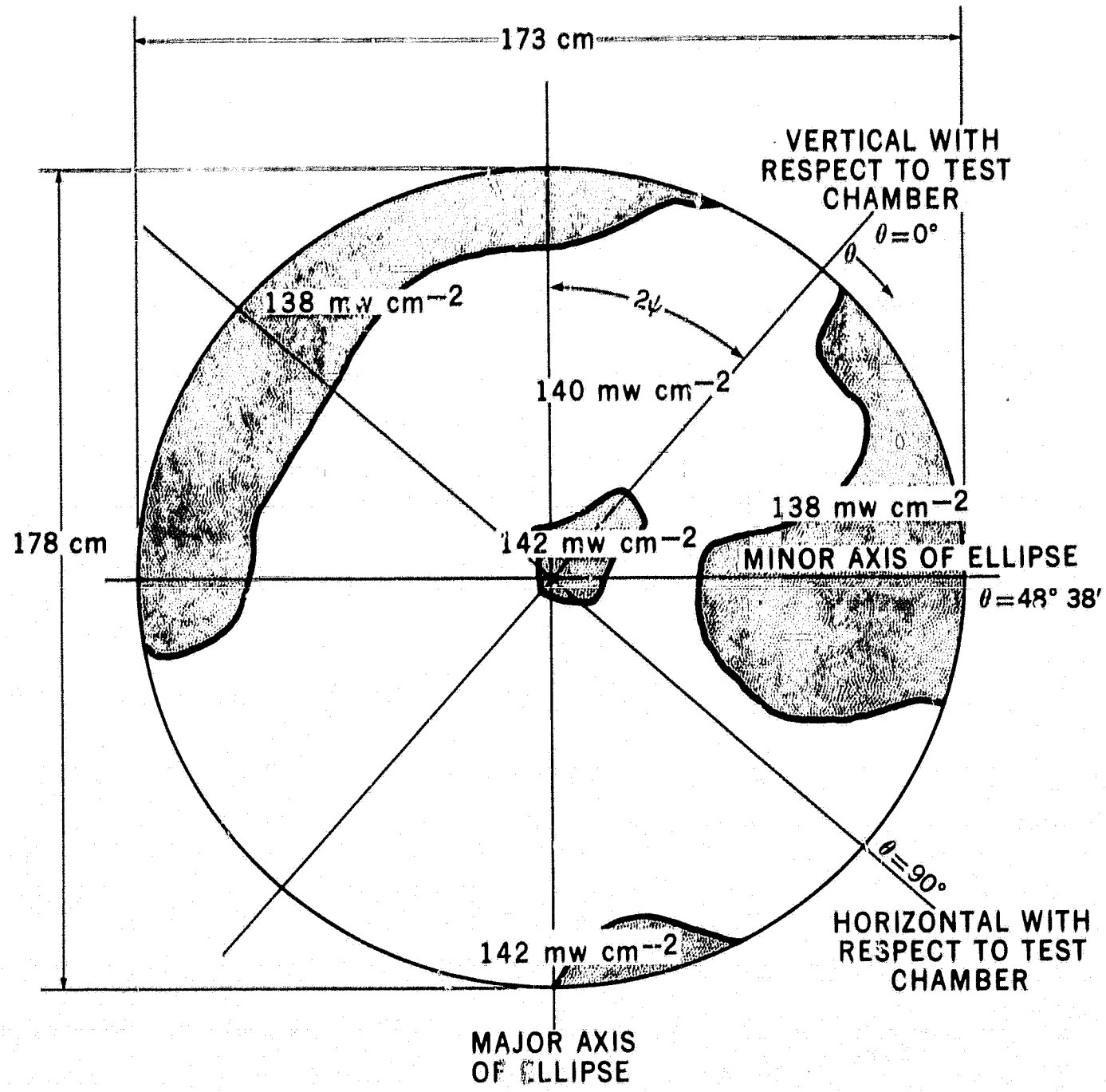

Figure 16. Contour Representation of Irradiance at z = 250 cm

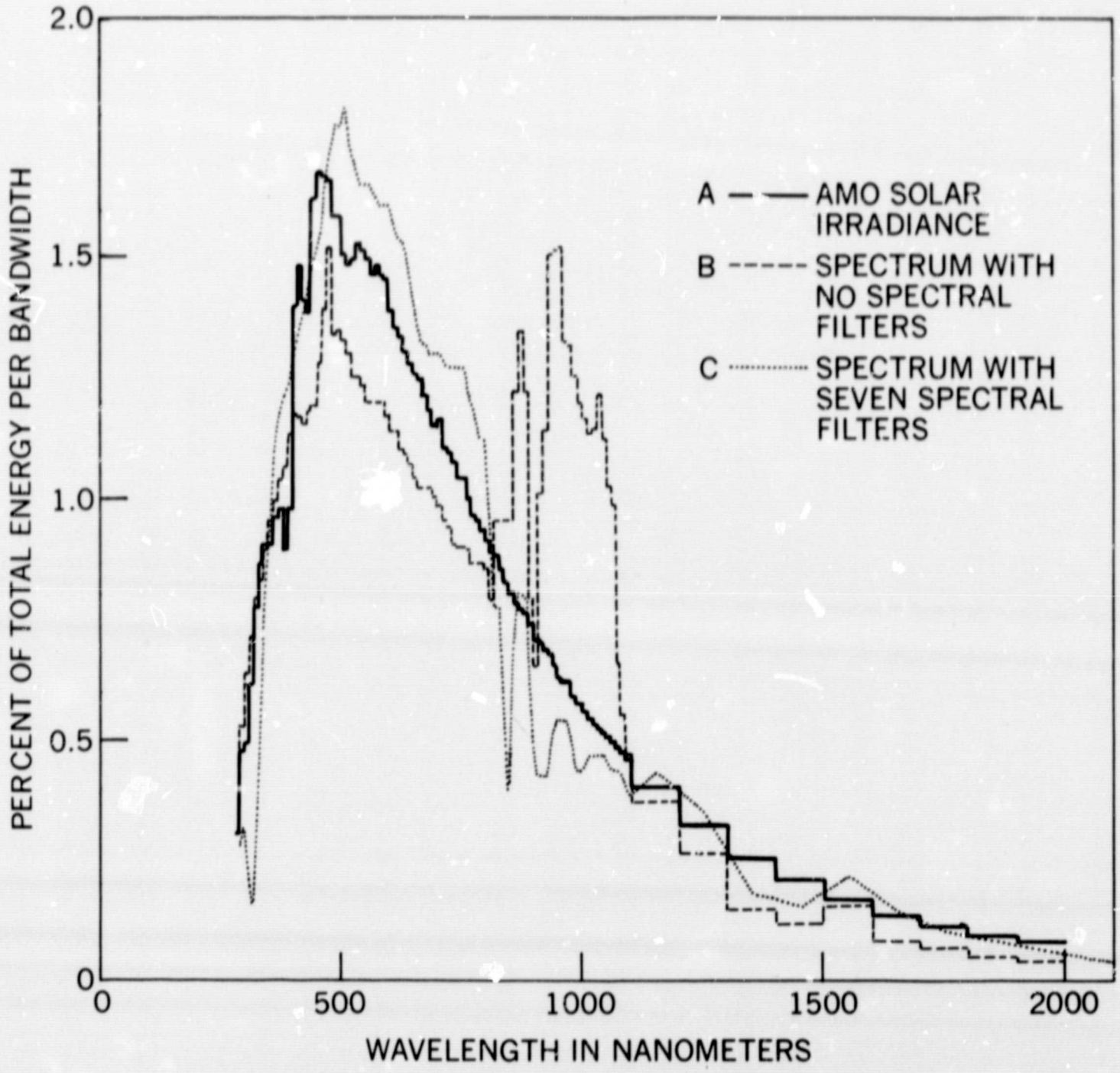

Figure 17. Spectra of Modified Simulator

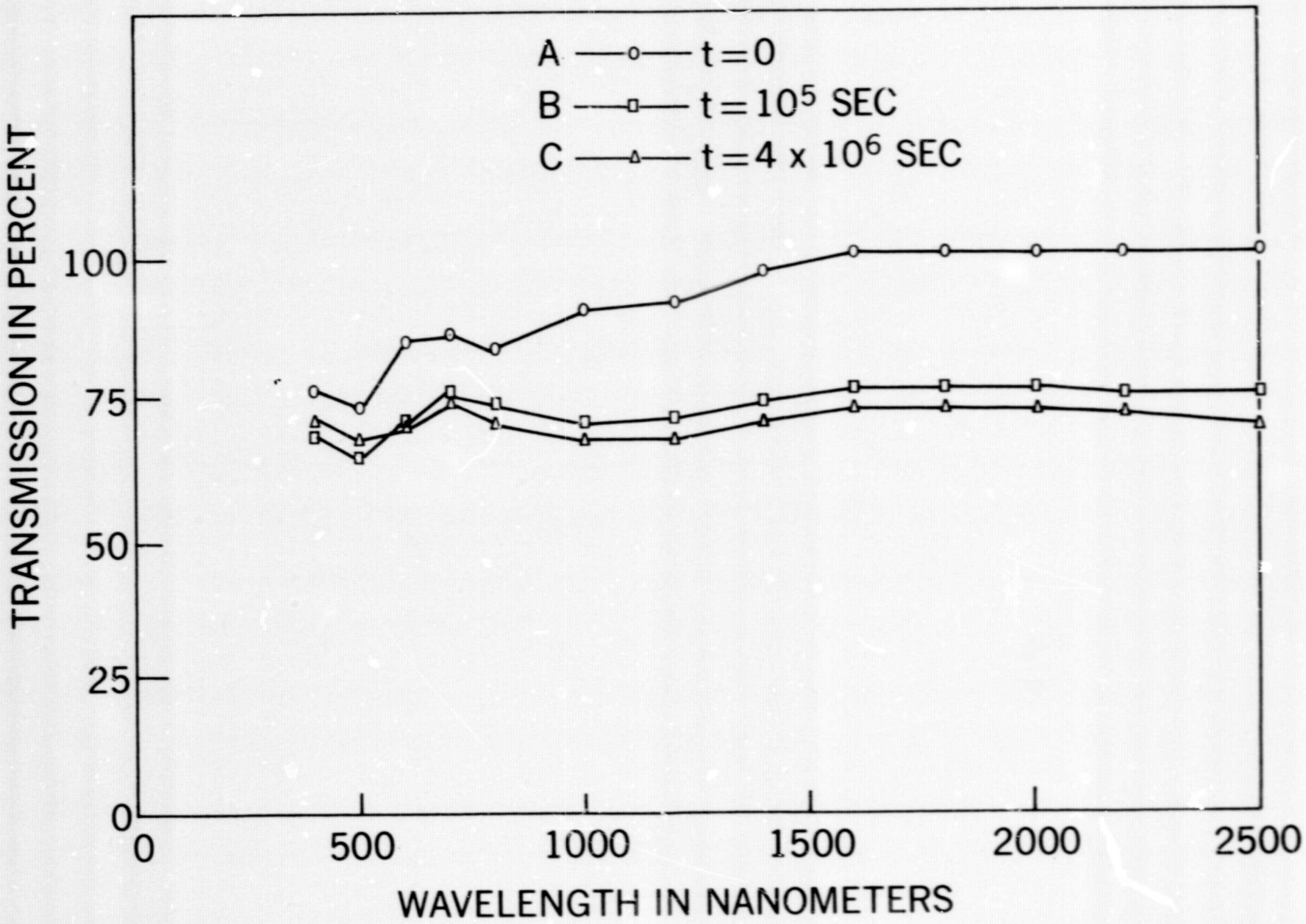

Figure 18. Spectral Transmission of Typical Uniformity Filter

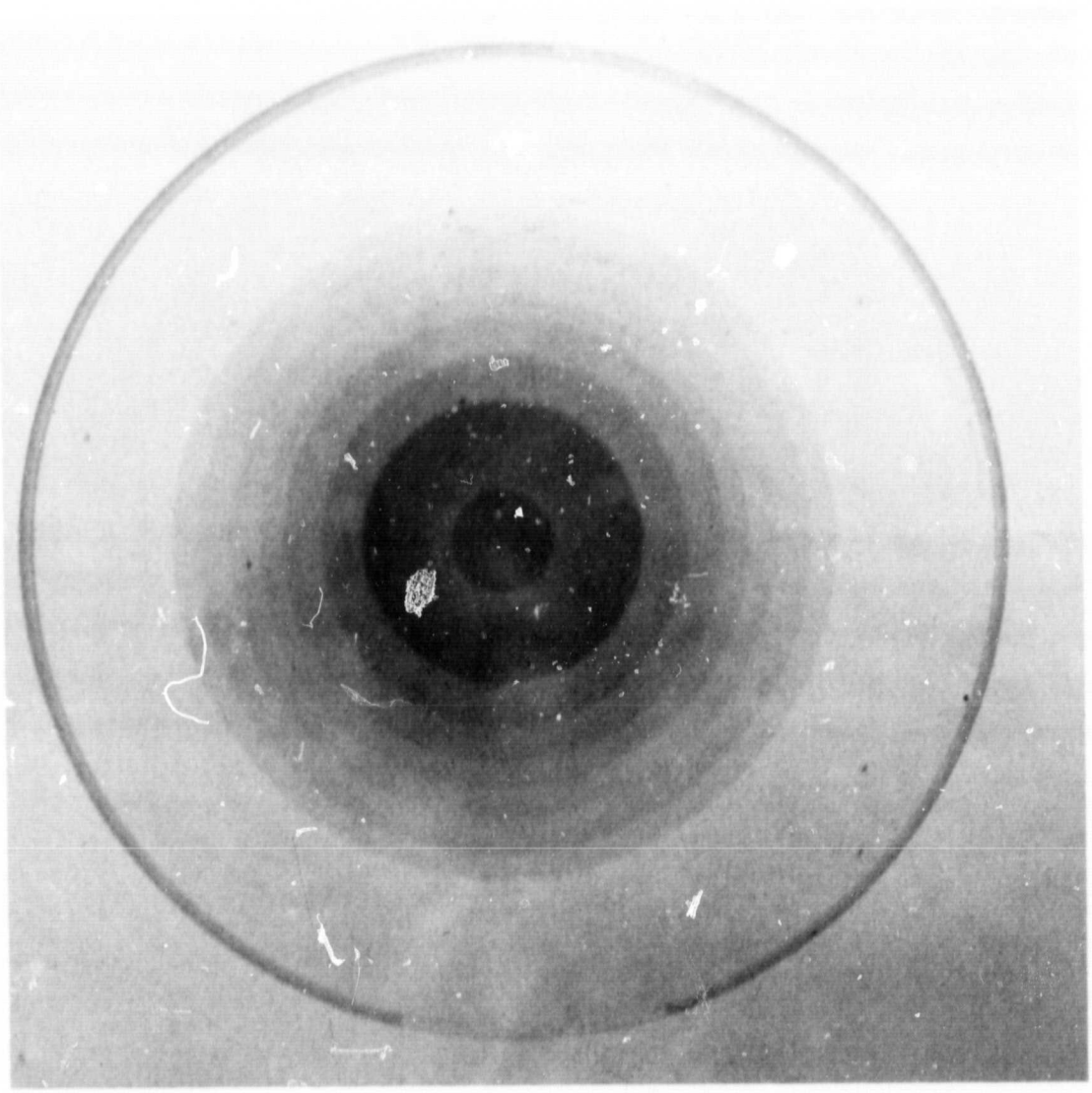

Figure 19. Uniformity Filter For Modified Simulator

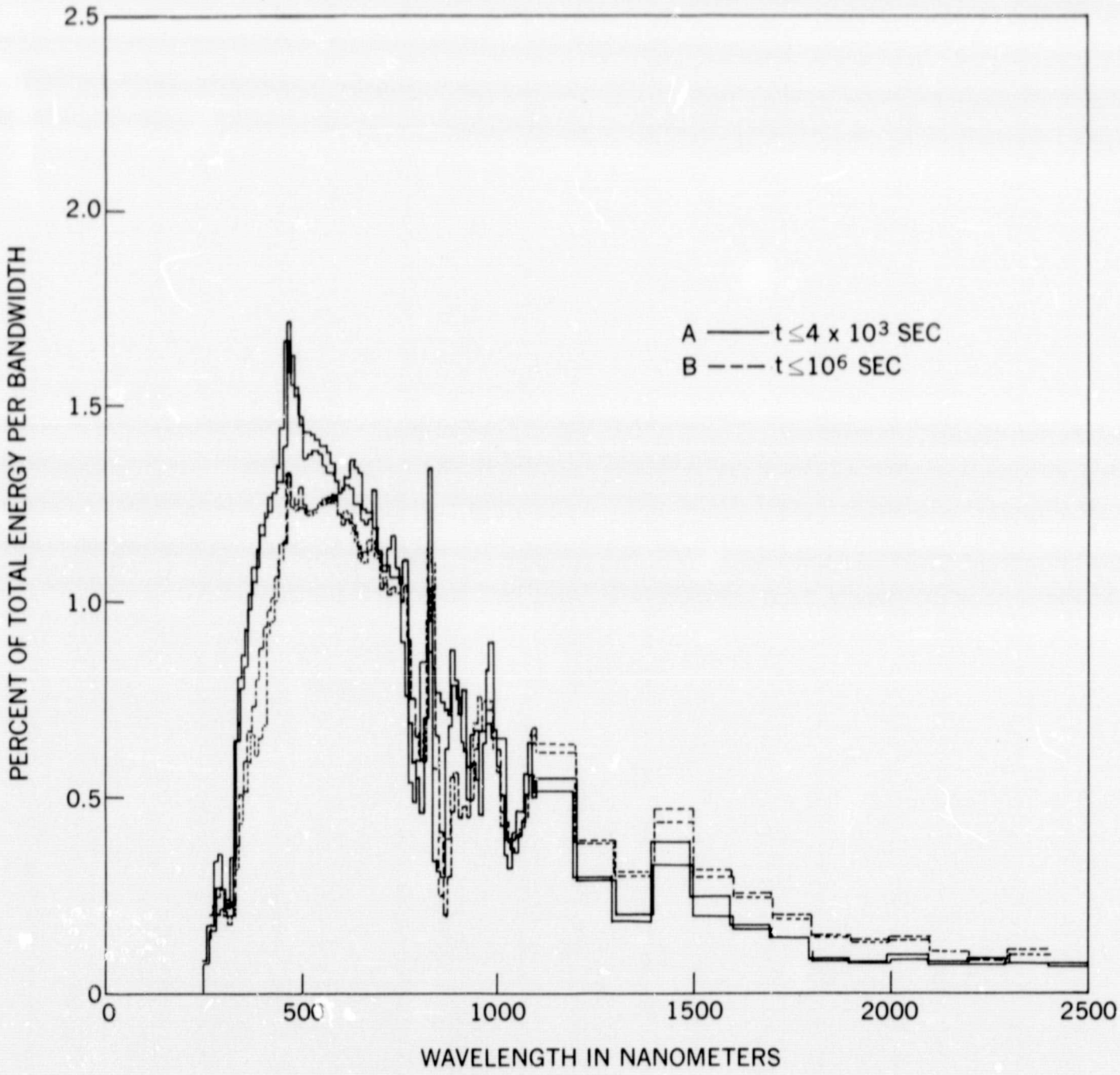

Figure 20. Spectrum Reproducibility of a Solar Simulation System as a Function of Operation Time

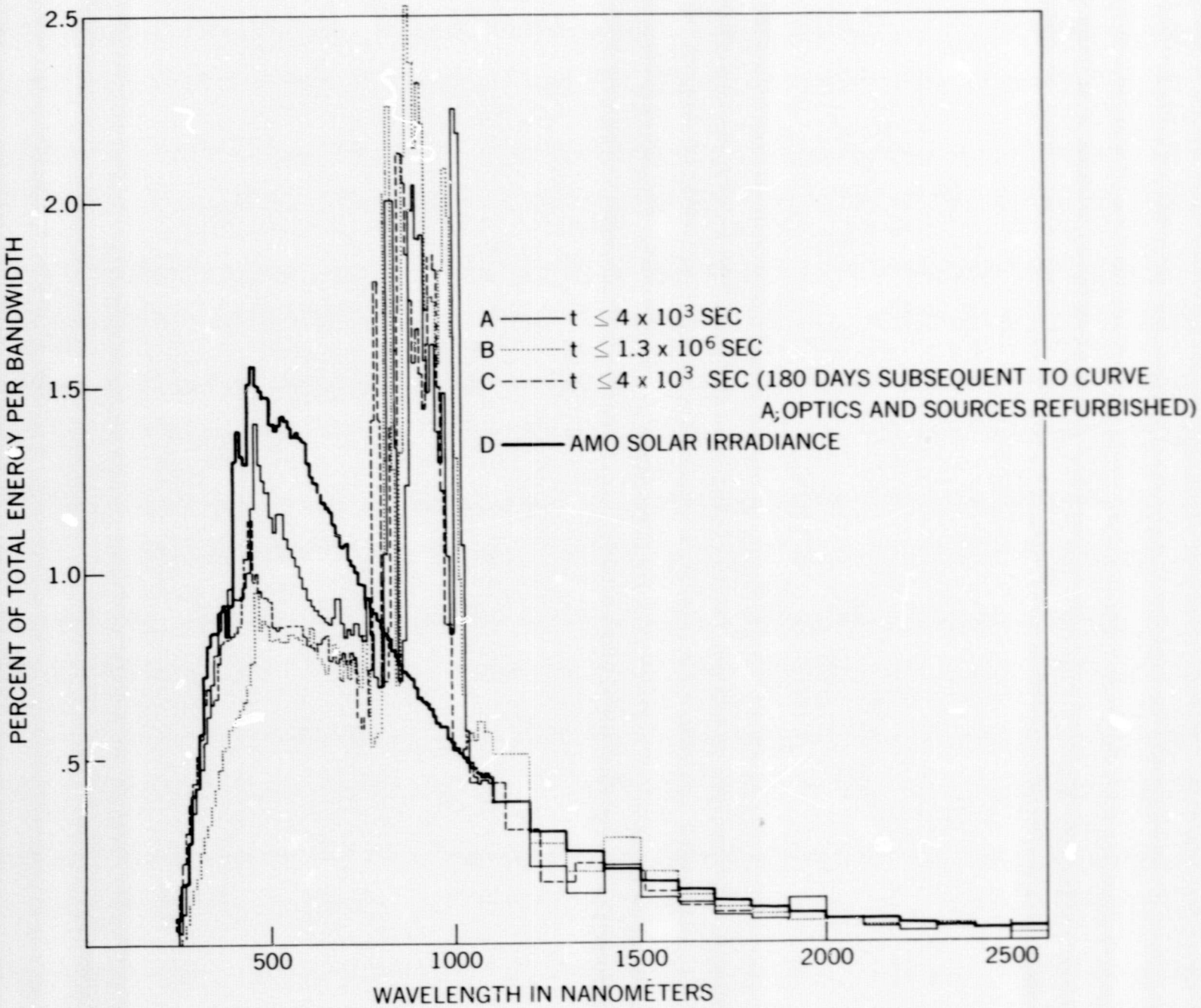

Figure 21. Spectrum Degradation With Elapsed Time of Simulator Operation Before Modification

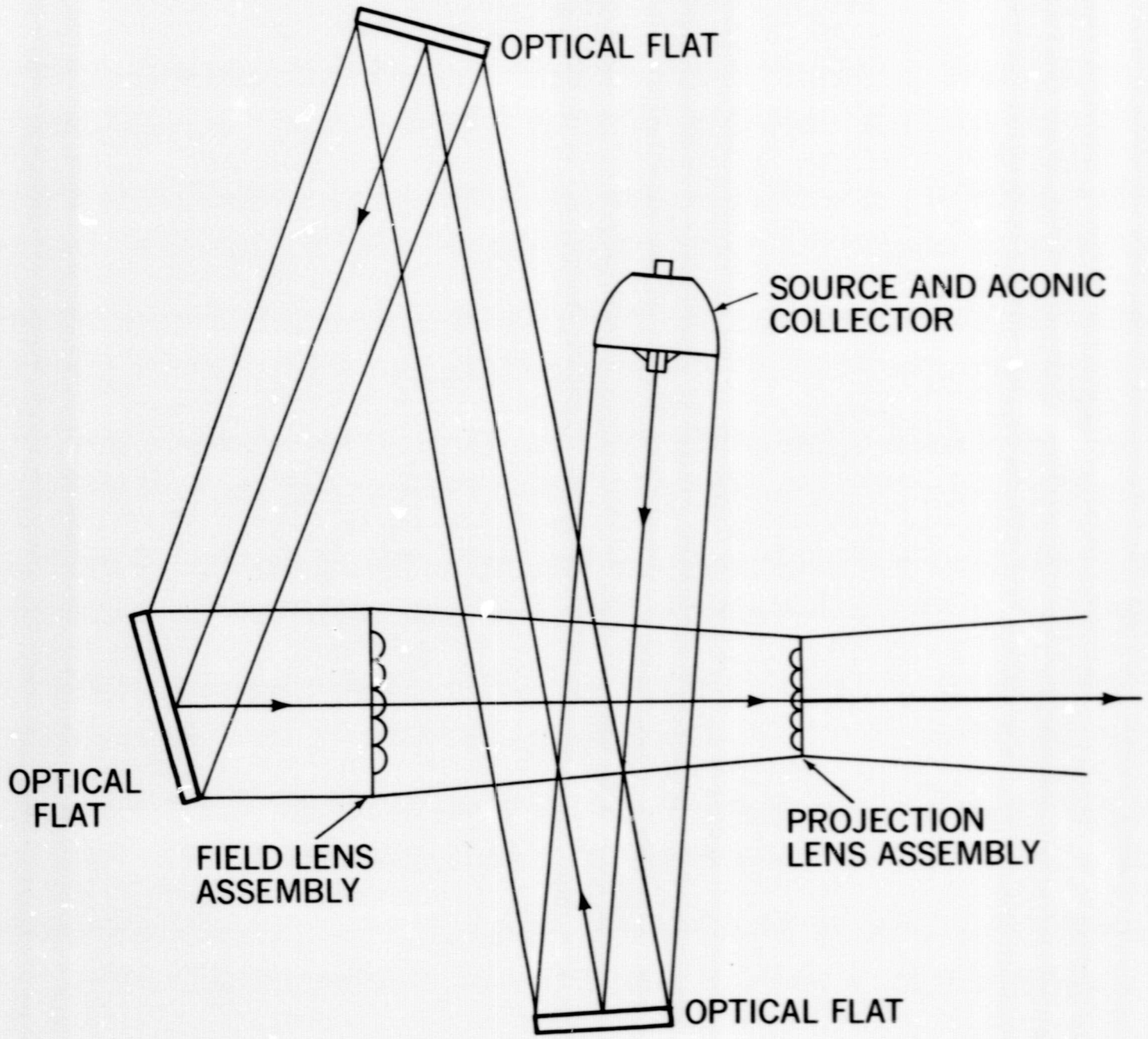

Figure 22. Optical Schematic of X-25 Solar Simulator

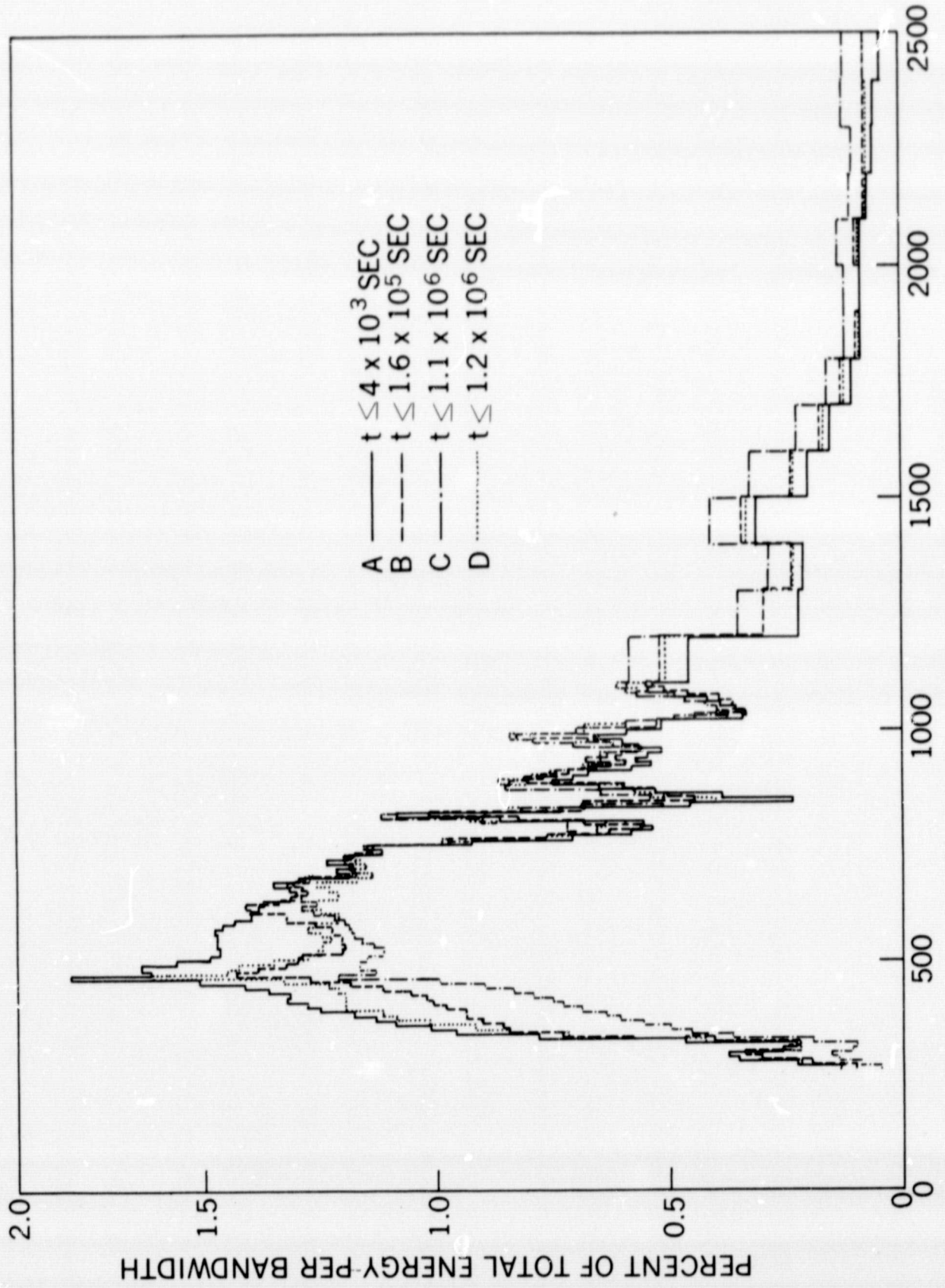

Figure 23. Spectrum Degradation With Elapsed Time of Simulator Operation for a Smaller System

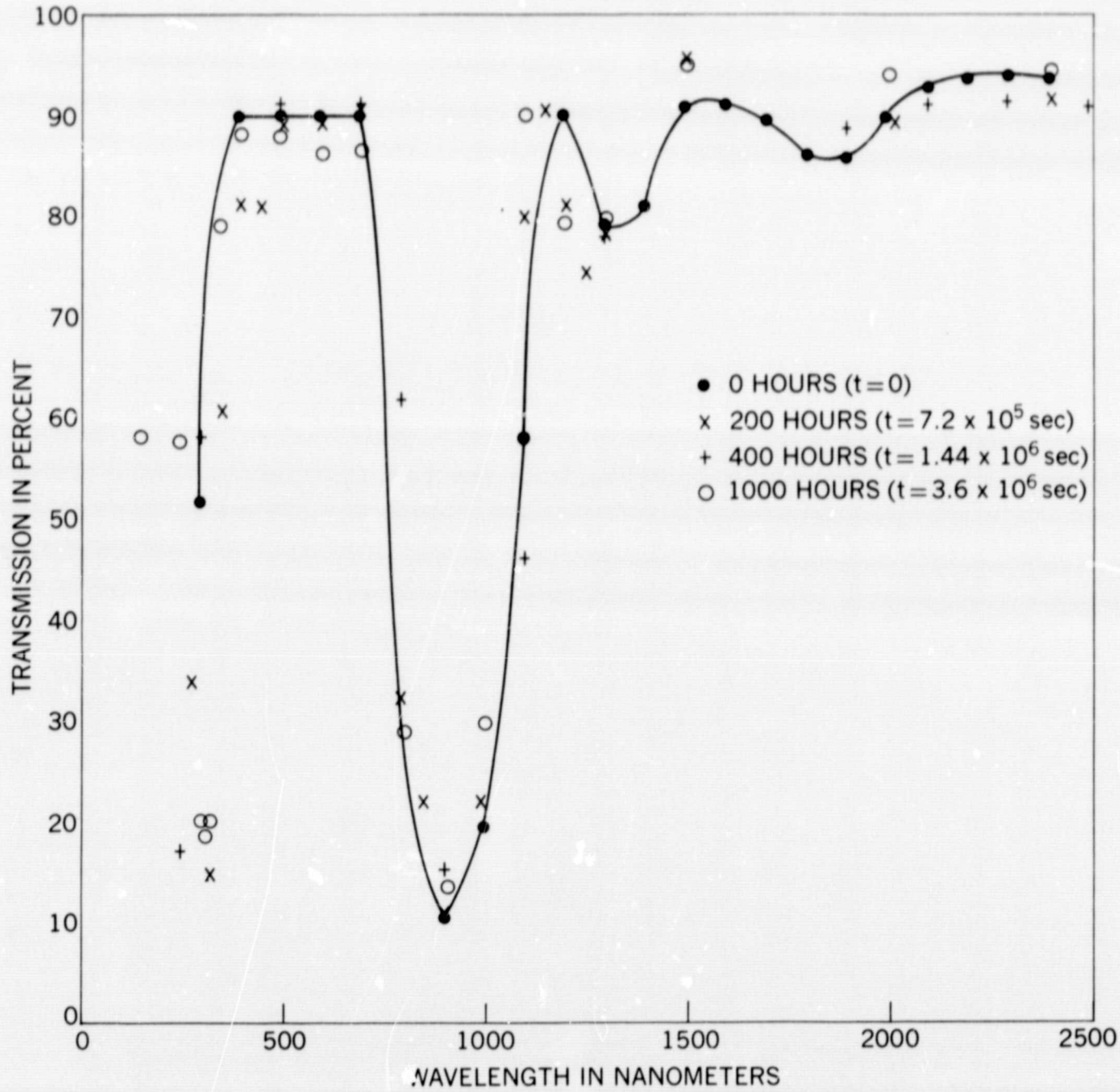

Figure 24. Spectral Transmission of Typical Spectral Filter For $\Delta t = 4 \times 10^6$ sec

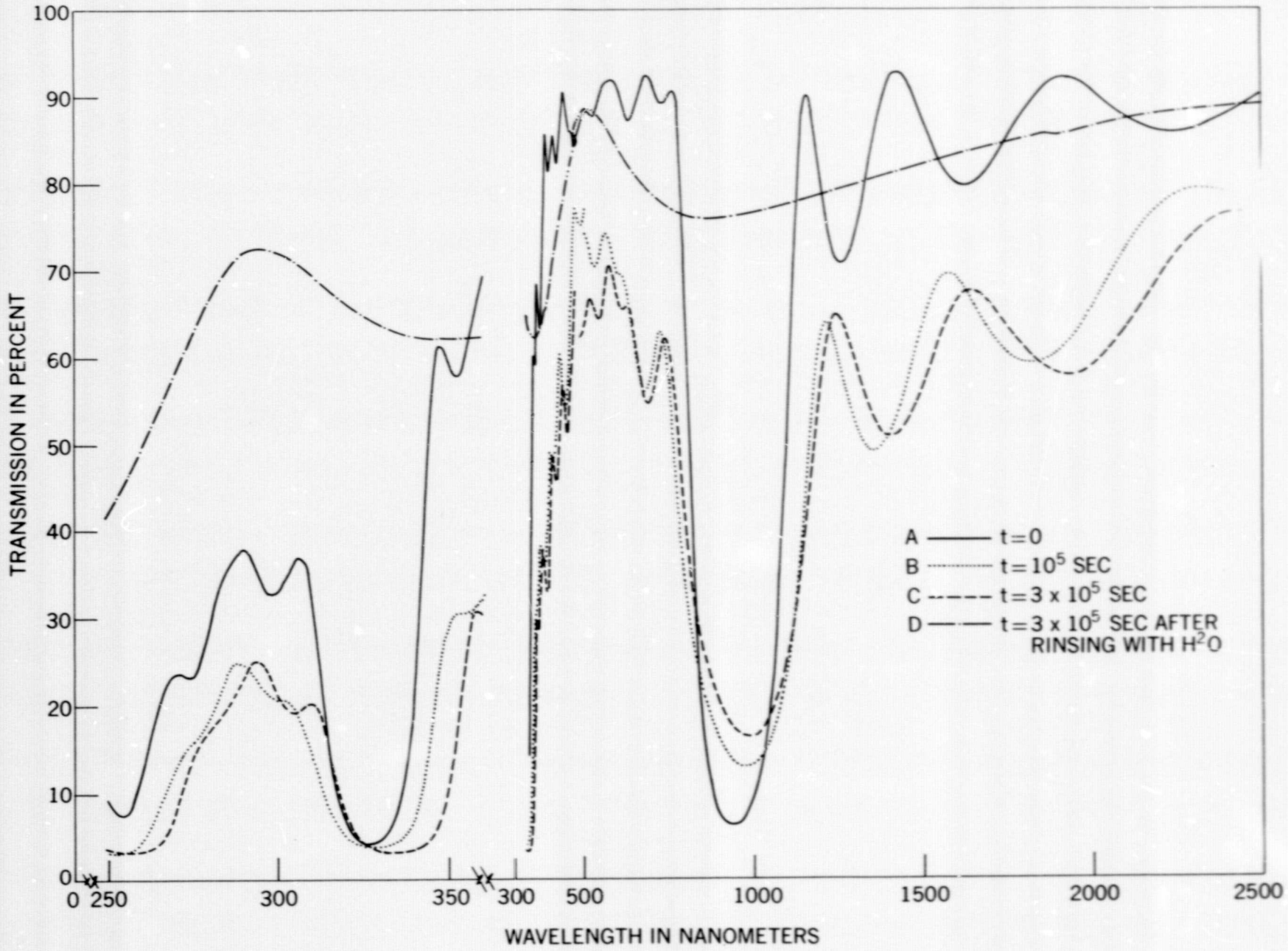

Figure 25. Effect of 540°C Temperature Upon Transmission of Spectral Filter

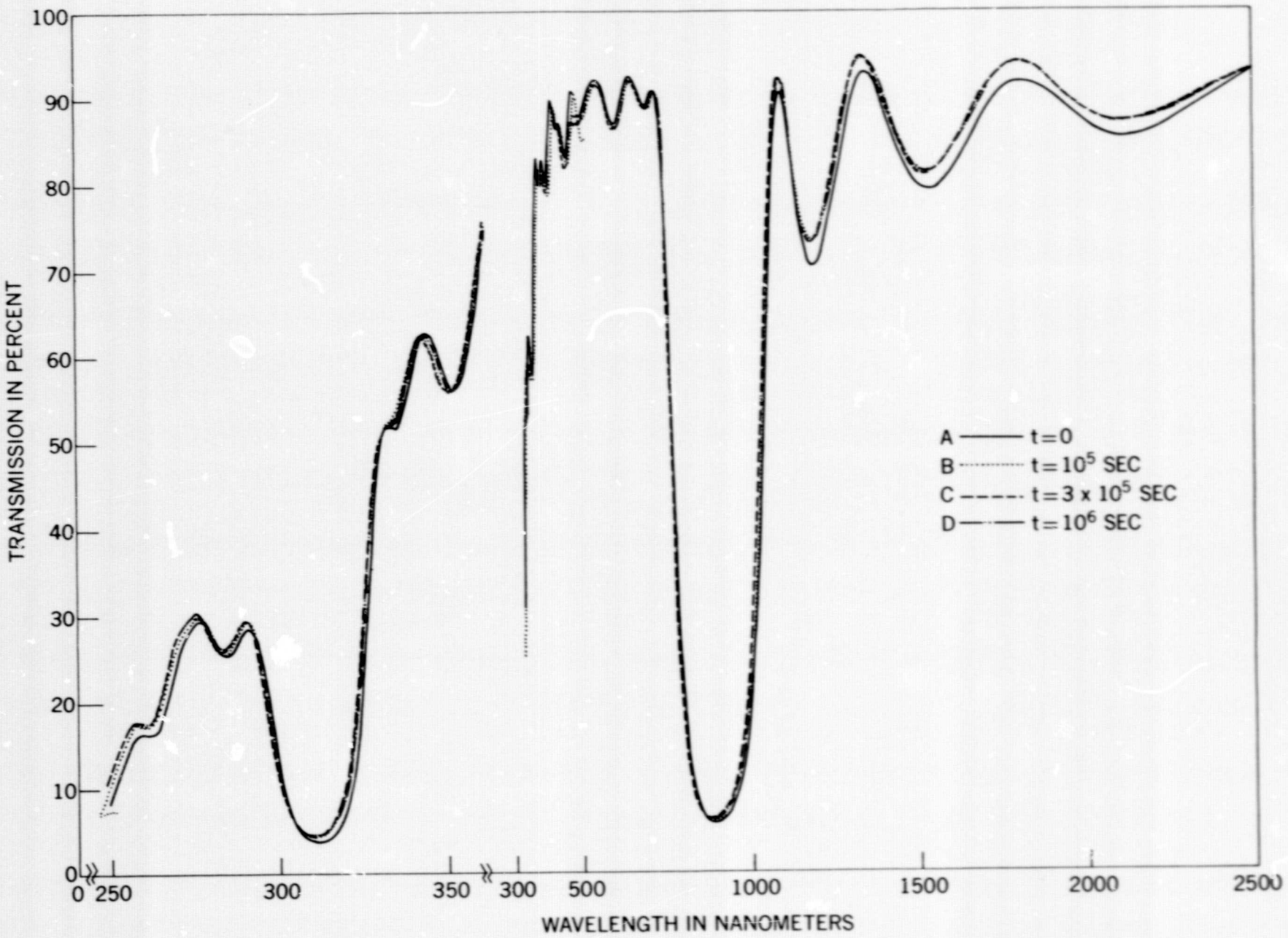

Figure 26. Effect of Ultra-Violet Irradiance Upon Transmission of Spectral Filter

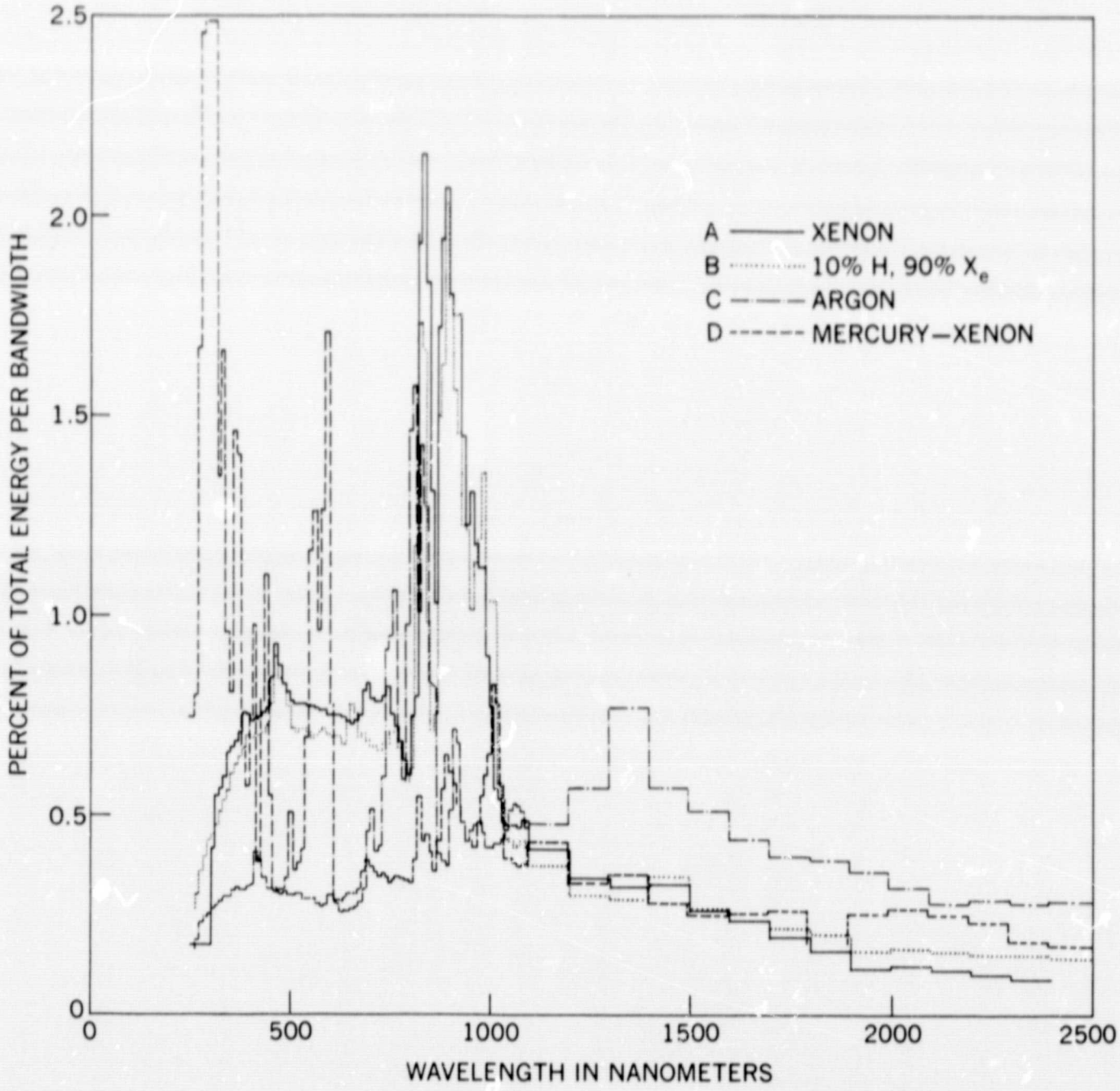

Figure 27. Spectra of Compact Arc Lamps

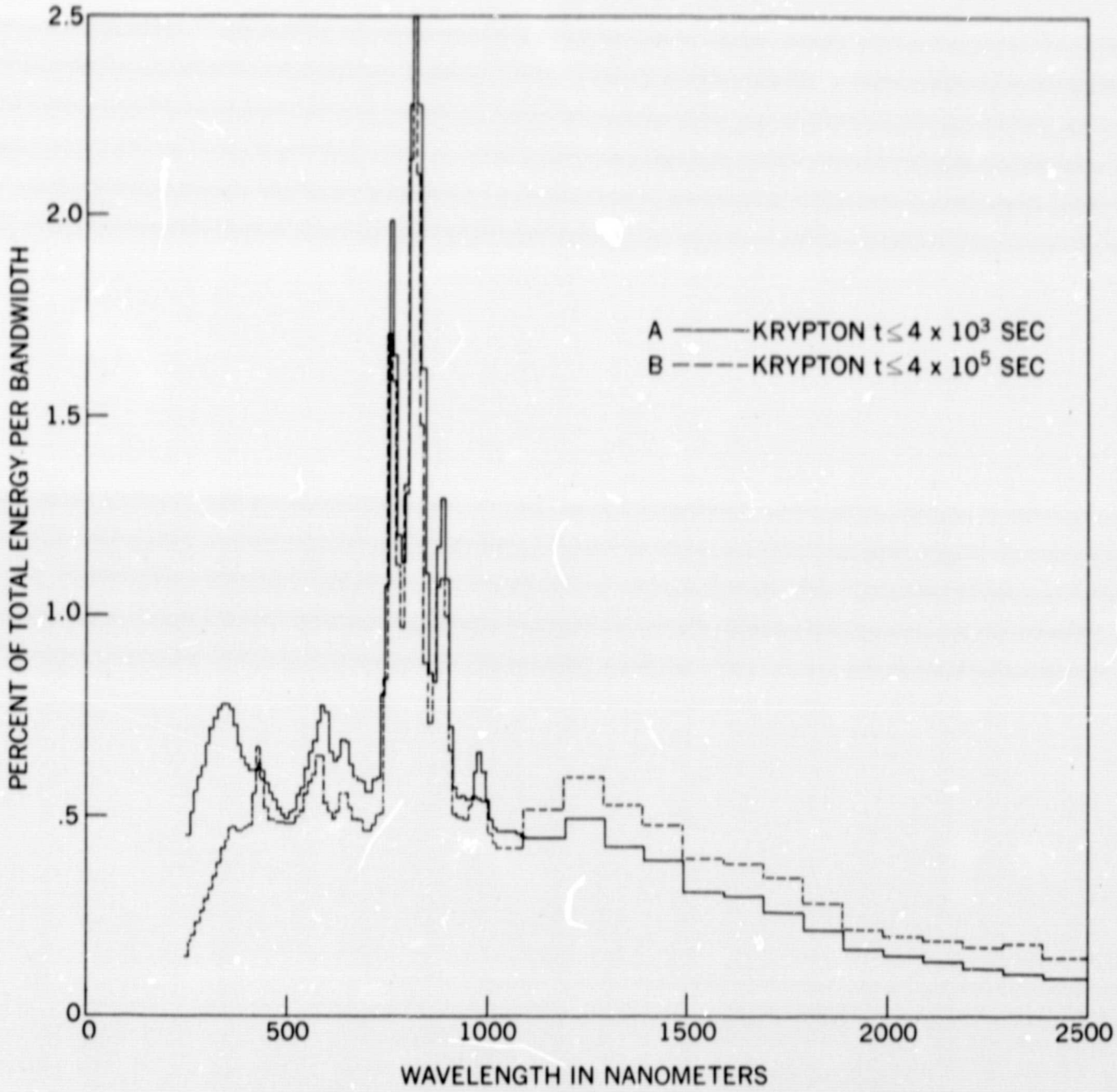

Figure 28. Spectrum Degradation of Krypton Compact Arc Lamp for $\Delta t = 3.5 \times 10^5$ sec

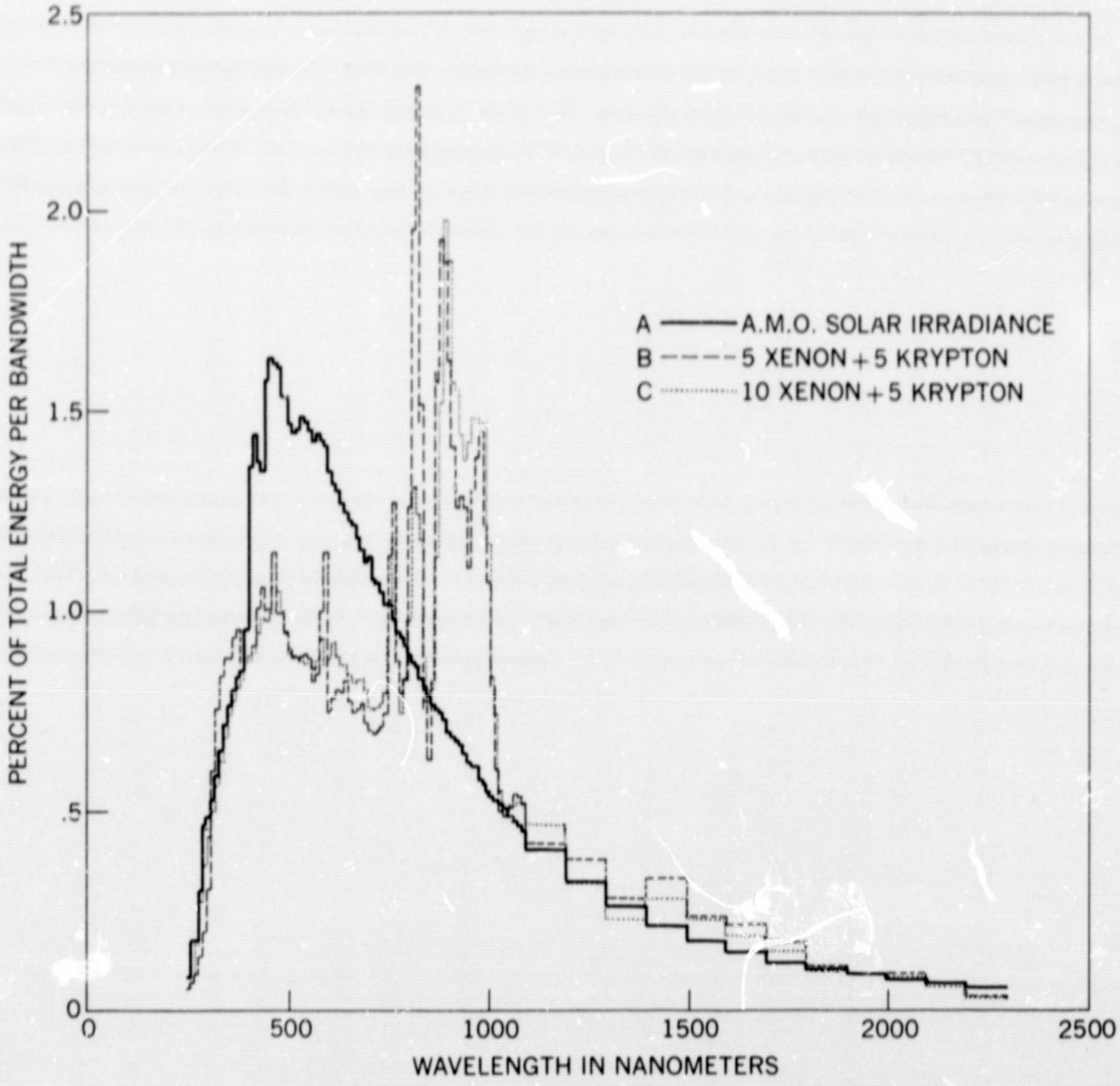

Figure 29. Spectra of Simulator Before Modification With Combination of Krypton and Xenon Arcs

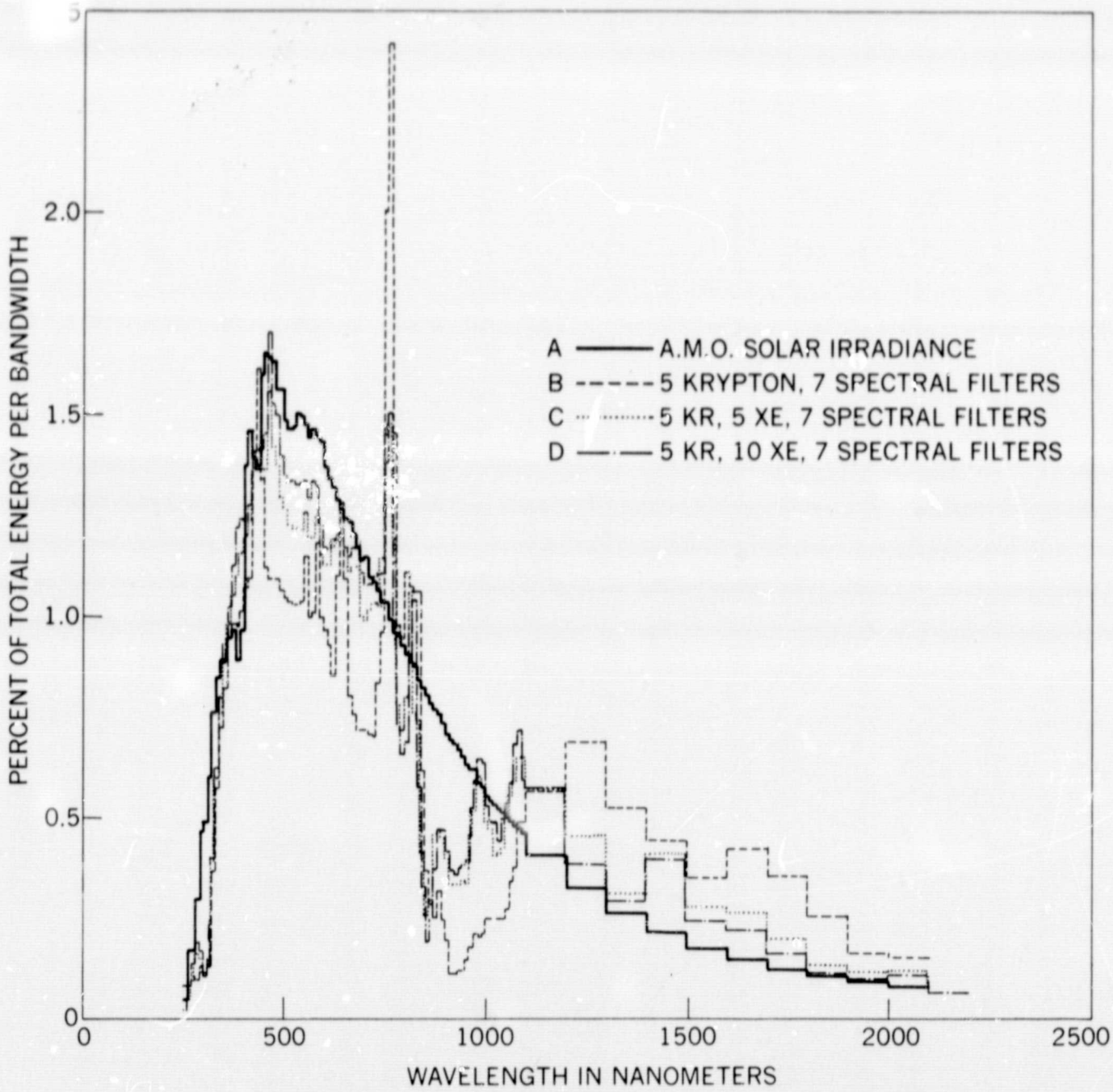

Figure 30. Spectra of Simulator Before Modification With Combination of Spectral Filters, Krypton and Xenon Arcs

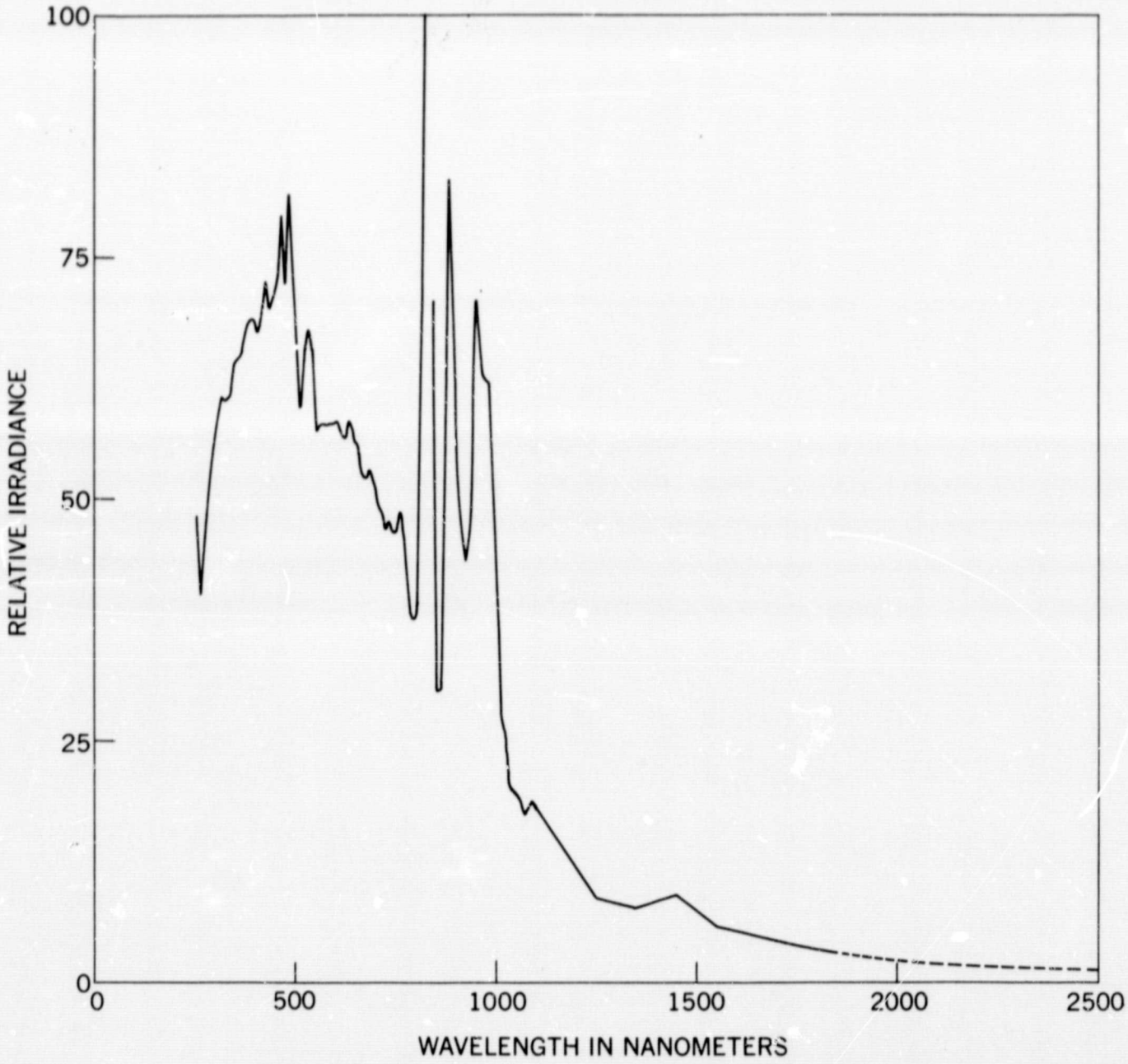

Figure 31. Spectrum of Vortex Stabilized Source With Neon-Xenon in an 8-1 Ratio

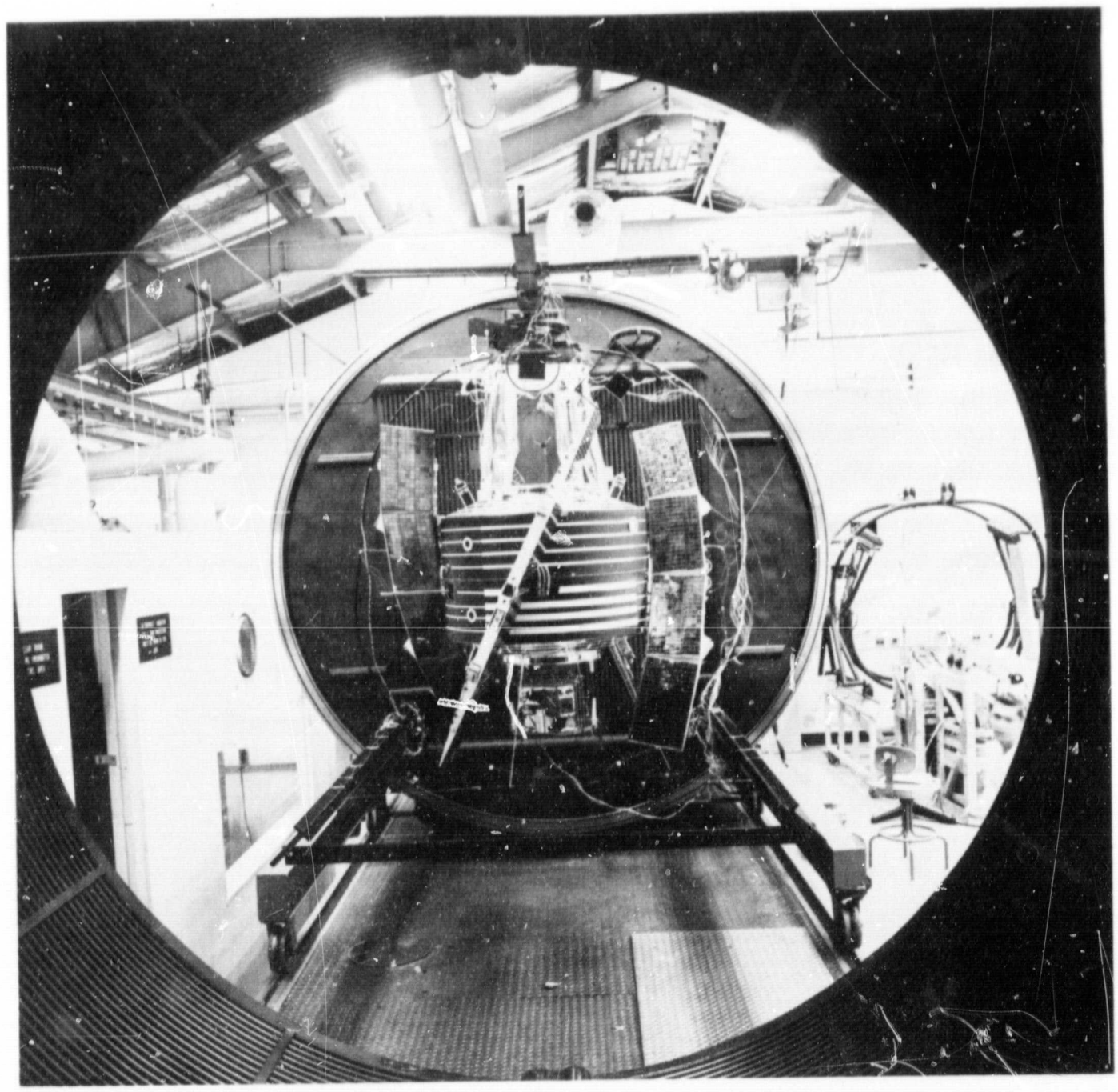

Figure 32. Explorer XXXVIII Before Solar Simulation Test

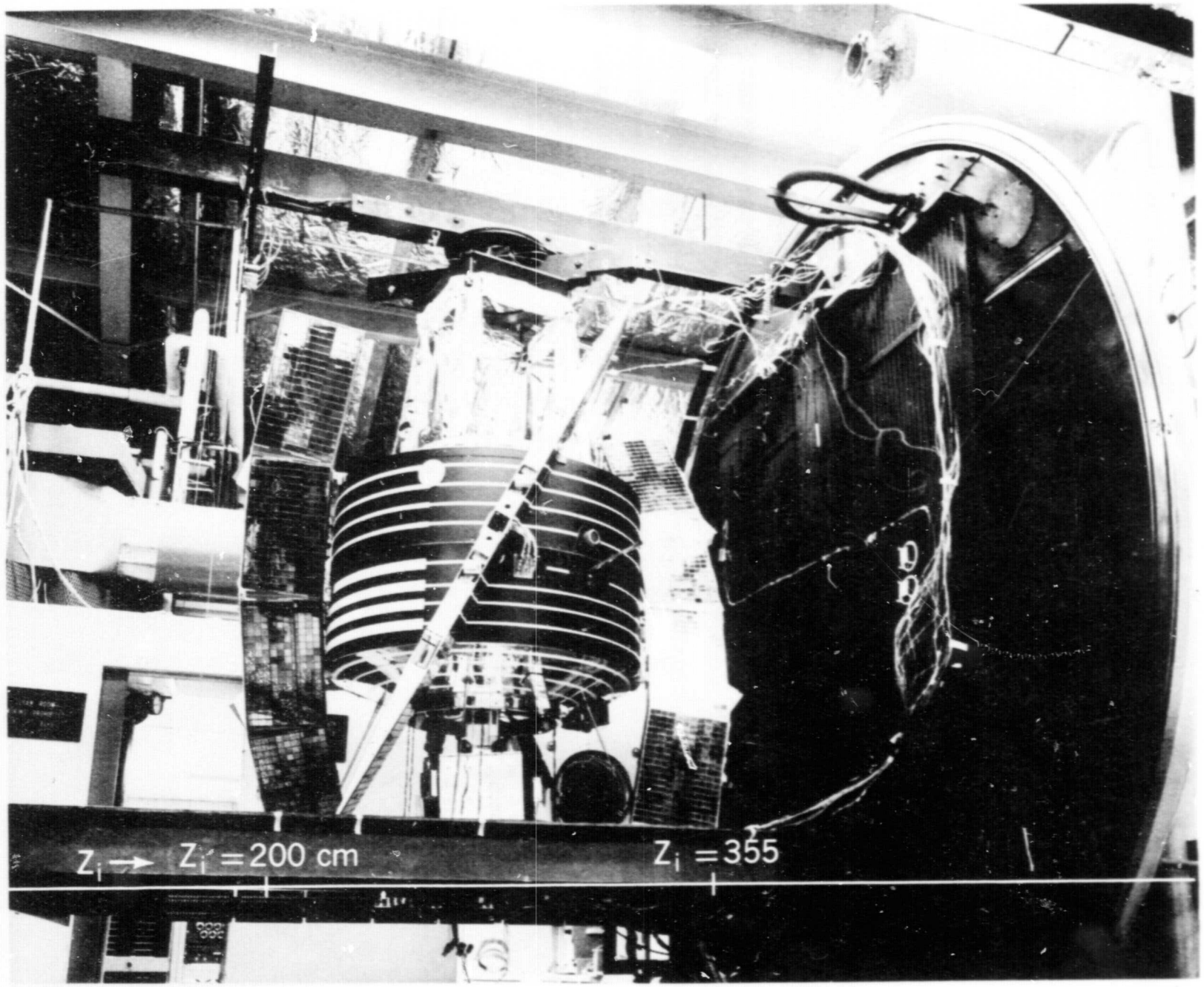

Figure 33. Side View of Explorer XXXVIII in Test Volume of Solar Simulator